NTNU
Norwegian University of
Science and Technology

Non-linear analysis methods in performance-based earthquake engineering

Fredrik Bjercke

Civil and Environmental Engineering
Submission date: June 2016
Supervisor: Amir Kaynia, KT
Co-supervisor: Nina Øystad-Larsen, Rambøll

Norwegian University of Science and Technology
Department of Structural Engineering

Department of Structural Engineering
Faculty of Engineering Science and Technology
NTNU- Norwegian University of Science and Technology

ACCESSIBILITY

MASTER THESIS 2016

SUBJECT AREA:	DATE:	NO. OF PAGES:
Computational Mechanics	09.06.2016	118

TITLE:

Non-linear analysis methods in performance-based earthquake engineering

BY:

Fredrik Bjercke

SUMMARY:

Over the last decades, increasing computational power is allowing engineers to do more advanced earthquake assessments on structures. The actual performance during seismic loading of buildings can be assessed using complicated material models, and analyses methods. Throughout this thesis, advanced non-linear analyses, both dynamic and static, are described, conducted and discussed. The structure that is used for the analyses is a reinforced concrete frame building, designed according to EN 1998-1 for ductility class medium. Analyses are primarily conducted using the open source finite element package OpenSees, but for some analyses the commercial FEA program Seismostruct is also used. A parameter study is done on the structure for comparison. Though expected, the analyses revealed that the design code is highly conservative, even when the structure remains in the elastic range. The sample structure is able to withstand major inelastic deformations. Assessing the structural behavior with performance-based earthquake engineering methods, the real collapse capacity are obtained and the safety assessed using probabilistic theory.

RESPONSIBLE TEACHER: Amir Kaynia (NTNU, KT)

SUPERVISOR(S): Nina Øystad-Larsen (Rambøll)

CARRIED OUT AT: NTNU, KT

Preface

The thesis was written over a 20 week period of time at the Norwegian University of Science and Technology (NTNU), Department of Structural Engineering, in the spring semester of 2016. This thesis marks the end of my five-year studies in Civil and Environmental Engineering with specialization in Computational Mechanics in Trondheim.

Throughout the semester, my supervisors Professor II Amir M. Kaynia (NTNU) and PhD-Candidate Nina Øystad-Larsen (Rambøll) has shown great support, knowledge, and encouragement about the subject, as well as my progression through the spring, which I am very thankful for.

Abstract

Over the last decades, increasing computational power is allowing engineers to do more advanced earthquake assessments on structures. The actual performance during seismic loading of buildings can be assessed using complicated material models, and analysis methods. Throughout this thesis, advanced non-linear analyses, both dynamic and static, are described, conducted and discussed. The structure that is used for the analyses is a reinforced concrete frame building, designed according to EN 1998-1 for ductility class medium. Analyses are primarily conducted using the open source finite element package OpenSees, but for some analyses the commercial FEA program Seismostruct is also used. A parameter study is done on the structure for comparison.

Though expected, the analyses revealed that the design code is highly conservative, even when the structure remains in the elastic range. The sample structure is able to withstand major inelastic deformations. Assessing the structural behavior with performance-based earthquake engineering methods, the real collapse capacity are obtained and the safety assessed using probabilistic theory.

Sammendrag

I løpet av de siste tiårene har kraftigere datamaskiner gjort det mulig for ingeniører å gjøre avanserte jordskjelvsberegninger. Den faktiske ytelsen av bygninger under jordskjelv, kan vurderes ved hjelp kompliserte materialmodeller og analysemetoder. Gjennom denne oppgaven er avanserte ikke-lineære analyser, både dynamiske og statiske, beskrevet, gjennomført og diskutert. Bygget som brukes for analysene er en armert betongrammebygning, utformet i henhold til EN 1998-1, for duktilitetsklasse medium. Analysene er i hovedsak utført ved bruk av åpenkildekode-programmet OpenSees, men for noen analyser er det kommersielle FEA-programmet Seismostruct også brukt. Et parameterstudie er gjennomført for å kunne gjøre sammenligninger.

Selv om det var forventet, avdekket analysene at standarden var meget konservativ, selv når resultatene forble i det elastiske området. Konstruksjonen viste seg å være i stand til å motstå store inelastiske deformasjoner. Den strukturelle oppførselen er vurdert med metoder basert på ytelsesbasert jordskjelvdimensjonering, den faktiske kapasiteten er funnet og sikkerheten vurdert med sannsynlighetsregning.

Contents

Preface i

Abstract iii

Sammendrag v

Table of Contents viii

List of Tables ix

List of Figures xiv

1 Introduction 1

2 Literature Review 3
- 2.1 Analysis procedures 3
  - 2.1.1 Linear static analysis 3
  - 2.1.2 Non-linear analysis 4
- 2.2 Software 11
- 2.3 Material modeling and element formulation 13
  - 2.3.1 Material modeling 13
  - 2.3.2 Element formulation 14
  - 2.3.3 Physical and numerical localization issues in distributed inelasticity elements 16
  - 2.3.4 Damping and Period elongation 18

3 Design of the building 21
- 3.1 Description 21
- 3.2 Seismic loading and design 21
  - 3.2.1 P-delta effects 23
  - 3.2.2 Damage limitation 25
  - 3.2.3 Ductility 26
  - 3.2.4 Columns 27

4 Non-linear static analysis 31
- 4.1 Results and discussion 31

5 Eigenperiods and stiffness reduction 35

6 Ground motion records **37**

7 Non-linear response history analysis **45**
7.1 Results and discussion 45

8 Incremental dynamic analysis **59**
8.1 Results and discussion 59
8.2 Probability of collapse and fragility curves 70

9 Parameter study **71**
9.1 Introduction 71
9.2 Results and discussion 74
9.3 Probability of collapse and fragility curves 77

10 Conclusion **79**

Bibliography **81**

Appendix **83**

List of Tables

3.1 Storey shear 23
3.2 $P - \delta$ effects 25
3.3 Updated $P - \delta$ effects due to increased stiffness 25
3.4 Drift limitations 25
3.5 Updated $P - \delta$ effects due damage limitations 26
3.6 Drift limitations after increased stiffness 26
3.7 Updated $P-$ effects due to ductility demands 27
3.8 Axial force level columns 27
3.9 Final Column dimensions 28

5.1 Eigenperiods uncracked state 35

6.1 The selected ground motions, and their properties: 38
6.2 Ground motion scaling factors, to match $S_d(T_1, 5\%)$ 38

7.1 Maximum base shear forces and displacement at control nodes from NRHA using S_d-scaling: 45

9.1 Updated ground motion scaling factors, to match $S_d(T_1, 5\%) = 1.458\,m/s^2$ 72

List of Figures

2.1 Idealized Static push-over curve. 5
2.2 Scaled response spectrum 7
2.3 IDA curves with first mode spectral acceleration as IM and maximum interstorey drift ratio as IM. 8
2.4 Limit states on a typical IDA curve, the characteristic elastic slope is also shown. 9
2.5 Probability of collapse: Cumulative distribution and the fitted fragility function. 10
2.6 The Seismostruct interface 11
2.7 The OpenSees interface 12
2.8 Confined concrete model, the red and black graph are the confined concrete with different transverse reinforcement ratios, and the dashed is the unconfined concrete. Illustration from OpenSees Wiki. [20] 13
2.9 Material models, illustrations from OpenSees Wiki [20] 14
2.10 Beam element with fiber sections along the element [18] 15
2.11 Illustration showing physical localization issues in uniaxial and flexural compression [18] 16
2.12 Illustration of hardening and softening behavior of a cantilever column [18] 17
2.13 Plot showing how the damping ratio depend on the frequency, and why a combination of both stiffness and mass proportional damping is favorable 19
2.14 Force-displacement curves illustrating stiffness reduction during an earthquake record 19

3.1 The building in Robot Structural Analysis 22
3.2 Plan and vertical projection of the building 23
3.3 Fundamental mode shape. Illustration from Robot Structural Analysis . . 24
3.4 Type 1 elastic and design response spectra. 24
3.5 Reinforcement of the columns 29
3.6 Reinforcement of the beams 30

4.1 Static pushover curve for both the OpenSees and Seismostruct analysis . . 32
4.2 SPO-result: Interstorey drift ratio at maximum base shear from OpenSees. 33
4.3 SPO-result: Interstorey drift ratio at 20% loss of maximum base shear from OpenSees. 33

5.1 The first four mode shape of the sample structure 36

6.1 RSN68 Unscaled ground motion time-history 39

6.2 RSN169 Unscaled ground motion time-history 39
6.3 RSN724 Unscaled ground motion time-history 39
6.4 RSN730 Unscaled ground motion time-history 39
6.5 RSN1634 Unscaled ground motion time-history 40
6.6 RSN4853 Unscaled ground motion time-history 40
6.7 RSN5786 Unscaled ground motion time-history 40
6.8 RSN68 Scaled ground motion time-history 41
6.9 RSN169 Scaled ground motion time-history 41
6.10 RSN724 Scaled ground motion time-history 41
6.11 RSN730 Scaled ground motion time-history 41
6.12 RSN1634 Scaled ground motion time-history 42
6.13 RSN4853 Scaled ground motion time-history 42
6.14 RSN5786 Scaled ground motion time-history 42
6.15 Unscaled response spectra for the selected earthquake records. 43
6.16 Scaled response spectra with $S_d(T_1, 5\%) = 1.96 m/s^2$, clearly different records have significantly different S_d for the lower periods. 43

7.1 NRHA Base shear vs RDR plotted with the SPO curve from OpenSees. Both the results from the scaling with $S_d(T_1, 5\%)$ and $S_e(T_1, 5\%)$ are included 46
7.2 Plot showing the lateral displacement of the building at maximum base shear for each earthquake motion record scaled to $S_d(T_1, 5\%)$ 47
7.3 RSN68 San Fernando scaled to $S_d(T_1, 5\%)$ 48
7.4 RSN169 Imperial Valley scaled to $S_d(T_1, 5\%)$ 48
7.5 RSN724 Superstition Hills-02 scaled to $S_d(T_1, 5\%)$ 49
7.6 RSN730 Spitak Armenia scaled to $S_d(T_1, 5\%)$ 49
7.7 RSN1634 Manjil Iran scaled to $S_d(T_1, 5\%)$ 50
7.8 RSN4853 Chuetsu-oki Japan scaled to $S_d(T_1, 5\%)$ 50
7.9 RSN5786 Iwate Japan scaled to $S_d(T_1, 5\%)$ 51
7.10 San Fernando earthquake hysteric base shear vs. roof displacement scaled to $S_d(T_1, 5\%)$ 52
7.11 Hysteric base shear vs. displacement at control node 53
7.12 Hysteric base shear vs. displacement at control node 53
7.13 Hysteric base shear vs. displacement at control node 54
7.14 San Fernando earthquake hysteric base shear vs. roof displacement scaled to $S_e(T_1, 5\%)$ 55
7.15 Hysteric base shear vs. displacement at control node 56
7.16 Hysteric base shear vs. displacement at control node 56
7.17 Hysteric base shear vs. displacement at control node 57

8.1 IDA curves showing maximum roof drift ratio, of the building with $T_1 = 0.790s$. 60
8.2 RDR Response of the last two scalings of RSN68, resulting in collapse at $T \approx 20$ s 61
8.3 RDR Response of the last two scalings of RSN169, resulting in collapse at $T \approx 78$ s 61

8.4 RDR Response of the last two converging scalings of RSN724, the time-history is not showing a collapse behavior, however the structure is collapsed at RDR=8% 61
8.5 RDR Response of the last converging two scalings of RSN730, the time-history is not showing a collapse behavior, however the structure is collapsed at RDR≈9% 62
8.6 RDR Response of the last two scalings of RSN1634, resulting in collapse at $T \approx 30$ s 62
8.7 RDR Response of the last two converging scalings of RSN4853, the time-history is not showing a collapse behavior, however the structure is collapsed at RDR≈8.5% 62
8.8 RDR Response of the last two scalings of RSN5786, resulting in collapse at $T \approx 50$ s 63
8.9 IDA curves showing maximum interstorey drift ratio for all the ground motion records. 65
8.10 IDA curves showing maximum interstorey drift ratio for each floor, for the RSN68 record 66
8.11 IDA curves showing maximum interstorey drift ratio for each floor, for the RSN169 record 66
8.12 IDA curves showing maximum interstorey drift ratio for each floor, for the RSN724 record 67
8.13 IDA curves showing maximum interstorey drift ratio for each floor, for the RSN730 record 67
8.14 IDA curves showing maximum interstorey drift ratio for each floor, for the RSN1634 record 68
8.15 IDA curves showing maximum interstorey drift ratio for each floor, for the RSN4853 record 68
8.16 IDA curves showing maximum interstorey drift ratio for each floor, for the RSN5786 record 69
8.17 Fitted collapse fragility curves and the empirical cumulative distribution. . 70

9.1 RSN68 Scaled ground motion time-history 72
9.2 RSN169 Scaled ground motion time-history 72
9.3 RSN724 Scaled ground motion time-history 72
9.4 RSN730 Scaled ground motion time-history 73
9.5 RSN1634 Scaled ground motion time-history 73
9.6 RSN4853 Scaled ground motion time-history 73
9.7 RSN5786 Scaled ground motion time-history 73
9.8 Scaled response spectra with $S_d(T_1, 5\%) = 1.458\, m/s^2$ 74
9.9 RDR from NRHA and SPO analysis, plotted with the results from the original building 75
9.10 IDA curves showing maximum roof drift ratio, of the building with $T_1 = 1.064\, s$ 76
9.11 IDA curves showing maximum interstorey drift ratio, of the building with $T_1 = 1.064\, s$ 76
9.12 Fitted collapse Fragility curves and the empirical cumulative distribution for the building with $T_1 = 1.064\, s$ 77

9.13 The fitted collapse fragility curves and the empirical cumulative distribution for both buildings 78

Chapter 1

Introduction

Earthquakes are often responsible for major damages or even collapse of buildings which in turn means major economical costs, and possible loss of human lives. Seismic loading acts on building such that the structure may exhibit highly non-linear behavior, which requires complicated material models and advanced dynamic analysis methods in order to accurately model the response. New analysis methods are emerging in research, and are being put into use in the industry. Alongside the development of increased computational capacity and intricate coding, engineers are able to conduct advanced non-linear analyses of structures, resulting in better buildings and a safer world. In performance-based earthquake engineering the actual performance of the building is evaluated, using advanced non-linear analysis methods. Different analysis methods can be used to assess capacity, and numerous ways to post-process the response and results. The thesis has a focus on the application of the different analyses methods, and how to assess the results.

The thesis consists of a Literature review, where the analysis methods, and its theory used later in the thesis are presented, followed by the description of the Design of the building. The design chapter goes through the procedures in EN 1998-1, and other governing codes for design of structures in Europe. Following that chapter are the result and discussion chapters, non-linear static analysis, non-linear response history analysis and finally incremental dynamic analysis. A parameter study is also included in the thesis, where the 1st floor is increased without changing the design, and the response is evaluated and compared to the original structure.

Chapter 2

Literature Review

2.1 Analysis procedures

In this section, the analysis procedures used in the thesis are presented. Assessing dynamic response of multi-degree of freedom system (MDOF), which applies to almost every building or structure in the world, the basis is the equation of motion:

$$\mathbf{M}\ddot{\mathbf{D}} + \mathbf{C}\dot{\mathbf{D}} + \mathbf{K}\mathbf{D} = \mathbf{R}^{ext} \tag{2.1}$$

Here, $\mathbf{M}$ is the mass matrix, $\mathbf{C}$ the damping matrix, $\mathbf{K}$ the stiffness matrix, and $\mathbf{R}^{ext}$ the externally applied forcing. $\ddot{\mathbf{D}}$,$\dot{\mathbf{D}}$, and $\mathbf{D}$ are nodal acceleration, velocity, and displacement vector, respectively. The most effective way to solve such a system of equations, is the *Finite Element Method* (FEM). Solving for the unknown nodal acceleration, velocity, and displacement, the element forces, stresses and strains can be obtained. An earthquake is basically an acceleration that the building is being subjected to. The earthquake comes from the ground, thus the foundations are subjected to the earthquake motion. In the equation of motion, acceleration from the seismic action is put into the vector $\ddot{\mathbf{D}}$, at the nodes connected to the ground. Since this acceleration is known, and mass times acceleration is force, the known parts of $\mathbf{M}\ddot{\mathbf{D}}$ is put into $\mathbf{R}^{ext}$. The known parts are now on the right hand side, and the unknown on the left. However, solving this requires an advanced integration scheme, thus simpler methods for assessing seismic action are developed.

2.1.1 Linear static analysis

Linear static analysis is often the preferred method when assessing seismic action due to the fact that it is the least time-consuming method. Eurocode 8 [5] presents a method, the Lateral Force method, which are simple guidelines for how to take the forces from potential earthquakes into account, without doing complicated dynamic analyses. The procedure gives shear forces at each floors and a base shear. Some of the drawbacks with this method is that it assumes that the contributions from higher order modes are negligible, which in some cases is not true, also if the structure deforms outside the elastic range the method does not give satisfying results, and since earthquakes are a dynamic load, inelastic or plastic behavior can likely occur. The procedure requires that the building has some regularity in plan and elevation, which is not always the case for buildings in the 21st century. Ground breaking architecture is challenging the existing codes, with slender columns, long spans, and complicated geometry. These limitations are often the motivation for conducting more advanced analyses of the earthquake response.

2.1.2 Non-linear analysis

Introduction

Linear analyses often overestimates forces since simplifications are made, and they are therefore often conservative. Knowing that large deformations will occur during the loading, inelastic material behavior in the elements or complicated structures that cannot be made code compliant, are incentives for conducting more accurate, non-linear analyses. Non-linear behavior can utilize the materials to its fullest, and is therefore the preferred method concerning accuracy, especially in the research field. Non-linear dynamic analyses are however time consuming even with the computational power available today. Non-Linear Response History Analysis (NRHA) also called non-linear time-history analysis, is the method with the highest accuracy, but with a high threshold for the analyst. NRHA are mostly used when the behavior of the higher modes are of interest, which they in many cases are not. Therefore simpler, but still accurate procedures for calculating non-linear response are developed.

Non-linear Static analysis

A well documented analysis type for assessing capacity is Static pushover analysis or SPO analysis. It is one of the easiest non-linear analyses that can be conducted, while still assessing the non-linear stress-strain relationships for all elements. A force-displacement curve is created by applying a monotonically increasing horizontal force to the structure, while still subject to gravitational loads, until collapse, or non-convergence. The vertical distribution of the lateral force at each storey level should be in proportion to the fundamental mode shape [2] [3], which is also one of the two suggested load-patterns in EN 1998-1 [5]. The other method in EN-1998-1 is an equal load pattern, and both patterns have to be applied. However, in this thesis only the modal pattern is applied, following FEMA P440 [3] recommendation. The lateral force is applied until a specified target displacement is reached or, the lateral forces are applied until a loss of 20% of the maximum base shear capacity is achieved [2], at this point the ultimate displacement is reached, this is directly linked to the displacement, the structure were to exhibit due to an earthquake. In Figure 2.1, an idealized static pushover curve is illustrated. A non-linear static pushover analysis is used to quantify the maximum base shear and the ultimate displacement, which are in turn used to compute overstrength and ductility. In Equation (2.2) the over strength factor formula is shown, where V_{max} is the maximum base shear resistance and V is the design base shear.

$$\Omega = \frac{V_{max}}{V} \tag{2.2}$$

By using the specified step-by-step method in EN 1998-1 Annex B. Point B.1 to B.6, the target displacement for different design situations can be calculated.

An important non-linear feature that are to be included in the SPO-analysis, is $P - \delta$ effects. Since the lateral loading is applied in combination with vertical gravitational loads, $P - \delta$ effects can be of great significance in determination of capacity.

However there are some disadvantages with the method, especially since the analysis is static, damping is not included, and neither can other time-dependent dynamic effects be. When the structure deforms and inelastic behavior occur, the modal properties change. This will not be included in the SPO, which is unfortunate since the forcing on the building in a SPO-analysis is dependent on the mode shape. For structures dominated by the first mode, SPO-analysis has satisfying accuracy, but for structures that depends highly on multiple modes, the method is not good enough [13].

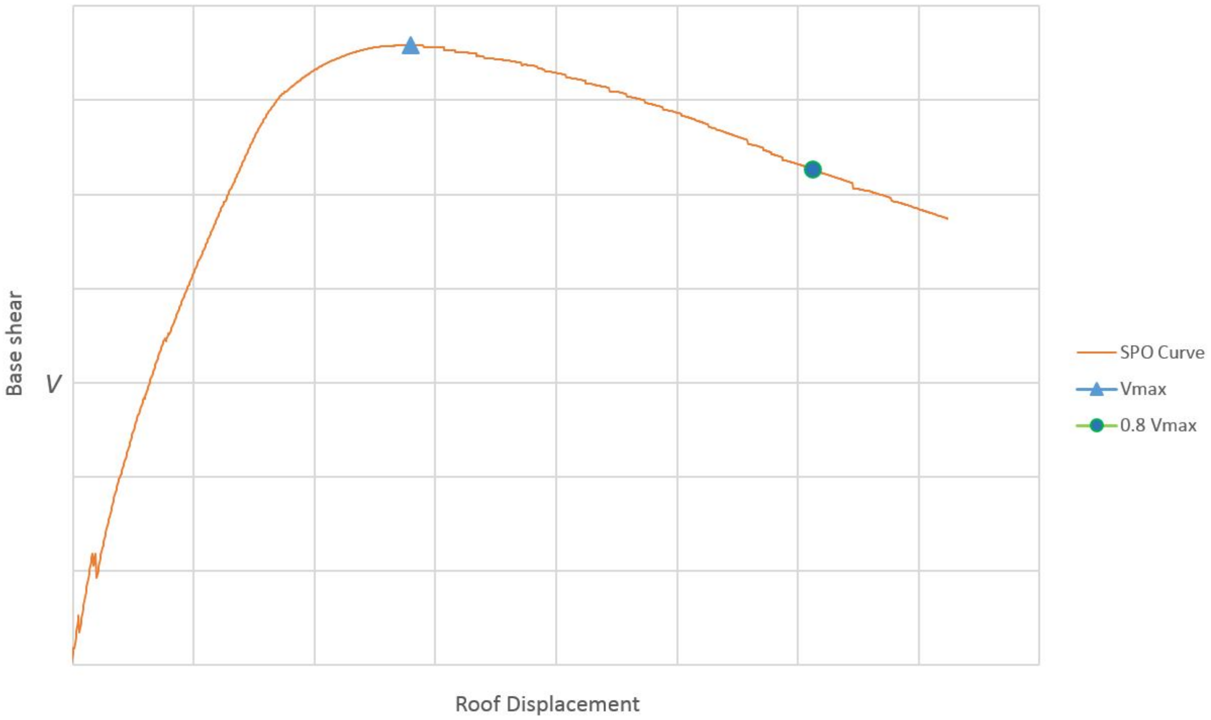

Figure 2.1: Idealized Static push-over curve.

Non-linear response history analysis

The most accurate way to model a structure and accessing the response due to dynamic loading is NRHA. It is a widely recognized method for simulating response of structures subjected to strong levels of seismic action [7]. As for the non-linear static analysis, non-linear material models are implemented, but since it is now a dynamic problem, damping, mass and ground acceleration must also be implemented to the model. For earthquake analysis assessment, a ground motion record from previous earthquakes or, an artificial record, are used for the seismic action. NRHA is suitable for structures that are likely to have significant behavior from higher order modes. When applying NRHA, strength and stiffness degradation can be accounted for, unlike in the SPO-analysis where this is completely neglected. Thus resulting forces and displacements from a NRHA are good estimates for the response a building is to exhibit during an earthquake.

By direct integration of the equation of motion (Eq. (2.1)), dynamic analysis can be performed. For non-linear dynamic analysis where the response period of interest is *long*, which is the case for earthquake motions, implicit integration of the equation of motion is the most accurate scheme, rather than explicit. Using an integration scheme such as the α-method, proposed by Hilbert, Hughes, and Taylor, algorithmic damping can be introduced, while still retaining second order accuracy [10]. The α-method is based on *The Average Acceleration Method* or *Newmark Difference Relations.* Since nonlinearities are to be introduced in the scheme, an incremental iterative solution procedure must be employed. Loads are applied incrementally, and an iterative scheme is used until equilibrium is reached, whereby internal forces, and displacement increments are computed. After each incremental solution is obtained, and prior to the next load increment, the stiffness matrix is updated to account for the geometric changes of the structure [7] [10].

The earthquake motion must be chosen when conducting a NRHA, and since the response is highly sensitive to the ground motion characteristics, multiple ground motions is needed. EN 1998-1 clause 4.3.3.4.3 demands at least seven time histories, where the average response from these analyses are used in the design. The different parameters such as *Peak Ground Acceleration* (PGA), *Magnitude*, and *Shear Wave Velocity* (V_s) should be in the same range for the NRHA. The time histories that are chosen should also be representative for the building site. In this thesis the earthquake motions are taken from the NGA-West2 database at PEER [17], which is discussed further in Chapter 6.

After the ground motions are selected, they are manipulated to match the response spectrum, this can be done using scaling or spectrum matching [12]. Using the scaling method, each individual ground motion response is scaled to match a specific natural period or over a range of periods in the design response spectrum, created using the EN-1998-1 procedure. Resulting in a unique integer factor for each ground motion. Spectrum matching is done by taking each ground motion, and manipulating them to match the design response spectrum, resulting in modification of the ground motion. There is for the time being, no specific agreement on which method is preferable in NRHA. Further insight on the topic can be found in the literature [12]. The scaling method is used in this thesis. In Figure 2.2 the scaled response spectra for the chosen seven time-histories are shown. They are scaled to match the period $T_1 \approx 0.8s$.

The significant difference between a static analysis and a dynamic one, is time, and time is a very important property in earthquake engineering. The duration of the earthquake, thus the number of cycles can influence the damage caused by the ground motion [24], however the research community does not agree on whether the duration have any effect on the structural damage [24,25]. Strong-motion duration must in some way effect the structural damage, the cyclic loading is causing the structure to exhibit stiffness and strength degradation and with more cycles, more damage is likely caused, longer-duration strong motion records is suggested to increase inelastic base shear. On the other hand, studies suggests that when the ground motions are scaled to the same spectral acceleration, the duration has no influence on inelastic displacements [25]. The governing seismic design codes today [5] states that duration can be neglected.

Incremental dynamic analysis

In the past decade more advanced analysis methods for assessing structural performance during seismic loading have emerged. Incremental Dynamic analysis (IDA) is a parametric

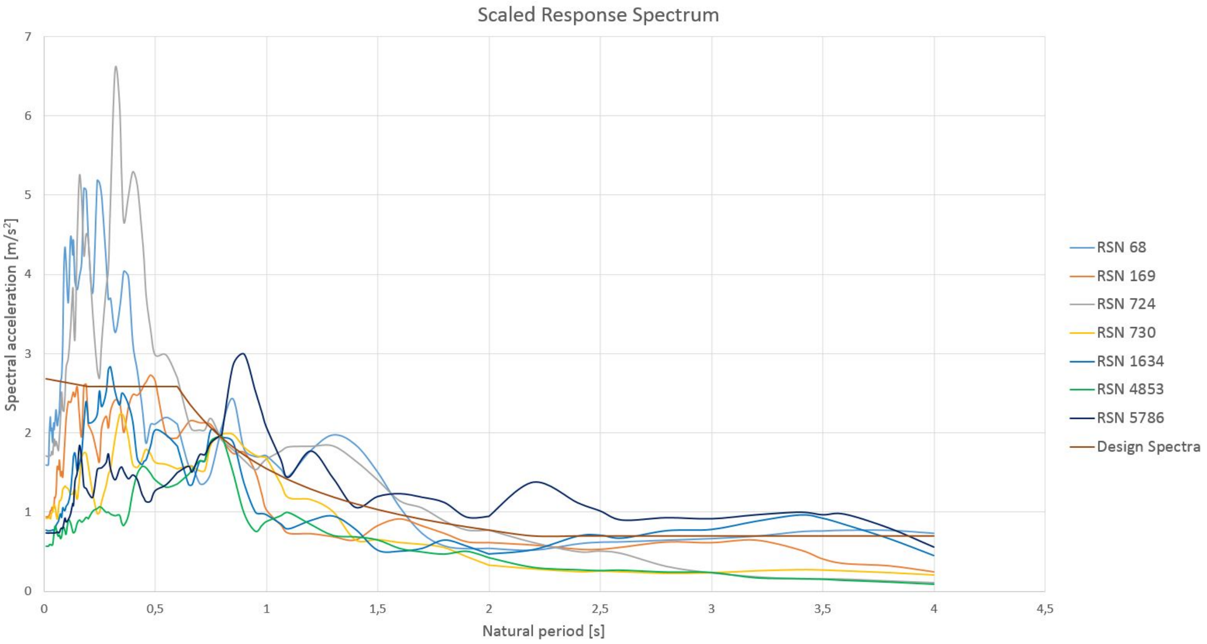

Figure 2.2: Scaled response spectrum

analysis method, where the structure is subjected to one or more ground motion records, scaled to multiple intensity levels, and subsequently producing several response curves. IDA is using the same solver for the equation of motion, as a NRHA, thus the procedure for solving the dynamic problem is the same. IDA is basically a set of NRHA, where the response from one or multiple records, scaled up and down, is plotted in the same graph. When using multiple records, the engineer is able to see how the structure is responding to different earthquakes scaled upwards, and can therefore design the columns, beams, and other structural members more efficiently for the seismic loading, as well as assess the structural performance. IDA is becoming more and more relevant, and important in Performance Based Earthquake Engineering (PBEE) [8] [9].

The IDA plot consist of an Intensity measure and a Damage measure, see Figure 2.3. Where the intensity measure is usually on the vertical axis and the damage measure on the horizontal. The intensity measure (IM) or *Monotonic Scalable Ground Motion Intensity Measure*, is a non-negative scalar that depends on an unscaled accelerogram, and is increased monotonically until collapse is reached [8]. There is proposed several different intensity measures that are scalable. Peak Ground Acceleration, Peak Ground Velocity, 5% damped Spectral Acceleration at the buildings fundamental period ($S_d(T_1, 5\%)$), and the yield reduction factor are such scalable IMs. The building analyzed in this thesis is first-mode dominated, and therefore the $S_d(T_1, 5\%)$ IM is used, which is appropriate for such structures. It is proven to be an efficient IM, by minimizing the scatter in the results, thus requiring fewer ground motions [9].

Damage measure (DM) or *Structural State Variable* is a non-negative scalar that describes the response of the structure, due to the seismic action on the building. In other words, DM is the output from the non-linear dynamic analysis. The selection of the Damage Measure (DM) highly depends on the application and the structure at hand. A suitable DM for a multi-storey building might be Maximum Interstorey drift ratio, while for a suspension bridge, base shear at the towers or mid-span acceleration would be a more appropriate DM. It is reasonable to look at multiple DM for each IDA, to assess the structural performance of the building or structure.

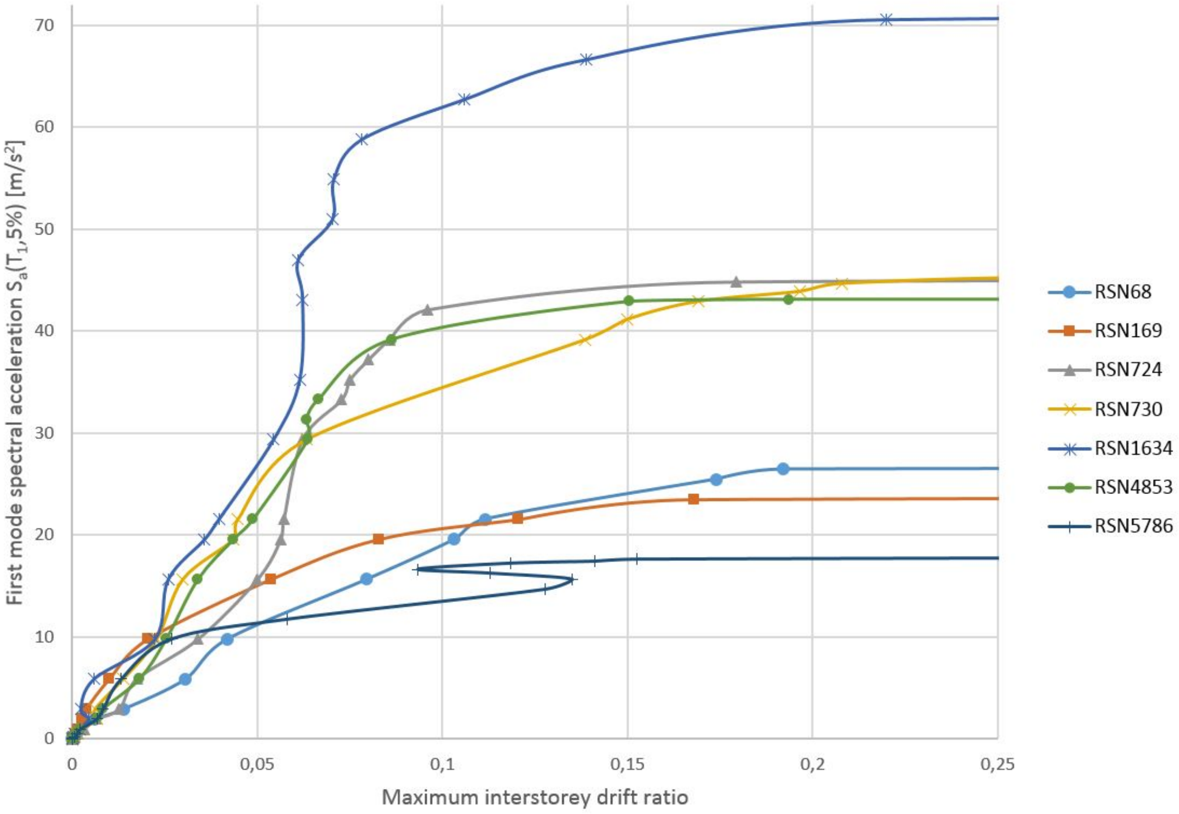

Figure 2.3: IDA curves with first mode spectral acceleration as IM and maximum interstorey drift ratio as IM.

The analyses are performed with increasing scaling factors until collapse of the structure, e.g. *Global Dynamic Instability*(GI) [9]. This is usually when convergence is not reached any more, but this can also mean localization issues, which will be discussed later on. Looking at the IDA curves in Figure 2.3, it is however not easy to determine where collapse actually occurs. Determining the limit state can be done by the DM-based rule or IM-based rule [8]. The DM-based rule is being imposed by the statement if $DM \geq C_{DM}$, then the limit state is exceeded. Here, C_{DM} is an indicator for the limit, that can be obtained through experiments, theory or experience. The IM-based rule is for assessing the collapse capacity better. Thus a point on the IDA curve clearly divides the curve into a collapse and non-collapse state. It is based on the same statement as a DM-rule, $IM \geq C_{IM}$. There are a number of limit-states that can be chosen, to determine the capacity on an IDA curve. Three types that are used in research, as described by Vamvatsikos et.al. [9], immediate occupancy (IO), collapse prevention and the before mentioned GI. In Figure 2.4 a typical IDA curve is shown with the different limit states. GI occurs when the flatline is reached, where a small increase in IM will result in an infinite increase in DM.

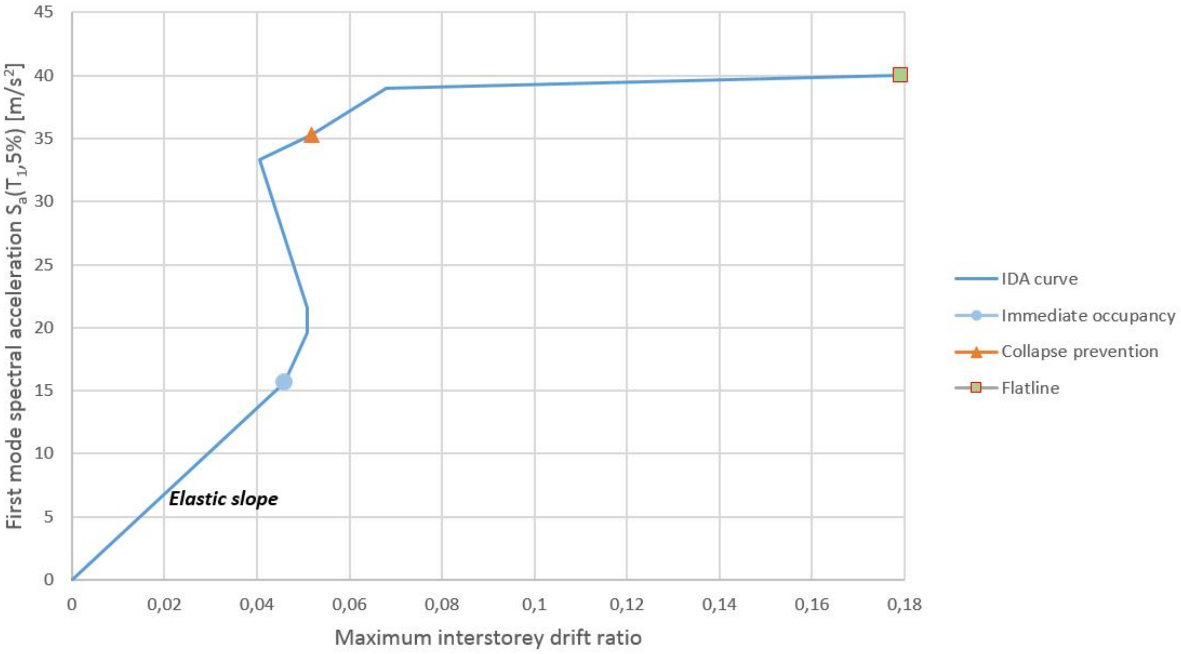

Figure 2.4: Limit states on a typical IDA curve, the characteristic elastic slope is also shown.

The different earthquakes have quite dissimilar response after the elastic range. As seen from the curves in Figure 2.3, some records may cause a softening behavior, others hardening and also weaving behavior is not unusual in an IDA study. Therefore, multi-record IDA is preferred, since single-record IDA's can not completely capture the behavior that the building may have in a possible earthquake. The response is highly dependent on the records chosen, thus the building must be subjected to a suite of ground motions.

Fragility functions

Fragility functions are useful post-processor tools in performance-based earthquake engineering. The results from an IDA can be used to assess the probability of collapse, and give the engineer a broader picture regarding the structural performance, and safety of the building. To define an analytical fragility function a log-normal cumulative distribution function is often used, as seen in Equation (2.3).

$$P(C \mid IM) = \Phi(\frac{ln(IM/\theta)}{\beta}) \tag{2.3}$$

Here $P(C \mid IM)$, is the probability of structural collapse at the given IM level, Φ is the standard normal cumulative distribution function, often abbreviated CDF, θ is the median collapse capasity e.g. the spectral acceleration where half of the ground motions cause collapse of the structure. However some literature such as J. Baker [11] suggests that the mean should be used when estimating θ, and β is the standard deviation of $ln(IM)$ which is often refereed to as the dispersion of IM [11], however FEMA P695 [2] demands that β is set to a fixed value, namely $\beta = 0.4$ for systems with period-based ductility greater than 3. Figure 2.5 shows a typical cumulative distribution which is obtained from the collapse

IMs in Figure 2.3. Here the fragility curve is created from seven earthquake record IMs, however multiple records would be favorable. If more ground motion recordings where to be used, the cumulative distribution function would pass through more points, and therefore be more accurate.

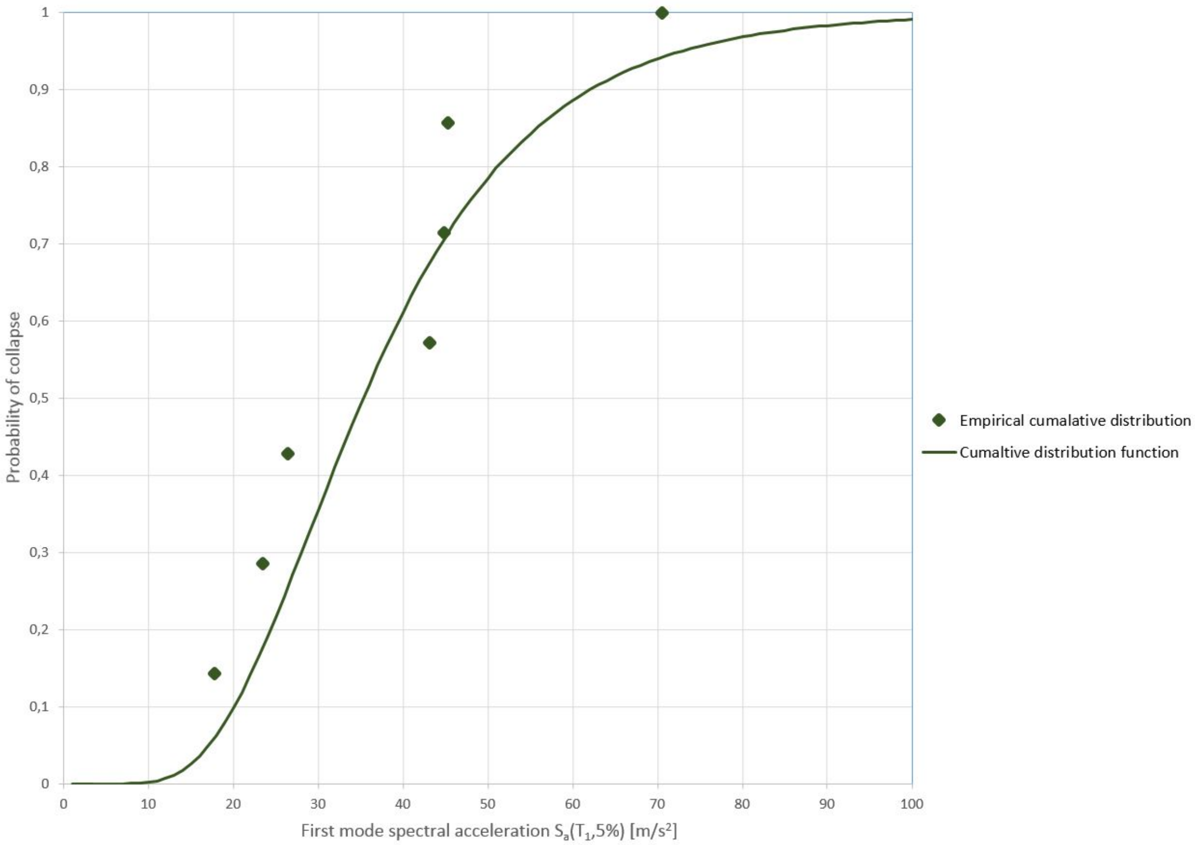

Figure 2.5: Probability of collapse: Cumulative distribution and the fitted fragility function.

2.2 Software

The analyses in this thesis are conducted in OpenSees and Seismostruct. OpenSees is an abbreviation for the full name, *The Open System for Earthquake Engineering Simulation*. The program is developed at the University of California Berkeley, at The Pacific Earthquake Engieneering Research Center (PEER). It is first of all used in research and for academic purposes, therefore it comes with a vast number of material modeling options, state of the art integrators for static and transient analysis, an arsenal of algorithms for solving the non-linear equations, and the ability to record the outputs you as an analyst need. OpenSees is one of the most advanced anaysis programs for structural engineering, and it is extremely powerful. However it lacks a graphical interface, so the user must write script in the programming language *tcl*, and using built in OpenSees commands, which is loaded into the OpenSees program. Subsequently building up structural models for analyses in OpenSees is a cumbersome process, and there is a lot of room for errors. Since OpenSees is an open source software, users can contribute to the development of the program, and it is free.

For verification of the structural model and analyses, some of the analyses are conducted in Seismostruct as well. This is a commercial finite element package, and therefore has a more user friendly interface. Seismostruct is also able to account for complicated concrete material models, and nonlinearities in both static and dynamic analysis. As seen from Figure 2.6 the Seismostruct user interface is much more convenient from a user point of view compared to the OpenSees Interface, which is depicted in Figure 2.7. Seismostruct is however not that robust, and does not have the almost endless modeling options that are in the OpenSees software package.

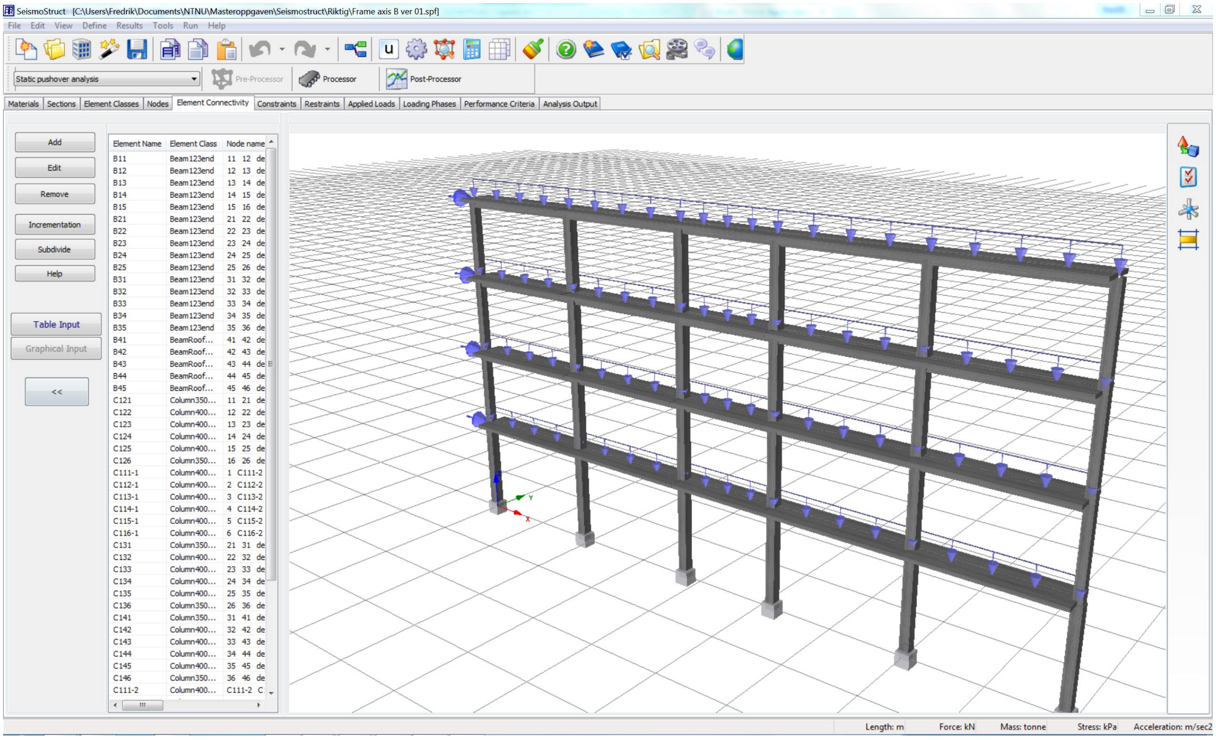
SeismoStruct [C:\Users\Fredrik\Documents\NTNU\Masteroppgaven\Seismostruct\Riktig\Frame axis B ver 01.spf]
File Edit View Define Results Tools Run Help
Static pushover analysis
Pre-Processor
Processor
Post-Processor
Materials
Sections
Element Classes
Nodes
Element Connectivity
Constraints
Restraints
Applied Loads
Loading Phases
Performance Criteria
Analysis Output
Add
Edit
Remove
Incrementation
Subdivide
Help
Table Input
Graphical Input
<<
Y
X
Length: m
Force: kN
Mass: tonne
Stress: kPa
Acceleration: m/sec2

Element Name	Element Class	Node name
B11	Beam123end	11 12 de
B12	Beam123end	12 13 de
B13	Beam123end	13 14 de
B14	Beam123end	14 15 de
B15	Beam123end	15 16 de
B21	Beam123end	21 22 de
B22	Beam123end	22 23 de
B23	Beam123end	23 24 de
B24	Beam123end	24 25 de
B25	Beam123end	25 26 de
B31	Beam123end	31 32 de
B32	Beam123end	32 33 de
B33	Beam123end	33 34 de
B34	Beam123end	34 35 de
B35	Beam123end	35 36 de
B41	BeamRoof…	41 42 de
B42	BeamRoof…	42 43 de
B43	BeamRoof…	43 44 de
B44	BeamRoof…	44 45 de
B45	BeamRoof…	45 46 de
C121	Column350…	11 21 de
C122	Column400…	12 22 de
C123	Column400…	13 23 de
C124	Column400…	14 24 de
C125	Column400…	15 25 de
C126	Column350…	16 26 de
C111-1	Column400…	1 C111-2
C112-1	Column400…	2 C112-2
C113-1	Column400…	3 C113-2
C114-1	Column400…	4 C114-2
C115-1	Column400…	5 C115-2
C116-1	Column400…	6 C116-2
C131	Column350…	21 31 de
C132	Column400…	22 32 de
C133	Column400…	23 33 de
C134	Column400…	24 34 de
C135	Column400…	25 35 de
C136	Column350…	26 36 de
C141	Column350…	31 41 de
C142	Column400…	32 42 de
C143	Column400…	33 43 de
C144	Column400…	34 44 de
C145	Column400…	35 45 de
C146	Column350…	36 46 de
C111-2	Column400…	C111-2 C

Figure 2.6: The Seismostruct interface

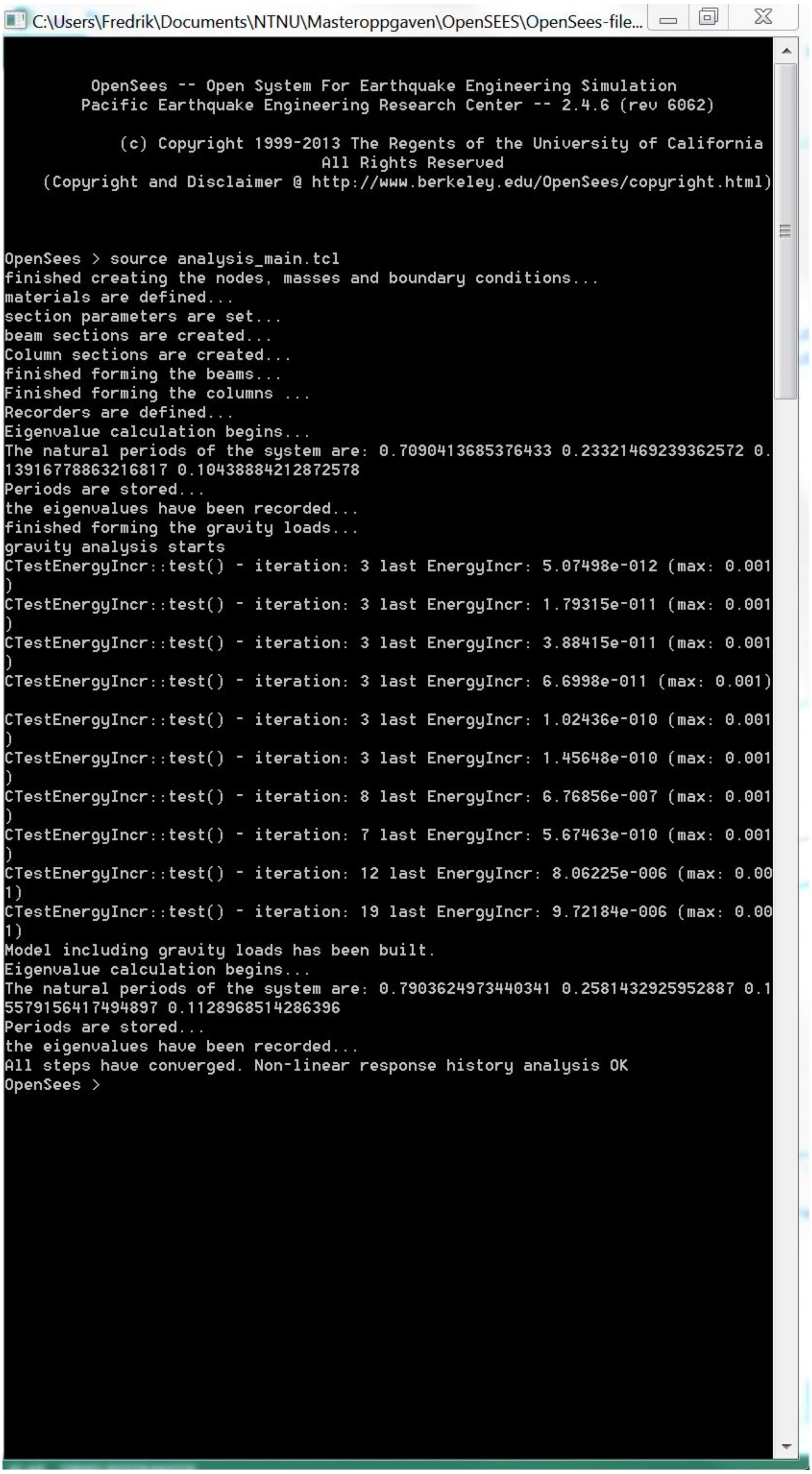
C:\Users\Fredrik\Documents\NTNU\Masteroppgaven\OpenSEES\OpenSees-file...

```


         OpenSees -- Open System For Earthquake Engineering Simulation
        Pacific Earthquake Engineering Research Center -- 2.4.6 (rev 6062)

            (c) Copyright 1999-2013 The Regents of the University of California
                                 All Rights Reserved
    (Copyright and Disclaimer @ http://www.berkeley.edu/OpenSees/copyright.html)



OpenSees > source analysis_main.tcl
finished creating the nodes, masses and boundary conditions...
materials are defined...
section parameters are set...
beam sections are created...
Column sections are created...
finished forming the beams...
Finished forming the columns ...
Recorders are defined...
Eigenvalue calculation begins...
The natural periods of the system are: 0.7090413685376433 0.23321469239362572 0.
13916778863216817 0.10438884212872578
Periods are stored...
the eigenvalues have been recorded...
finished forming the gravity loads...
gravity analysis starts
CTestEnergyIncr::test() - iteration: 3 last EnergyIncr: 5.07498e-012 (max: 0.001
)
CTestEnergyIncr::test() - iteration: 3 last EnergyIncr: 1.79315e-011 (max: 0.001
)
CTestEnergyIncr::test() - iteration: 3 last EnergyIncr: 3.88415e-011 (max: 0.001
)
CTestEnergyIncr::test() - iteration: 3 last EnergyIncr: 6.6998e-011 (max: 0.001)

CTestEnergyIncr::test() - iteration: 3 last EnergyIncr: 1.02436e-010 (max: 0.001
)
CTestEnergyIncr::test() - iteration: 3 last EnergyIncr: 1.45648e-010 (max: 0.001
)
CTestEnergyIncr::test() - iteration: 8 last EnergyIncr: 6.76856e-007 (max: 0.001
)
CTestEnergyIncr::test() - iteration: 7 last EnergyIncr: 5.67463e-010 (max: 0.001
)
CTestEnergyIncr::test() - iteration: 12 last EnergyIncr: 8.06225e-006 (max: 0.00
1)
CTestEnergyIncr::test() - iteration: 19 last EnergyIncr: 9.72184e-006 (max: 0.00
1)
Model including gravity loads has been built.
Eigenvalue calculation begins...
The natural periods of the system are: 0.7903624973440341 0.2581432925952887 0.1
5579156417494897 0.1128968514286396
Periods are stored...
the eigenvalues have been recorded...
All steps have converged. Non-linear response history analysis OK
OpenSees >
```

Figure 2.7: The OpenSees interface

2.3 Material modeling and element formulation

2.3.1 Material modeling

Concrete is a brittle material, and modeling concrete accurately for non-linear analysis requires vast knowledge about the parameters and the properties of concrete. Dynamic and cyclic horizontal loading is causing large deformation which in turn causes the concrete to crack, resulting in a highly non-linear material behavior. One of the most important parts of modeling concrete elements in a structural model, is the confined concrete. The confined concrete is the part of the cross section of the columns and beams that have transverse reinforcement. In a building, all columns and beams will have rectangular hoops or spirals, but in seismic design, an increased number of hoops are placed near the member ends. This is to ensure that shaking from potential earthquakes does not cause collapse of the building or structure, but instead have ductile behavior. Compressed concrete also have confinement in order to prevent buckling of the longitudinal bars, and to avoid shear failure, which is often the reason for collapse of concrete structures. Confined concrete have a much higher compressive strength than the unconfined concrete as seen in Figure 2.8.

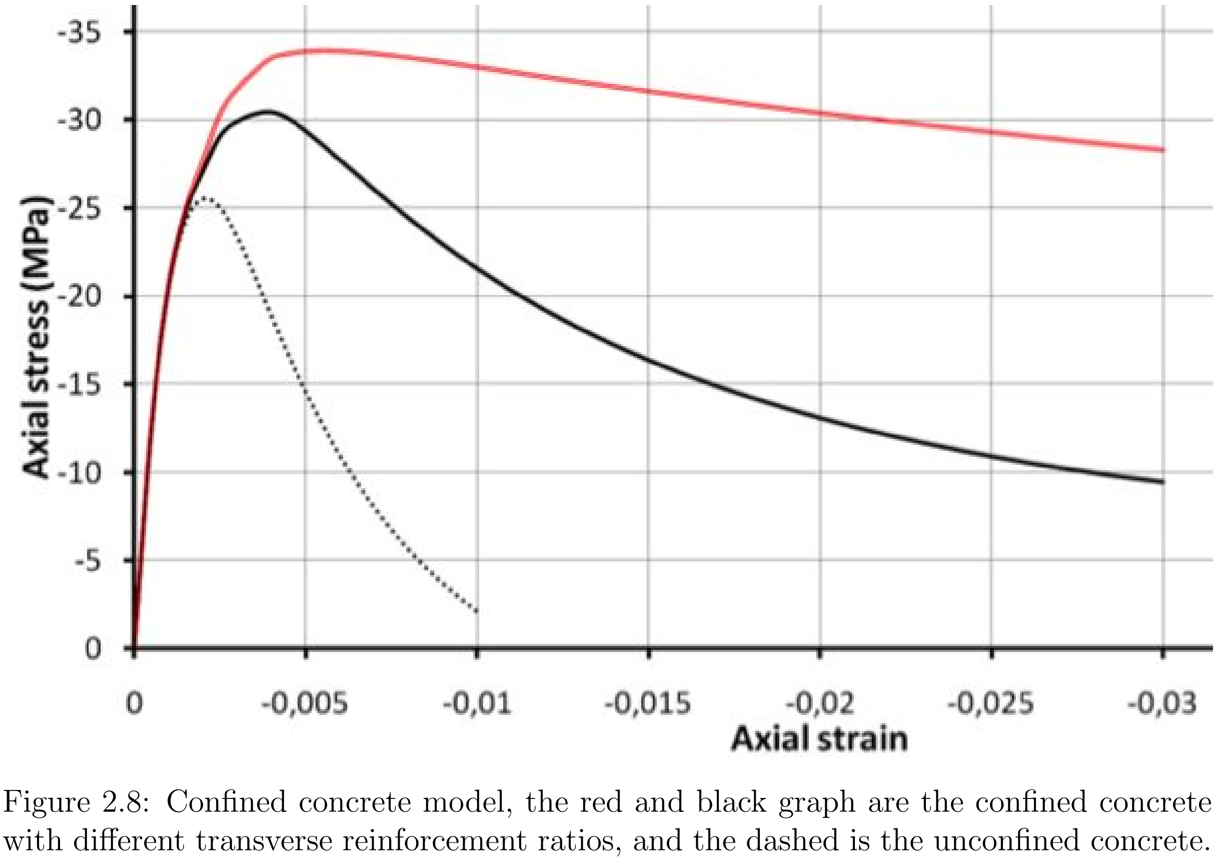

Figure 2.8: Confined concrete model, the red and black graph are the confined concrete with different transverse reinforcement ratios, and the dashed is the unconfined concrete. Illustration from OpenSees Wiki. [20]

In this thesis the confined concrete parameters was calculated according to Mander et al. [1], allowing a significant increase in both strength and stiffness when loading at higher strain rate occurs. The quasi-static compressive strength is magnified by the dynamic magnification factor D_f, which depends on the rate of strain. The dynamic stiffness and dynamic strain at peak stress are also increased by D_E and D_ϵ, respectively.

In Equations (2.4), (2.5) and (2.6) the dynamic strength, stiffness, and strain parameters are shown, respectively. Depending on the transverse reinforcement and its spacing, the parameters can be calculated.

$$(f'_{co})_{dyn} = D_f f'_{co} \tag{2.4}$$

$$(E_c)_{dyn} = D_E E_c \tag{2.5}$$

$$(\epsilon_{co})_{dyn} = D_\epsilon \epsilon_{co}, \tag{2.6}$$

Here, f'_{co}, E_c, and ϵ_{co} is the quasi-static compressive strength, modulus of elasticity, and strain at peak stress, respectively. The material model *Concrete04* is used in OpenSees, which is based on the Material model Mander et. al. presents [1]. In the analyses conducted in this thesis, the beam and column ends have increased shear capasity, thus increased transverse reinforcement according to EN 1998-1 [5], this is described more thoroughly in Chapter 3. The steel model used in the analyses, is a bilinear steel material model with kinematic and isotropic hardening. In OpenSees the model is called *Steel01*. In Figure 2.9 an illustration of the material models in OpenSees is depicted. Seismostruct offers the same concrete material model, a uniaxial nonlinear confinement model (con_ma), which is also based on the model proposed by Mander et al. [1] [19]. The steel model in Seismostruct, (stl_bl) is also a uniaxial bilinear steel model as the one used in OpenSees.

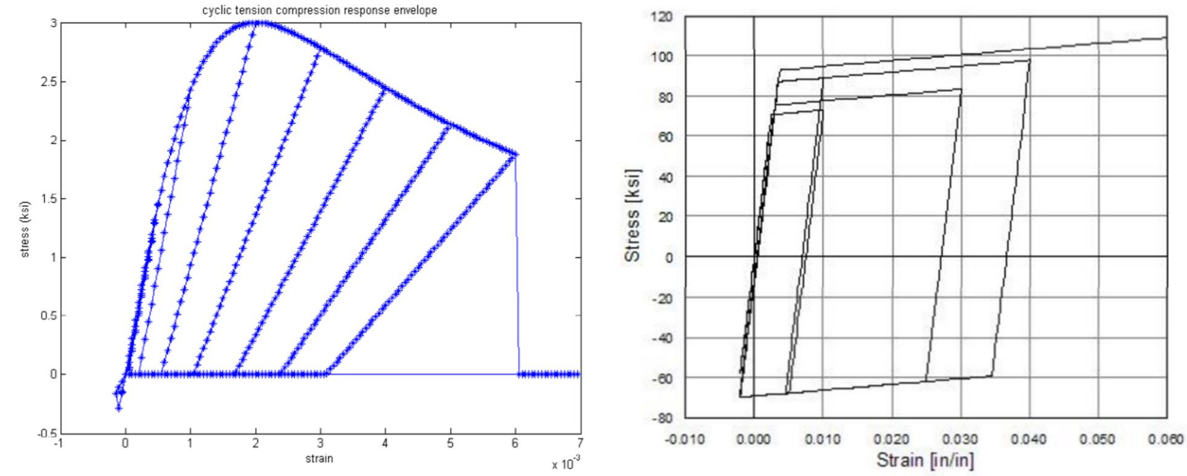

(a) Concrete model in OpenSees, envelope under cyclic tension compression

(b) Steel model in OpenSees, with isotropic hardening in tension

Figure 2.9: Material models, illustrations from OpenSees Wiki [20]

2.3.2 Element formulation

Modeling of material nonlinearities in a Finite element model for structural analysis is usually done by lumped or distributed inelasticity. Dissipating energy introduced by earthquake loads, is best done by inelastic deformation mechanisms, modeled with one of the two mentioned inelastic modeling approaches [7]. The structure is likely to form plastic hinges when responding to strong ground motions and plastic hinge regions must therefore be carefully detailed for ductility to ensure response from larger earthquakes does not cause collaps [1]. The elements are modeled using a distributed inelastic material model, which in the recent years with the increased computational power is favorable to the lumped plasticity model [18]. A distributed inelasticity-model is able to form plastic hinges in regions anywhere along the element length, even though they are likely to form at the ends. This formulation is resulting in a more realistic behavior of the structure. The only drawback with this model compared to a lumped inelastic model, is the computational cost.

Figure 2.10 shows a typical beam-element with sections along its length. The number of integration points is set to at least three for all members, to ensure sufficient accuracy and computational efficiency, it is however increased initially for more critical members, up to six points for the columns in the first floor. The integration rule that is used is the Gauss-Lobatto quadrature rule, which is the most used quadrature rule in generating element matrices. Up to the level of desired accuracy, Gauss-Lobatto quadrature uses fewer integration points than other rules available [10]. The element formulation shown in Figure 2.10 is also called a fiber model, where fibers are modeled at each integration section. At each section, the number of fibers is specified by the user, allowing for accurately modeling the confined, and unconfined concrete, and steel fibers. This allows for higher levels of accuracy in certain areas where inelastic behavior is more likely to occur, by increasing or decreasing the number of fibers.

The elements are formulated using a *force-based* (FB) formulation, rather than the more conventional *displacement-based* (DB) formulation. The DB element is the commonly used formulation, where a displacement field is imposed, and by energy considerations the element forces are found. In a FB formulation, there is an imposed force field, and the element displacement is found using a work equivalence balance [18]. In the DB approach the displacement shape functions are not able to capture the real deformed shape, because the curvature field can be highly non-linear, and with linear variation along the element, it is not able to capture this behavior. The FB formulation is however always exact, since it does not depend on any assumed behavior, as the DB formulation does. The result is an extremely effective formulation since only one element is needed for each structural member, and the approximation can be done by a discrete number of integration sections along the element [18]. Having been made clear that the FB formulation has a clear advantage to the DB formulation, FB elements are used in the analyses

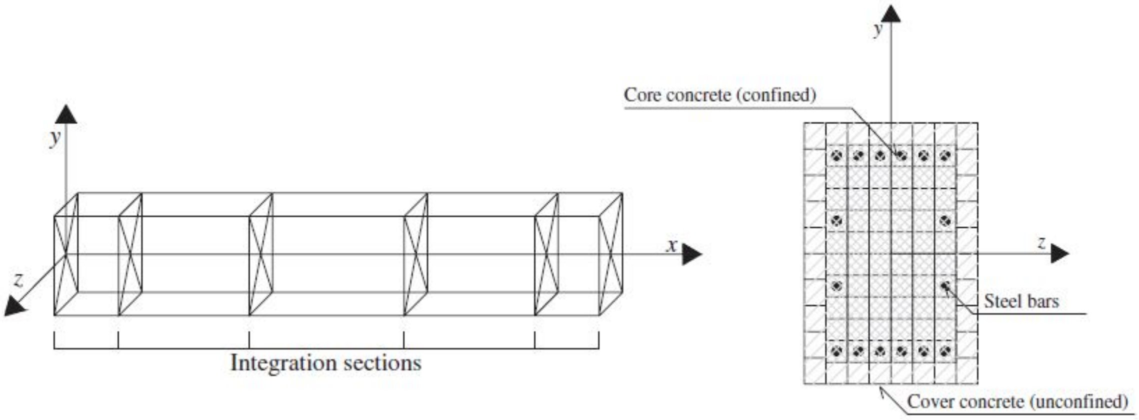

Figure 2.10: Beam element with fiber sections along the element [18]

in this thesis. In OpenSees this element type is called *Force-Based Beam-Column Element*, offering a variety of integration options, distributed plasticity, and plastic hinge integration. As mentioned above, distributed plasticity and Gauss-Lobatto quadrature is used throughout this thesis. In Seismostruct, the *inelastic force-based frame element type* (infrmFB) is used [19].

2.3.3 Physical and numerical localization issues in distributed inelasticity elements

The term *localization issue* is a widely researched area in fracture mechanics [18]. Localization issues are affecting the structural properties of the concrete members due to size effects [14] [18]. Localization is causing strain softening, meaning a descending stress-strain curve. This phenomenon can occur in concrete in both tension and compression. In the case of compression damage zones occurs and in tension, cracks can cause localization issues. Most concrete structures including the one in this thesis, are reinforced with steel, and thus the steel bars are responsible for the tensile forces. Localization in tensile is therefore not an issue here. In Figure 2.11 two conceptual response curves are shown for localization issues in compression. The plots are showing that localization is size dependent in both uniaxial and flexural compression. When strains are concentrated on a limited region of the member, collapse occurs due to the local mechanism, hence the term *localization*.

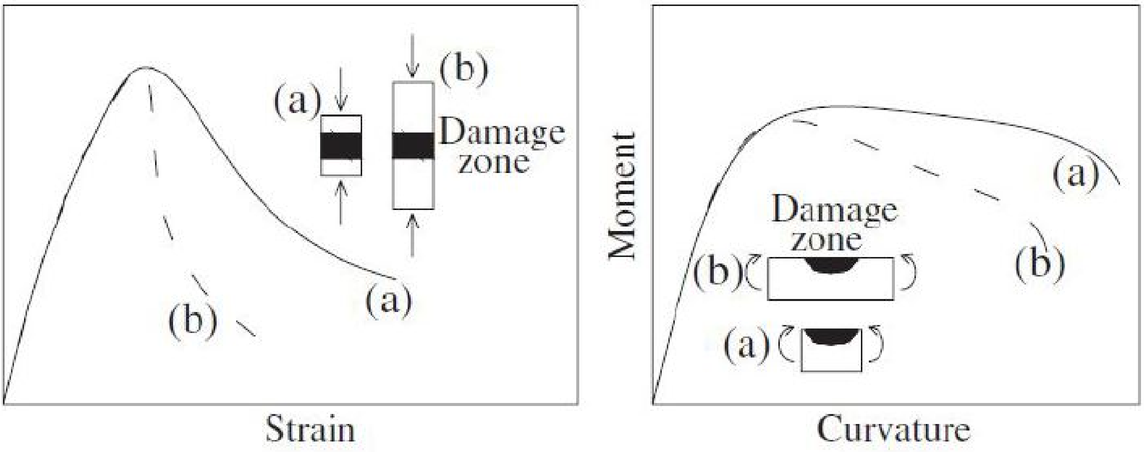

Figure 2.11: Illustration showing physical localization issues in uniaxial and flexural compression [18]

In computational mechanics, numerical localization can be accounted for, by altering the stress-strain relationship [14]. The same behavior is exhibited as in fracture mechanics; a softening behavior or non-objective response, however this is causing numerical problems for both DB and FB elements. Concentration of inelasticity is highly dependent on the number of elements or mesh refinement in DB elements and the number of integration points or sections in the FB formulation [18]. Figure 2.12 clearly shows this, and how a hardening behavior or objective response is causing the opposite, namely converging to a stable solution. The numerical localization issue is only due to finite element assumption, and as opposed to physical localization, it is only a numerical issue, and will not happen in reality. In the FB formulation, which is only modeled with one element per structural member, will in the non-objective response experience an increase of local strains at the base integration point for the cantilever, illustrated in Figure 2.12, with an increase of integration points along the element. The same goes for the sample building in this thesis, which is subjected to high axial loading and strong horizontal forces, due to earthquake motion. In DB elements, the main reason for numerical localization is that the elements are not able to maintain force equilibrium. When the applied lateral displacement increases, the elements near the base starts softening, and loosing their capacity. To ensure force equilibrium, the other elements that are not loosing their capacity, must unload elastically. In the DB formulation the numerical issues arises in the assembling of the stiffness matrix, when these elements does not do that, and instead continue to take bending moment, whilst the base elements are unloading [14]. For the FB formulation there is not an issue with force equilibrium regarding localization, however, other problems arise. As the number of integration points increases and smaller plastic hinge regions, the result is growing strains. With the growing strains, material stiffness will lower, thus material degradation occur. This is will effect the load carrying capacity, and result in a non-objective response.

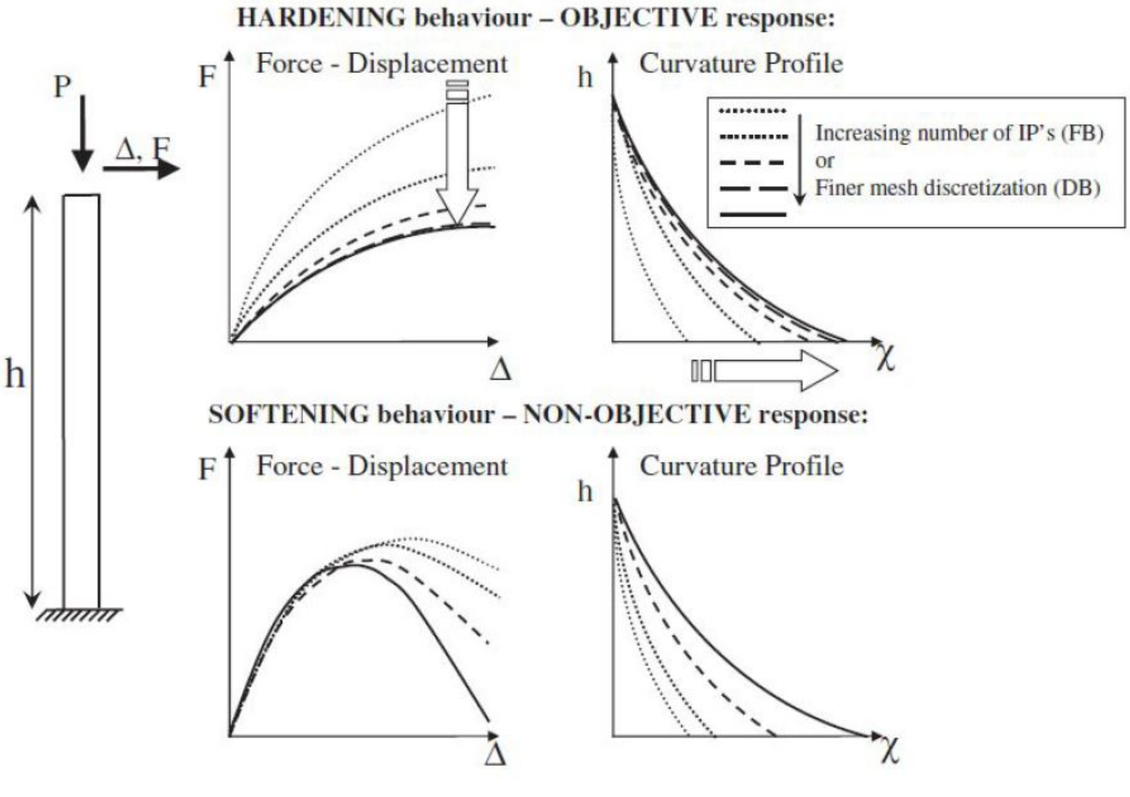
HARDENING behaviour – OBJECTIVE response:
P
Δ, F
h
F
Force - Displacement
Δ
h
Curvature Profile
χ
Increasing number of IP's (FB)
or
Finer mesh discretization (DB)
SOFTENING behaviour – NON-OBJECTIVE response:
F
Force - Displacement
Δ
h
Curvature Profile
χ

Figure 2.12: Illustration of hardening and softening behavior of a cantilever column [18]

2.3.4 Damping and Period elongation

Damping is a phenomenon that dissipates energy, thus causing the amplitude of the free vibration to decay [10]. If buildings did not have any damping, they would vibrate forever, and subsequently be inhabitable. Luckily all structures naturally have damping, but modeling damping is a research field where arguments and results are widely discussed. There are different types of physical damping that influences structural dynamics, such as Hysteresis, Coloumb, Radiation, and Viscous damping. The latter is used in this thesis, and the reader is refereed to the literature for further insight on the other types [10]. Viscous damping exerts force proportional to the velocity term $\dot{\mathbf{D}}$ in the equation of motion in Equation (2.1). Proportional damping or *Rayleigh damping* is a common device for modelling viscous damping, and is defined by the global damping matrix $\mathbf{C}$. Propotional damping can be mass proportional, stiffness proportional, or a combination of the two. By having mass proportional damping, the damping of the lower modes are ensured, while the contribution from the stiffness proportional damping, take care of the higher modes, thus a combination of the two is adequate in earthquake engineering. Rayleigh damping is a linear combination of the global mass and stiffness matrices, shown in Equation (2.7), and is used in this thesis.

$$\mathbf{C} = a_0\mathbf{M} + a_1\mathbf{K}, \tag{2.7}$$

The damping ratio, ξ_n for the *n-th* mode of the structural system is defined in Equation (2.8). Here ω_n is the frequency of the *n-th* mode, where the coefficients a_0 and a_1 are determined by the expressions in Equation (2.9), assuming that the *i-th* and *j-th* modes have the same damping ratios. In Figure 2.13 the frequency dependent damping ratio scheme is depicted.

$$\xi_n = \frac{a_0}{2\omega_n} + \frac{a_1}{2}\omega_n \tag{2.8}$$

where

$$a_0 = \xi\frac{2\omega_i\omega_j}{\omega_i + \omega_j} \quad ; \quad a_1 = \xi\frac{2}{\omega_i + \omega_j} \tag{2.9}$$

There are a number of different approaches for calculating the coefficients that could give satisfying results. According to Erduran [16], Rayleigh damping anchored at the reduced first mode frequency, and $T_3 = 0.2s$ thus $\omega_j = \frac{2\pi}{T_3}$ can be regarded as a good option. This model limits the contributions of damping forces to the response, preventing overestimation of acceleration, and makes sure that higher order modes are not suppressed. The reader is referred to the literature [10], [16] for further insight on Rayleigh damping, and the different models. With the direct integration scheme discussed earlier in this chapter, it is also possible to introduce algorithmic damping or numerical dissipation. This is introduced solely by the HHT-algorithm, and is built into the program.

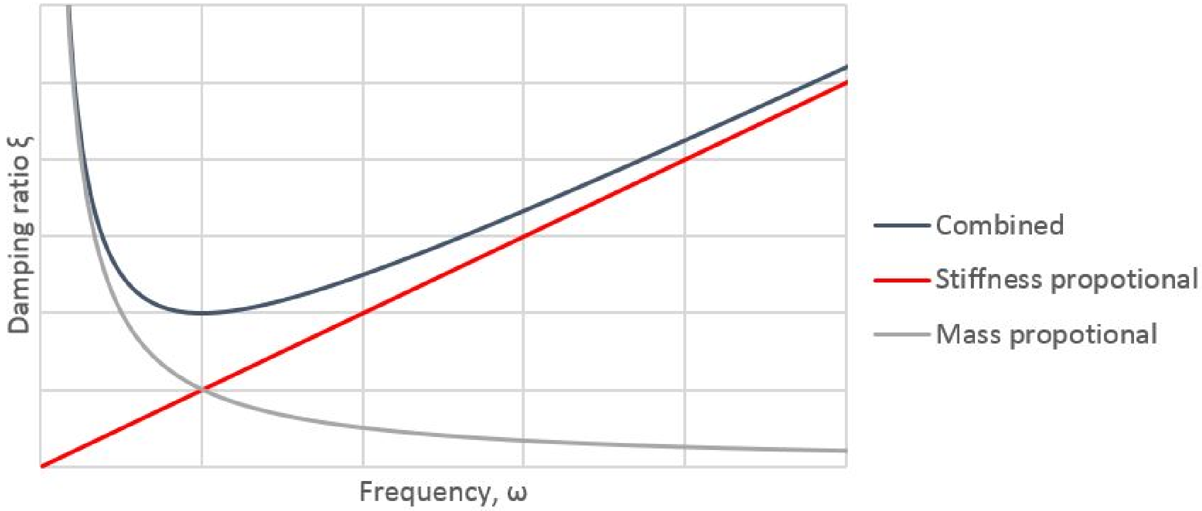

Figure 2.13: Plot showing how the damping ratio depend on the frequency, and why a combination of both stiffness and mass proportional damping is favorable

Period elongation occurs when the structure suffers from stiffness degradation. In earthquake engineering this can happen over the course of the ground motion, resulting in a change of the period during the time-history. The natural period of the undamped, free vibration system is defined in Equation (2.10) [10].

$$T = 2\pi\sqrt{\frac{\mathbf{M}}{\mathbf{K}}}, \tag{2.10}$$

Clearly a significant decrease of the global stiffness will result in a higher natural period, called period elongation. In Figure 2.14 the force-displacement curve for a column in the first and fourth floor of a building is shown. Since the stiffness is the tangent in the force-displacement curve, the stiffness is drastically reduced at $T = 20s$ in the first floor column, resulting in reduced global stiffness, thus a higher period.

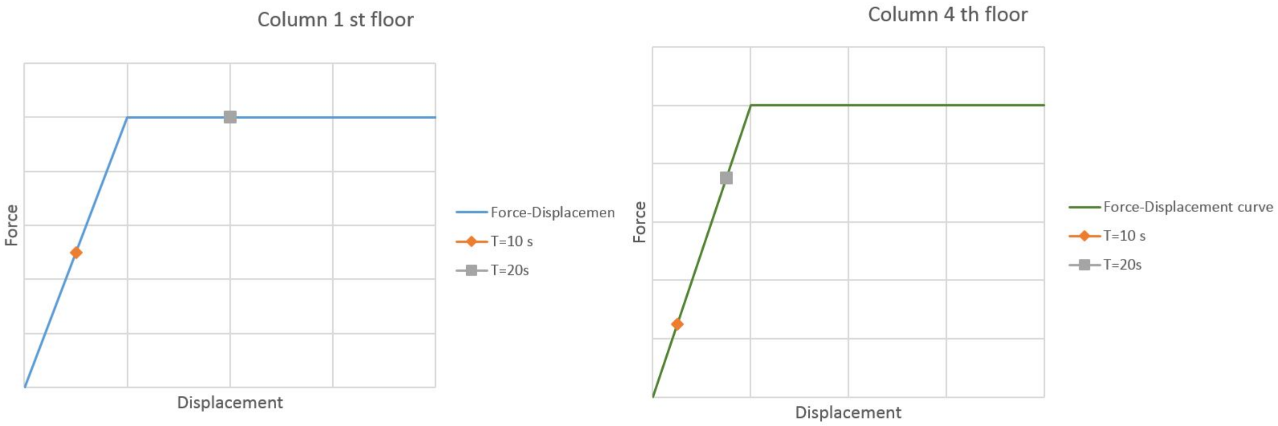

(a) Force-displacement curve 1st floor

(b) Force-displacement curve 4th floor

Figure 2.14: Force-displacement curves illustrating stiffness reduction during an earthquake record

Chapter 3

Design of the building

This chapter is a summary of the design of the building that is to be analyzed in this thesis, and calculations relevant to the seismic design are shown here. The building is designed and analyzed according to EN 1998-1 for medium ductility by the author's co-supervisor Nina Øystad-Larsen. It is expected that the reader is familiar with analysis, design, and response of structure for gravity loads. Thus these calculations are not included in this section nor later on.

3.1 Description

The structure is located in Southern Europe, in a high seismity region. It is a four-storey reinforced concrete frame building for residential purposes. Øystad-Larsen conducted a lateral force method analysis in the Finite Element program Robot Structural Analysis. In Figure 3.1 and 3.2 the structure is depicted. It is only subjected to gravity loads, and the seismic loading described in the next section, according to EN 1990 [4]. The live load for residential buildings are 2 kN/m^2 and the dead load is the weight of the concrete members, which is 25 kN/m^3 and 0,5kN/m^2 due to light walls, ceilings etc. The loads are combined according to EN 1990/EN 1998-1 [4, 5], and beams, and columns are designed according to EN 1992-1-1 [6] and EN 1998-1 DCM demands. The concrete and reinforcement quality is C30/37 and B500NC, respectively. It is worth mentioning that the materials are determined according to the Norwegian NS-EN 1992-1-1+NA:2008 in order to save time.

3.2 Seismic loading and design

When analysing a structure due to seismic loading the structure must first be designed for the before mentioned gravitational forces. An eigenvalue analysis is performed to determine the natural periods and modes. In Figure 3.3, the fundamental mode shape is depicted.

The building at hand was designed using the spatial Lateral force method, which is described in EN 1998 clause 4.3.3.2. This method requires that the analyst creates a response spectrum for the site of the building. The peak ground acceleration (PGA) was set to $0.35g$, approximately $3.5m/s^2$, which is representative for the region the building is located, according to the 2013 European Seismic Hazard model [15].

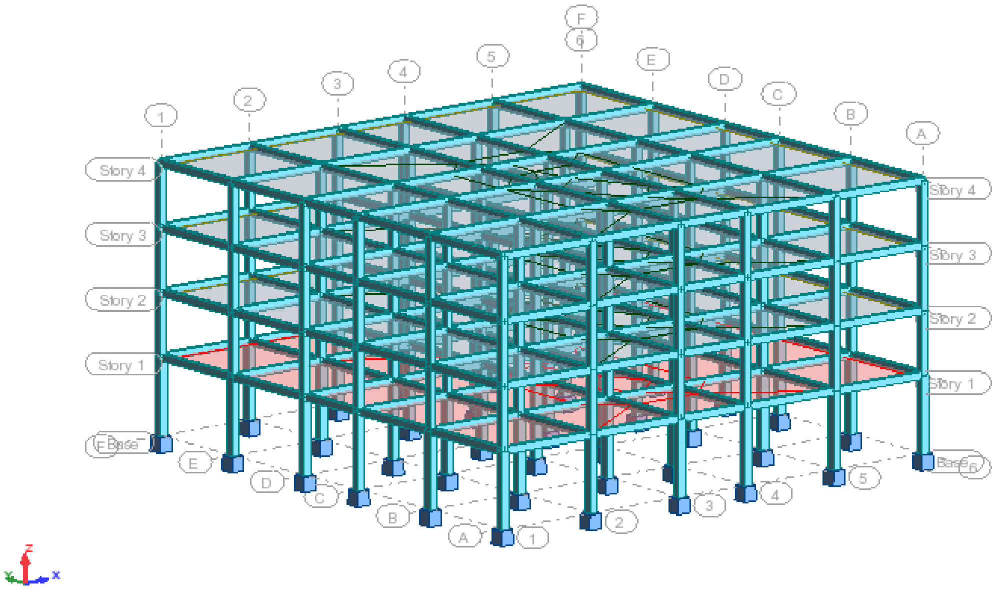

Figure 3.1: The building in Robot Structural Analysis

Table 3.2 in EN 1998-1 gives the recommended soil factor and control periods for different ground types, that are to be used to create the elastic response spectra. In this case the Type 1 spectrum is used, since the site is in a high seismity region. The elastic response spectra were created, using the expressions in EN 1998-1-1 clause 3.2.2.2. This acceleration response spectrum is however not the one being used in the determination of the seismic action, the design response spectra need to be determined. This is done by establishing the behavior factor, q, according to EN 1998-1-1 clause 5.2.2.2.

$$q = q_0 k_w \geq 1.5 \tag{3.1}$$

As stated previously the frame is to be designed for medium ductility (DCM). EN 1998-1-1 clause 5.2.2.2(2) states that $q_0 = 3.0\alpha_u/\alpha_1$, where $\alpha_u/\alpha_1 = 1.3$ according to EN 1998-1 clause 5.2.2.2(5a). The factor k_w in equation 3.1 is determined by EN 1998-1-1 clause 5.2.2.2(11)P, as 1.00 for frames. This results in a behavior factor $q = 3.9$. The design and elastic response spectra are shown in Figure 3.4.

Now the loading can be determined, and the procedure is described in EN 1998-1 4.3.3.2. The base shear force, F_b is obtained, according to the expression in EN 1998-1 4.3.3.2.2 shown in Equation (3.2).

$$F_b = S_d(T_1) \cdot m \cdot \lambda \tag{3.2}$$

Here $S_d(T_1)$ is the ordinate of the design response spectrum at the first natural period, T_1, m is the total mass of the building an λ is a correction factor that is 1.0 for this building according to EN 1998-1 clause 4.3.3.2.2(1)P. With a total mass of 1623 *tons* and $S_d(1.54) = 1.01 m/s^2$ the resulting base shear is $F_b = 1639kN$. The base shear is distributed over the storeys of the building according to EN 1998-1 4.3.3.2.3. F_i is the seismic shear in the i-th floor, calculated from Equation (3.3) and the resulting forces are shown in Table 3.1.

$$F_i = F_b \cdot \frac{z_i \cdot m_1}{\sum z_j \cdot m_j} \tag{3.3}$$

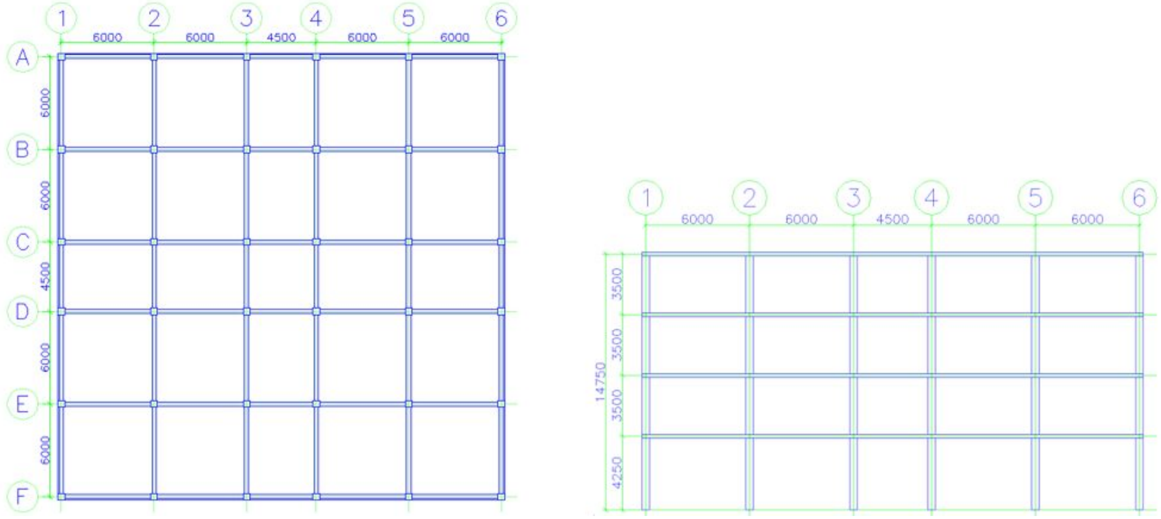

Figure 3.2: Plan and vertical projection of the building

Table 3.1: Storey shear

Storey	$z_i(m)$	$m_i(tons)$	$F_i(kN)$
1	4.250	428	198
2	7.750	419	353
3	11.250	413	506
Roof	14.750	363	582
			$\sum F_i = F_b = 1639kN$

The forces are applied to the FEM-model, and since the spatial lateral force method is used, the loads are applied in one main direction combined with 30% of the load in the other, and vice versa [5].Accidental torsional effects are accounted for as specified in EN 1998-1 clause 4.3.2, by applying the load with an eccentricity $e_{ai} = \pm 0.05 \cdot L_i$, where e_{ai} is the accidental eccentricity of storey mass i from its nominal location and L_i is the length of the floor, perpendicular to the acting seismic force in the storey.

3.2.1 P-delta effects

In clause 4.4.2.2(2) in EN 1998-1 it is demanded that second-order effects also known as $P-\delta$ effects are accounted for to ensure resistance in structural elements. $P-\delta$ effects are to be accounted for if the condition in Equation (3.4) is not fulfilled for any of the storeys in the building of interest.

$$\theta = \frac{P_{tot} \cdot d_r}{V_{tot} \cdot h} \leq 0.10 \tag{3.4}$$

Here, θ in Equation (3.4) is the interstorey drift sensitivity coefficient, P_{tot} is the total gravity load at and above the storey in question, d_r is the average lateral displacement between the stories, V_{tot} is the total seismic shear in the storey, and h is the height of the storey. Preferably θ should be less than 0.10, then the second-order effects can be neglected. However as seen from Table 3.2 this is not the case for most of the floors in this building. If θ is less then 0.2, the $P-\delta$ effects can be approximately taken accounted for,

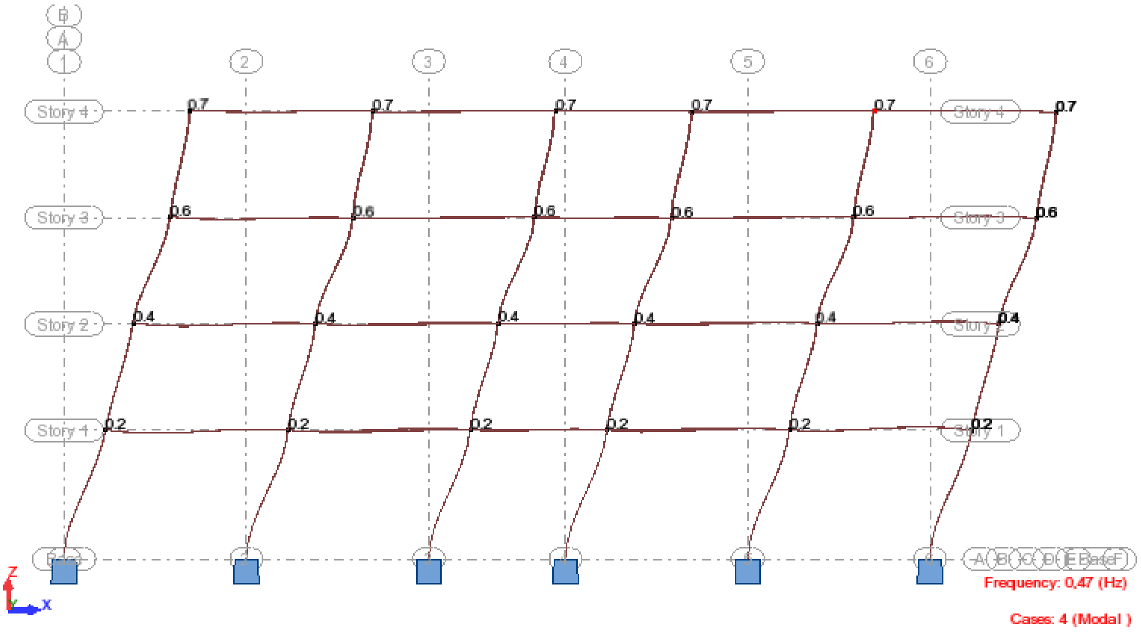

Figure 3.3: Fundamental mode shape. Illustration from Robot Structural Analysis

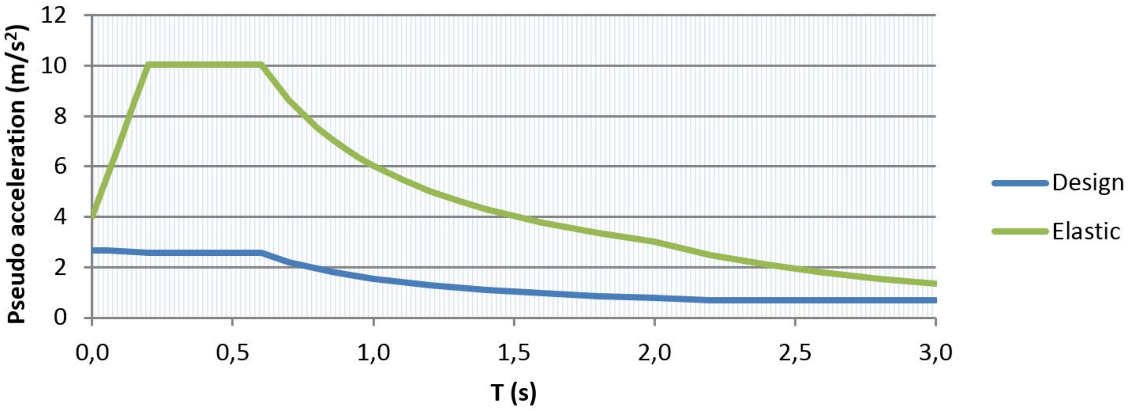

Figure 3.4: Type 1 elastic and design response spectra.

as described in EN 1998-1 clause 4.4.2.2(3). The solution here is to increase the stiffness of the structure such that θ is reduced. Increasing the column sizes in the first floor is an effective way to do this. Thus these columns are increased from 320 × 320 mm to 350 × 350 mm cross sections.

The increased stiffness results in a higher total mass, new natural periods and change in design spectral acceleration, thus the base shear is also increased. The updated first natural period is $T_1 = 1.45s$, the total mass is now 1634 $tons$, Spectral acceleration, $S_d(1.45) = 1.04m/s^s$. The resulting base shear is $F_b = 1749kN$. Then updated values for θ are calculated, and as seen from Table 3.3, θ is now lower than 0.2 for all storeys. $P - \delta$ effects can be included in the analysis, using the approximated method mentioned above. The second order effects are accounted for by multiplying the seismic force in each storey by the factor $\frac{1}{1-\theta}$.

Table 3.2: $P-\delta$ effects

Storey	$P_{tot}(kN)$	$d_r(mm)$	$V_{tot}(kN)$	θ
1	16068	106	1711	0.23
2	11821	70	1505	0.16
3	7662	95	1136	0.18
Roof	3559	51	608	0.09

Table 3.3: Updated $P-\delta$ effects due to increased stiffness

Storey	$P_{tot}(kN)$	$d_r(mm)$	$V_{tot}(kN)$	θ
1	16179	84	1826	0.176
2	11821	74	1600	0.156
3	7662	100	1208	0.182
Roof	3559	54	646	0.086

3.2.2 Damage limitation

According to EN 1998-1 clause 4.4.3.2 the the design interstorey drift should be limited. The requirement in Equation (3.5) must be met:

$$d_r\nu \leq 0,010h \tag{3.5}$$

Here d_r is the design interstorey drift, h is the storey height and ν is reduction factor which is 0.5 for importance class II. In Table 3.4 the interstorey drift is shown, including the $P-\delta$ effects. Clearly the requirement in Equation (3.5) is not met, and again the stiffness must be increased. Thus the cross sections of the columns are increased to 350 × 350 mm in the 2^{nd} and 3^{rd} storeys and to 400 × 400 mm in the 1^{st} storey. The increased stiffness is again resulting in added mass, new natural periods, spectral acceleration and base shear. This means that now must also new sensitivity factors for accounting $P-\delta$ effects be recalculated. The updated first natural period, $T_1 = 1.19s$, the total mass is now 1658 $tons$, Spectral acceleration, $S_d(1.19) = 1.30\ m/s^2$. The base shear is $F_b = 1832kN$. In Table 3.5 the updated $P-\delta$ effects are recalculated after the increase in columns due to damage limitations. With accounting for the updated values in Table 3.5, the final storey drifts are shown in Table 3.6 which obviously satisfy the criterion in Equation (3.5).

Table 3.4: Drift limitations

Storey	$d_r(mm)$	$h(mm)$	$\frac{d_r\nu}{h}$
1	103	4250	0.012
2	90	3500	0.013
3	123	3500	0.018
Roof	67	3500	0.012

Table 3.5: Updated $P - \delta$ effects due damage limitations

Storey	$P_{tot}(kN)$	$d_r(mm)$	$V_{tot}(kN)$	θ
1	16415	59	1913	0.118
2	12025	62	1678	0.126
3	7749	46	1261	0.081
Roof	3559	56	668	0.085

Table 3.6: Drift limitations after increased stiffness

Storey	$d_r(mm)$	$h(mm)$	$\frac{d_r \nu}{h}$
1	67	4250	0.008
2	71	3500	0.010
3	53	3500	0.008
Roof	64	3500	0.009

3.2.3 Ductility

An important part of designing a structure for earthquake action, is to ensure ductile behavior. When plastic deformation occurs it is expected that plastic hinges form at beam ends. EN 1998-1 clause 5.4.3.1.2 requires that these critical areas are detailed carefully. The length of the critical area, l_{cr}, from the beam-column-joint shall be set to the height of the beam in question. Within the critical area over-capacity on shear is demanded. To ensure local ductility at beam ends, the curvature ductility factor must be assessed. According to EN 1998-1 clause 5.2.3.4(3) the curvature ductility factor μ_ϕ of the potential plastic regions, defined as the ratio of the post-ultimate strength curvature at 85% of the moment resistance, to the curvature at yield, provided that the limiting strains of concrete and streel ϵ_{cu} and $\epsilon_{su,k}$ are not exceeded, is at least equal to the values in Equation (3.6) and (3.7).

$$\mu_\phi = 2q_0 - 1 \qquad if \qquad T_1 \geq T_C \tag{3.6}$$

$$\mu_\phi = 1 + 2(q_0 - 1)\frac{T_C}{T_1} \qquad if \qquad T_1 < T_C \tag{3.7}$$

Here $q_0 = 3.9$, still is the corresponding basic value of the behaviour factor and T_1 is the fundamental period of the building. With $T_1 = 1.19s$, and $T_C = 0.6s$ Equation (3.6) is determining $\mu_\phi = 2 \cdot 3.9 - 1 = 6.8$. Detailing for local ductility must the be done for all beam-ends, demanding that at least half the reinforcement in the tension zone is placed in the compression zone and the reinforcement ratio in the tension zone, ρ does not exceed ρ_{max} according to EN 1998-1 clause 5.4.3.1.2. This procedure requires some iterations both regarding reinforcement and size of cross-sections. After all beams have been checked and adjusted, the stiffness of the structure is changed and new natural periods must be found. The updated fundamental period $T_1 = 1,6s$, the spectral acceleration $S_d = 1.33m/s^2$ and the base shear, $F_b = 1875$ kN. Due to the increased stiffness of the structure, $P - \delta$-effects are reduced as seen from Table 3.7.

Table 3.7: Updated $P-$ effects due to ductility demands

Storey	$P_{tot}(kN)$	$d_r(mm)$	$V_{tot}(kN)$	θ
1	16415	57	1957	0.113
2	12025	58	1717	0.116
3	7749	44	1290	0.075
4	3559	56	684	0.083

3.2.4 Columns

The ductility of the columns must also be assessed. EN 1998-1 clause 5.4.3.2.1 requires that the maximum axial force, in Equation (3.8) is satisfied.

$$\nu_d = \frac{N_{Ed}}{A_c f_{cd}} \leq 0.65 \tag{3.8}$$

The axial forces are checked in each storey of the building, and as seen from Table 3.8 none of the columns does not meet the criteria in Equation (3.8).

Table 3.8: Axial force level columns

Storey	$min\ \ N_{Ed}(kN)$	$max\ \ N_{Ed}(kN)$	$Column(mm)$	$\nu_{d,max}$
1	-148	-984	400×400	0.37
2	-123	-714	350×350	0.35
3	-86	-462	350×350	0.23
Roof	-44	-214	260×260	0.19

According to EN 1998-1 clause 5.6.2, anchorage of reinforcement must be checked. For interior beam-column joints Equation (3.9) must be satisfied and for exterior beam-column joints Equation (3.10) must be satisfied, as described in EN 1998-1 clause 5.6.2.2(2)P.

$$\frac{d_{bL}}{h_c} \leq \frac{7.5 \cdot f_{ctm}}{\gamma_{Rd} \cdot f_{yd}} \cdot \frac{1 + 0.8 \cdot \nu_d}{1 + 0.75 k_D \cdot \rho' / \rho_{max}} \tag{3.9}$$

$$\frac{d_{bL}}{h_c} \leq \frac{7.5 \cdot f_{ctm}}{\gamma_{Rd} \cdot f_{yd}} \cdot (1 + 0.8 \cdot \nu_d) \tag{3.10}$$

where,

h_c	is the width of the column parallel to the bars
f_{ctm}	is the mean value of the tensile strength of concrete
f_{yd}	is the design value of the yield strength of steel
ν_d	is the normalised design axial force in the column, taken with its minimum value for the seismic design situation
k_D	is the factor reflecting the ductility class, equal to 2/3 for DCM
ρ'	is the compression steel ratio of the beam bars passing through the joint
ρ_{max}	is the maximum allowed tension steel ratio
γ_{Rd}	is the model uncertainty factor on the design value of resistances, taken as being 1,0 for DCM.

Fulfilling this for all beam-column joints require that the columns are adjusted again and the resulting column dimensions are listed in Table 3.9, used in the analysis. The principle of strong column - weak beam is strongly pursued in seismic design, since forming of plastic hinges in the columns rather than in beams is more likely to cause collapse. Making sure that the sum of the moment capacity of the columns in a joint, is 30% above the adjacent beam capacity, the criteria in EN 1998-1 clause 4.4.2.3(4) is met. In Equation (3.11) the condition is shown:

Table 3.9: Final Column dimensions

$Storey$	$InteriorColumns$	$BorderColumn$	$CornerColumns$
1	400×400	400×400	300×300
2	400×400	350×350	300×300
3	400×400	350×350	300×300
Roof	400×400	350×350	300×300

$$\sum M_{Rc} \geq 1.3 \cdot \sum M_{Rb} \tag{3.11}$$

Here, M_{Rc} is the sum of the design moment resistance in the columns in the joint and M_{Rb} is the sum of the design moment resistance in the beams. All joints in the structure are then checked, and to meet the requirement in Equation (3.11) the reinforcement is adjusted, such that all columns have sufficient moment capacity. EN 1998-1 clause 5.4.2.3 specifies the demanded shear capacity of the columns. Acording to EN 1998-1, in primary seismic columns the design values of shear forces shall be determined with the capacity design rule, which uses the end moments of the column for obtaining equilibrium. The end moments that forms plastic hinges are then used, and since equation 3.11 is satisfied, the plastic hinges will then form in the beam of the beam-column joint. The end moments that are to be used for determining the shear demand is specified in EN 1998-1 clause 5.4.2.3(2), shown in Equation (3.12) below:

$$M_{i,d} = \gamma_{Rd} M_{Rc,i} \cdot min(1, \frac{\sum M_{Rb}}{\sum M_{Rc}}) \tag{3.12}$$

where,

$M_{i,d}$	is the column end moments in end $i = 1, 2$
γ_{Rd}	is the factor accounting for overstrength due to steel strain hardening and confinement of the concrete, which is 1,1 in DCM
$M_{Rc,i}$	is the design value of the column moment of resistance at end i.
$\sum M_{Rb}$	is the sum of the design moment resistance in the beams in the joint
$\sum M_{Rc}$	is the sum of the design moment resistance in the columns in the joint

Based on the moments the shear demand is calculated in each storey, and the shear capacity of the columns is calculated. The necessary shear resistance is calculated according to EN 1992-1-1 6.2.3 and EN 1998-1 5.4.3.2.1. The stirrup spacing is adjusted such that the shear demand is met. The stiffness in the design of the building is however halved, due to cracking. Evidently designing a code compliant building for seismic loading is somewhat of an iteration procedure, where dimensions and materials must be adjusted throughout the process. The total mass of the is *1690 tons*, and the first fundamental period $T_1 = 1.09$ s. The resulting seismic base shear is 2040 kN and including the geometric imperfections it is 2084 kN. The final reinforcement in the columns is shown in Figure 3.5 and the reinforcement of the beams and its dimensions are depicted in Figure 3.6.

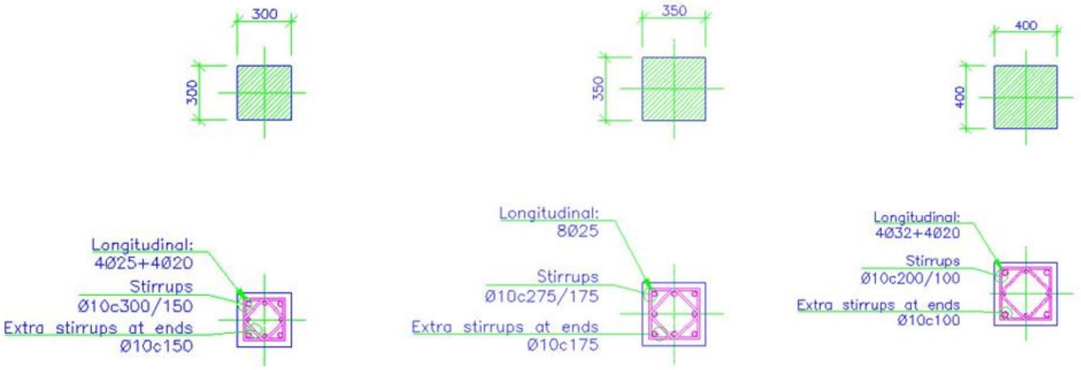
300
300
350
350
400
400
Longitudinal:
4Ø25+4Ø20
Stirrups
Ø10c300/150
Extra stirrups at ends
Ø10c150
Longitudinal:
8Ø25
Stirrups
Ø10c275/175
Extra stirrups at ends
Ø10c175
Longitudinal:
4Ø32+4Ø20
Stirrups
Ø10c200/100
Extra stirrups at ends
Ø10c100

Figure 3.5: Reinforcement of the columns

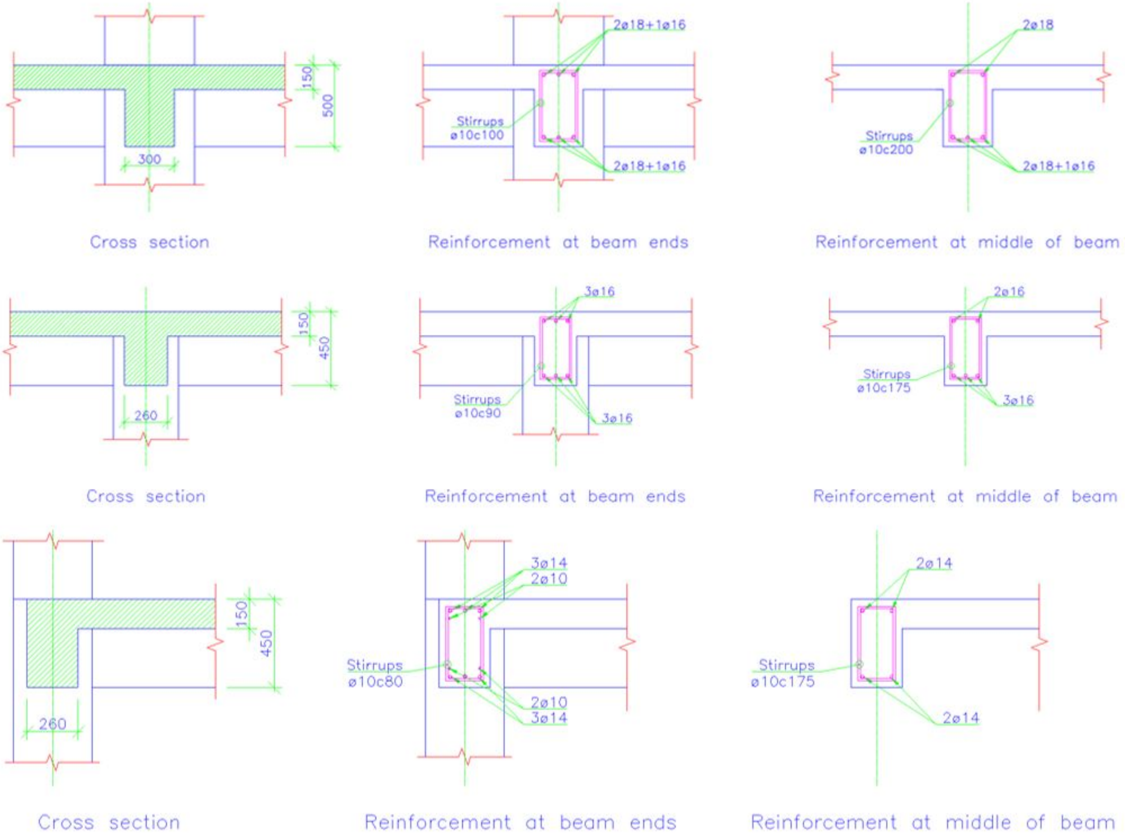
150
500
300
Cross section
2ø18+1ø16
Stirrups
ø10c100
2ø18+1ø16
Reinforcement at beam ends
2ø18
Stirrups
ø10c200
2ø18+1ø16
Reinforcement at middle of beam
150
450
260
Cross section
3ø16
Stirrups
ø10c90
3ø16
Reinforcement at beam ends
2ø16
Stirrups
ø10c175
3ø16
Reinforcement at middle of beam
150
450
260
Cross section
3ø14
2ø10
Stirrups
ø10c80
2ø10
3ø14
Reinforcement at beam ends
2ø14
Stirrups
ø10c175
2ø14
Reinforcement at middle of beam

Figure 3.6: Reinforcement of the beams

Chapter 4

Non-linear static analysis

4.1 Results and discussion

In this section the results from the non-linear static analysis or *Static Pushover* analysis are presented. As mentioned earlier, the analysis of the reinforced concrete frame is conducted using both *OpenSees* and *Seismostruct*, such that the results could be verified. The SPO-analysis is conducted on the frame section in axis B only, thus the structure is now in 2D in order to save time. The total seismic base shear found in the design of the building including geometric imperfections was 2084 kN. However, this is for the whole (3D) model. According to FEMA P695 [2] and as described in the Literature review, the loading is applied until a loss of 20% of maximum base shear is achieved. The displacement or roof drift ratio is obtained from the top node in the middle of the building in Seismostruct and OpenSees. From the analysis conducted in OpenSees, the maximum base shear was found to be 875 kN, that is for axis B alone. Expecting that at least the other internal frames in the building would withstand the same base shear and the end frames half of that, the SPO-analysis gives a total 4375 kN, which is more than double the total seismic base shear found in the design phase. The calculation of the over-strength factor is shown below. Note that the base shear obtained in OpenSees is used.

$$\Omega = \frac{4375kN}{2084kN} = 2.10$$

It is expected that the non-linear analysis would give a higher capacity than the linear analysis. The non-linear static analysis is utilizing the materials to its fullest. In Figure 4.1 the pushover curves are depicted. It is evident from Figure 4.1 that the OpenSees analysis is able to converge for much higher deformations than the Seismostruct analysis. However both of the curves are showing good ductile behavior. The maximum base shear is however close in the two analyses, where the maximum base shear for the analysis in Seismostruct is 885 kN. The OpenSees curve is plotted as recommended by FEMA P695, at 80% of maximum base shear, which is approximately 700 kN, the Seismostruct analysis is not able to converge until a 20% loss of maximum base shear, as seen in Figure 4.1. The first part of the curves, which is the linear elastic part of the response, is also correlating well, which is a good model verification. Since all the columns are the same in the different floors it is fairly obvious that it is the first floor that is contributing the most to the roof drift ratio since the seismic shear is largest in the first floor. Figure 4.2 shows the interstorey drift ratio for each floor at maximum base shear, and Figure

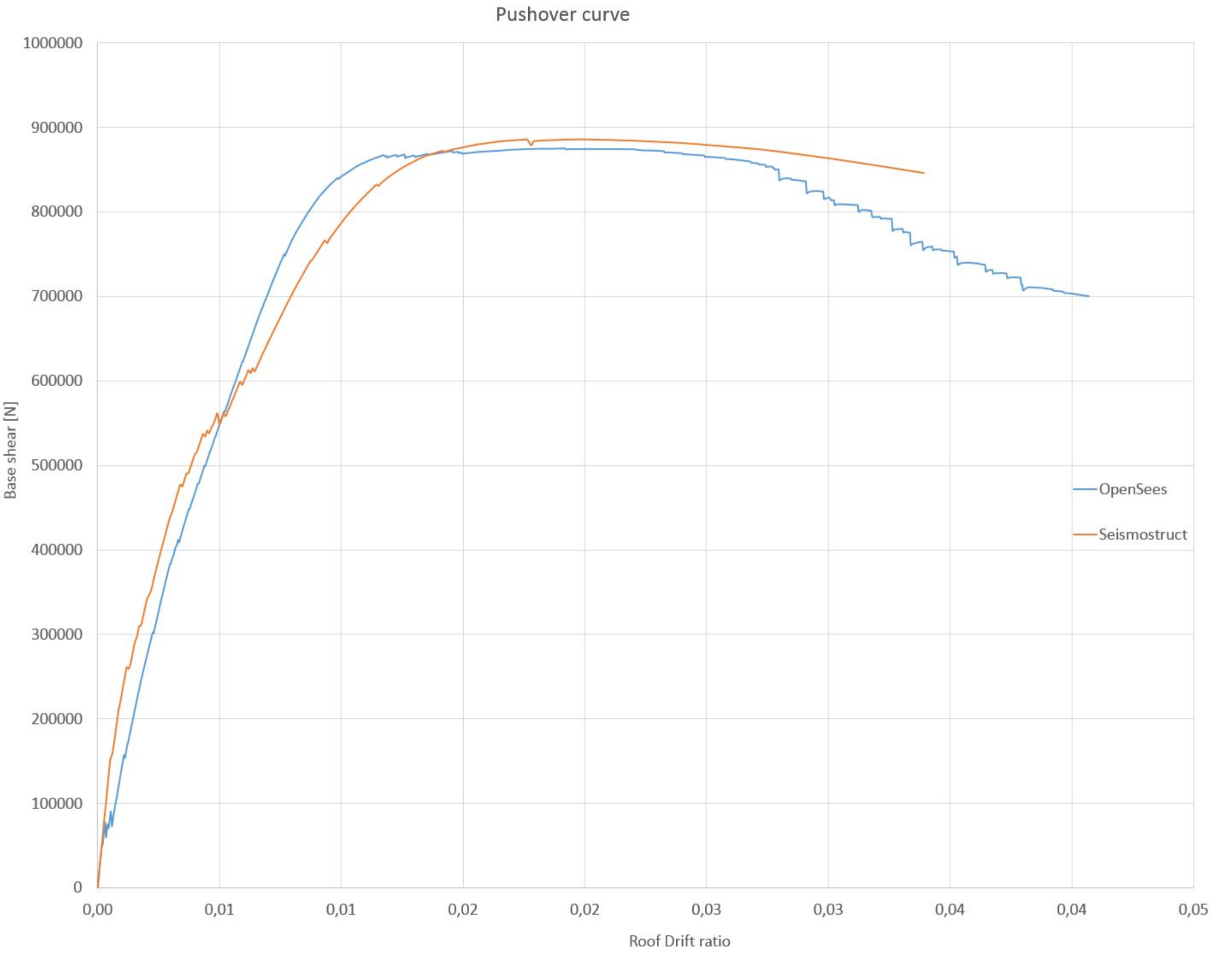

Figure 4.1: Static pushover curve for both the OpenSees and Seismostruct analysis

4.3 illustrates the interstorey drift ratio for each floor after a 20% loss of maximum base shear. From Figure 4.2 and 4.3 it is evident that it is the first floor that is drifting and causing collapse. Clearly the non-linear static pushover gives a higher capacity than the design obtained using the procedure from Eurocode 8.

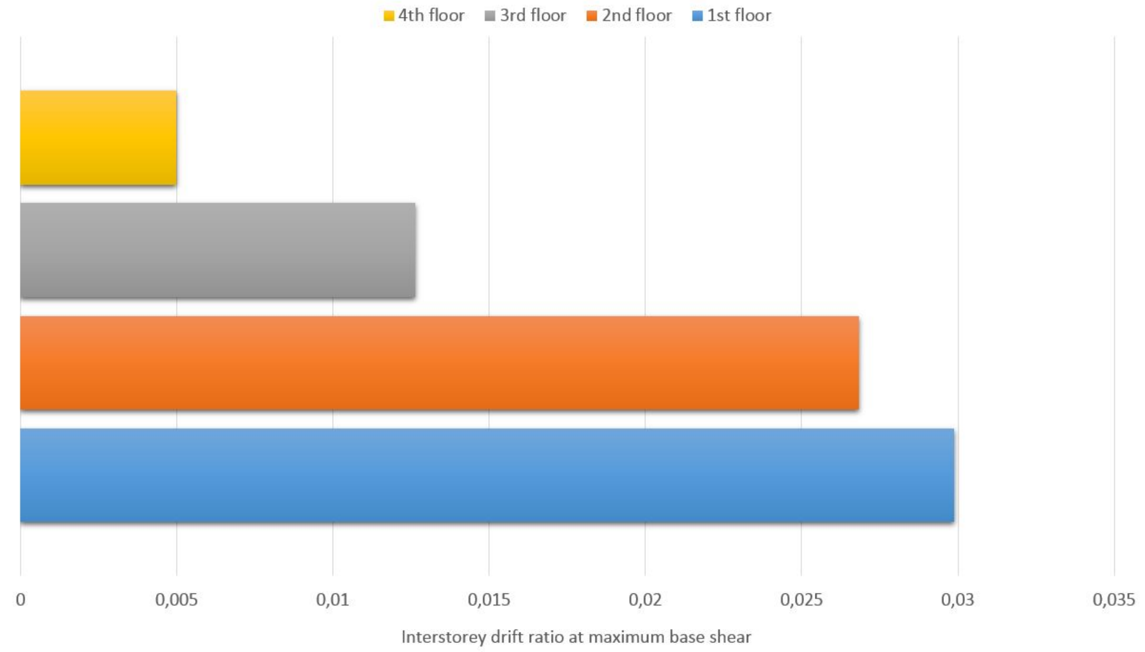

Figure 4.2: SPO-result: Interstorey drift ratio at maximum base shear from OpenSees.

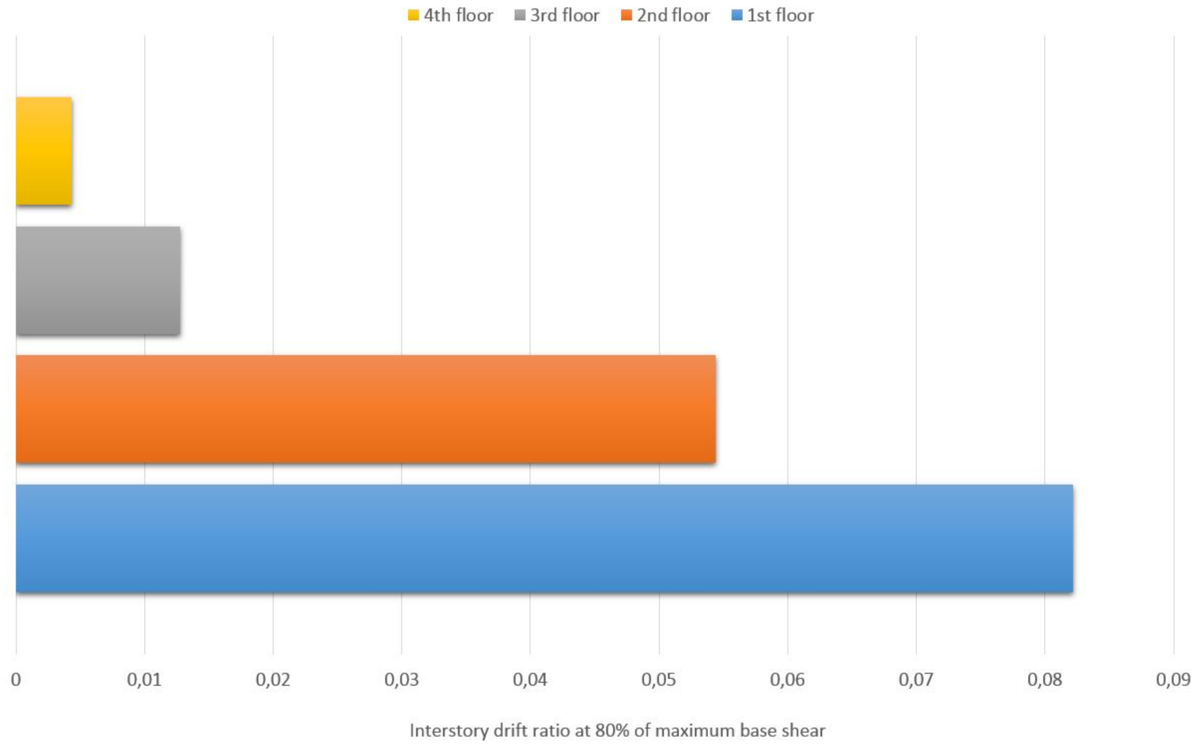

Figure 4.3: SPO-result: Interstorey drift ratio at 20% loss of maximum base shear from OpenSees.

Chapter 5

Eigenperiods and stiffness reduction

In the design phase, the stiffness of the structure was halved according to the requirement in EN 1998-1, clause 4.3.1. This reduction comes from the fact that the concrete will crack during loading. Unless a specific analysis of the cracked concrete members is performed, the stiffness is then set to half of the uncracked stiffnesses. This consequently affects the eigenperiods, and thus the scaling of the ground motions. However, the analyses that are conducted in Seismostruct and OpenSees are with the full stiffness, not reduced as the Eurocode states. The reason for this is that the goal of the thesis is to find the *real* capacity, strength and response of the structure. To verify that the modeling of the building is satisfying, the eigenperiods are compared. Recalling that the natural period of the undamped, free vibration system is defined as [10]:

$$T = 2\pi\sqrt{\frac{\mathbf{M}}{\mathbf{K}}} \tag{5.1}$$

where **K** is the stiffness matrix and **M** is the mass matrix. Equation (5.2) shows that the period obtained in Robot is approximately the same as the uncracked periods calculated in Seismostruct and OpenSees.

$$T_{Robot} \approx T_{Seismostruct} \times \sqrt{2} \approx T_{OpenSees} \times \sqrt{2}, \tag{5.2}$$

Table 5.1: Eigenperiods uncracked state

OpenSees	$0.710s \times \sqrt{2} = 1.004s$
Seismostruct	$0.680s \times \sqrt{2} = 0.961s$
Robot	$1.090s$

In Figure 5.1, the first four modeshapes are depicted. It should be mentioned that the first *cracked* eigenperiod is used in the scaling of the earthquake records. The first four, cracked natural periods, obtained using OpenSees and used for further analyses, are as follows:

$$\mathbf{T} = [0.790 \quad 0.258 \quad 0.155 \quad 0.113]$$

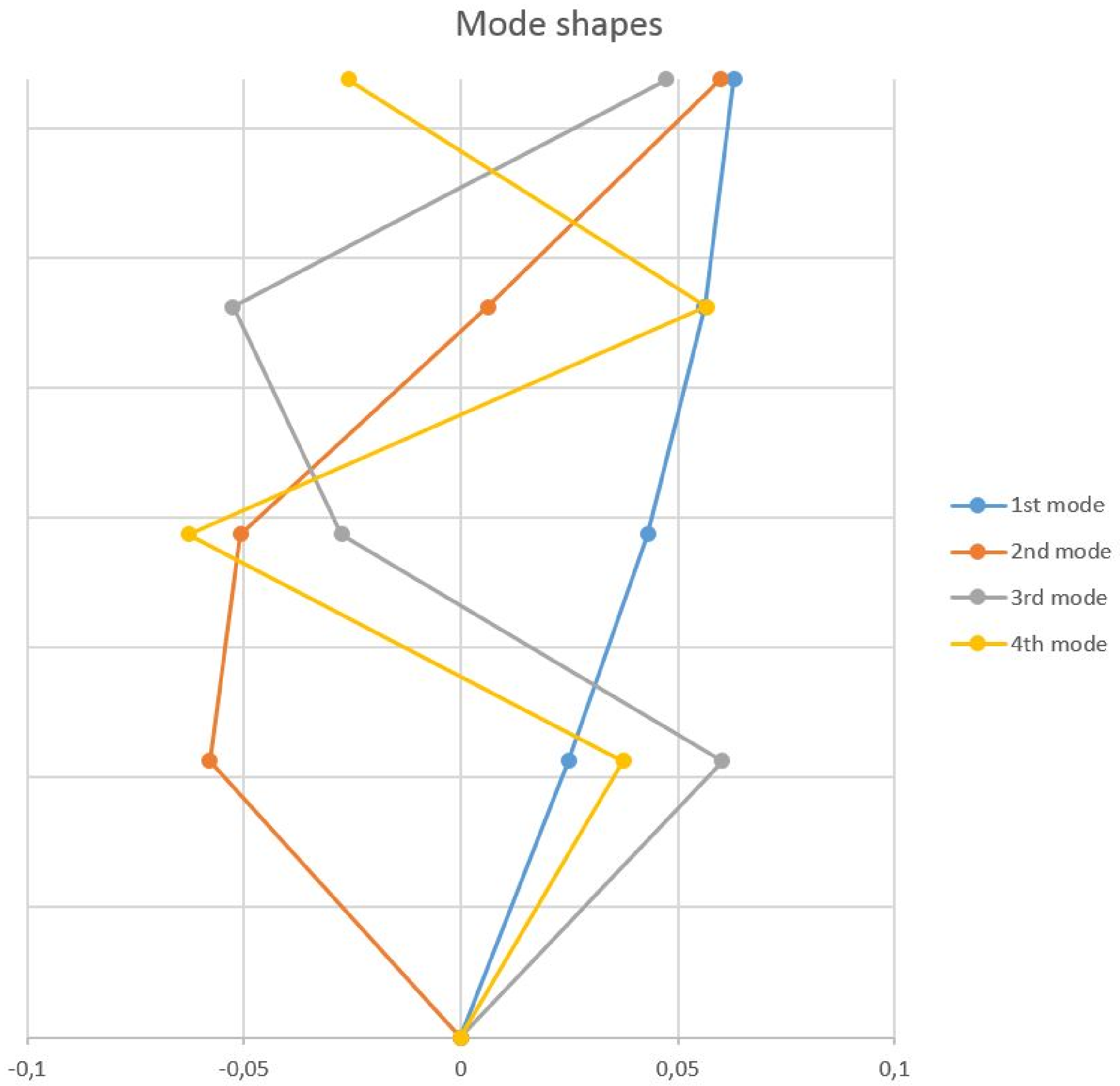

Figure 5.1: The first four mode shape of the sample structure

Chapter 6

Ground motion records

Prior to conducting a Nonlinear response history analysis, the ground motions records must be chosen. The earthquake records used in this thesis are the same used by M. Cemalovic [13]. The selection is based upon some criteria and the reader is referred to Cemalovics thesis [13] for further insight. In Table 6.1 the relevant earthquakes with their properties are listed. As seen from the table the records have similar properties. All of the earthquake records and data are downloaded from the PEER Ground Motion Database, NGA-West2 [17]. The NGA-West2 is one of the most comprehensive databases of earthquake records and data sets available in the world. In Figure 6.1 to 6.7 the chosen, unscaled ground motions time histories are depicted and in Figure 6.8 to 6.14 the scaled ground motion time histories are shown.

All of the selected ground motions are scaled such that the spectral acceleration at the fundamental period match the design spectral acceleration at the fundamental period of the design spectrum, as suggested by Vamvatsikos et. al. [8]. The scaling factors for the selected ground motion records are shown in Table 6.2. The unscaled spectra are shown in Figure 6.15 and the scaled spectra in Figure 6.16. The design spectral acceleration at the first natural period, which is the base for the scaling, is $S_d(T_1, 5\%) = 1.96\,m/s^2$. For the NRHA the records has also been scaled to match the spectral acceleration of the elastic spectrum, $S_e(T_1, 5\%) = 7.64\,m/s^2$. Even though the spectral acceleration at the first period is the same, as seen clearly in Figure 6.16, the records have significantly different modal properties and some higher spectral acceleration for the lower periods than others.

Table 6.1: The selected ground motions, and their properties:

RSN	Earthquake name	Magnitude	Rrup [km]	PGA[m/s^2]	V_{s30} [m/s]
68 Horizontal-1	*San Fernando*	6.61	22.77	3.04	316.46
169 Horizontal-1	*Imperial Valley*	6.53	22.03	4.21	242.05
724 Horizontal-1	*Superstition Hills-02*	6.54	22.25	2.16	316.64
730 Horizontal-1	*Spitak Armenia*	6.77	23.99	2.65	343.53
1634 Horizontal-1	*Manjil Iran*	7.37	75.58	2.45	302.64
4853 Horizontal-1	*Chuetsu-oki Japan*	6.8	27.9	3.43	294.71
5786 Horizontal-1	*Iwate Japan*	6.9	34.52	2.45	300.21

Table 6.2: Ground motion scaling factors, to match $S_d(T_1, 5\%)$

RSN	Scale factor
68	0.70
169	0.40
724	1.26
730	0.46
1634	0.59
4853	0.27
5786	0.41

In Figure 6.1 to 6.7 the chosen, unscaled ground motions time histories are depicted.

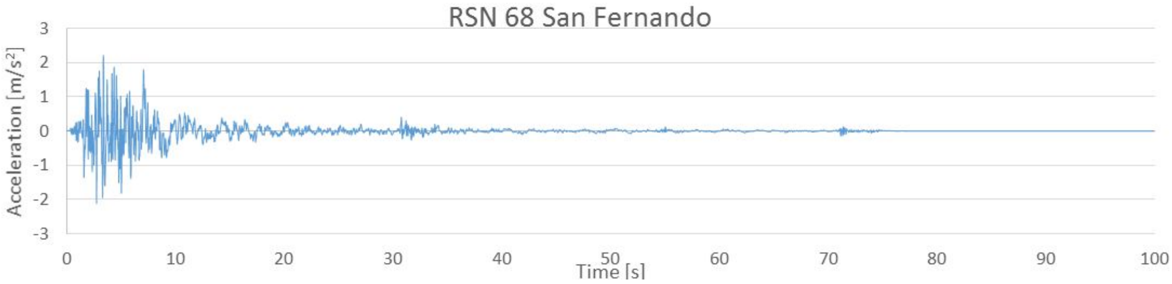

Figure 6.1: RSN68 Unscaled ground motion time-history

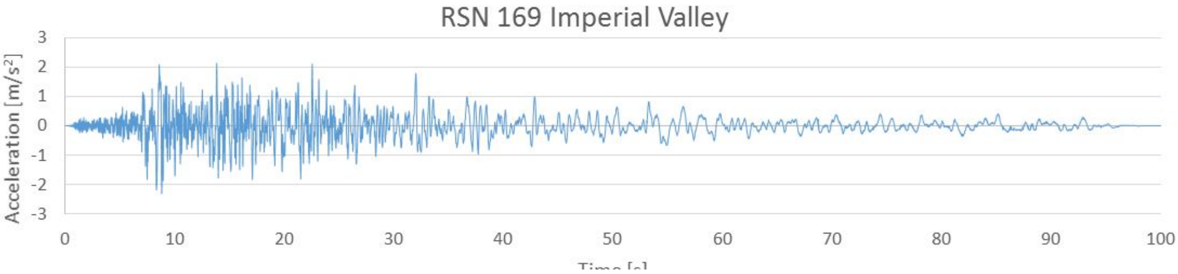

Figure 6.2: RSN169 Unscaled ground motion time-history

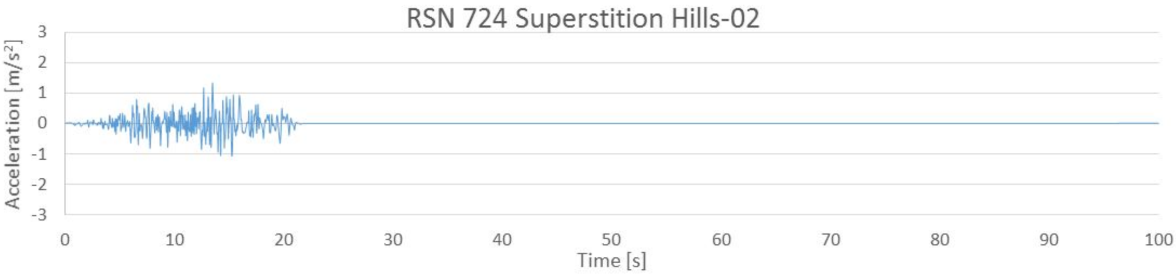

Figure 6.3: RSN724 Unscaled ground motion time-history

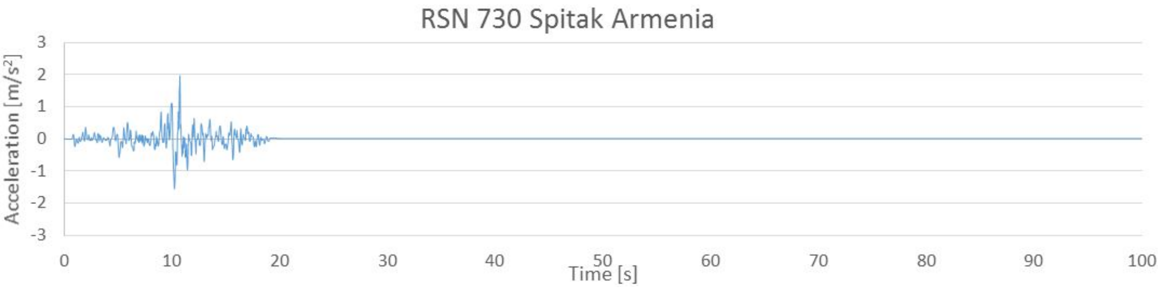

Figure 6.4: RSN730 Unscaled ground motion time-history

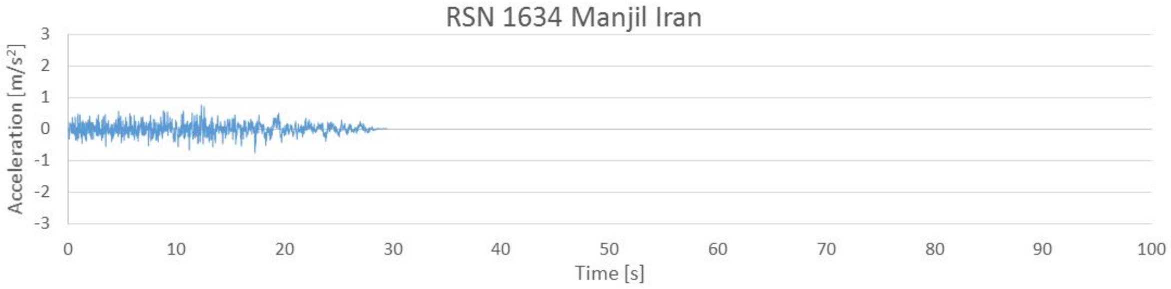

Figure 6.5: RSN1634 Unscaled ground motion time-history

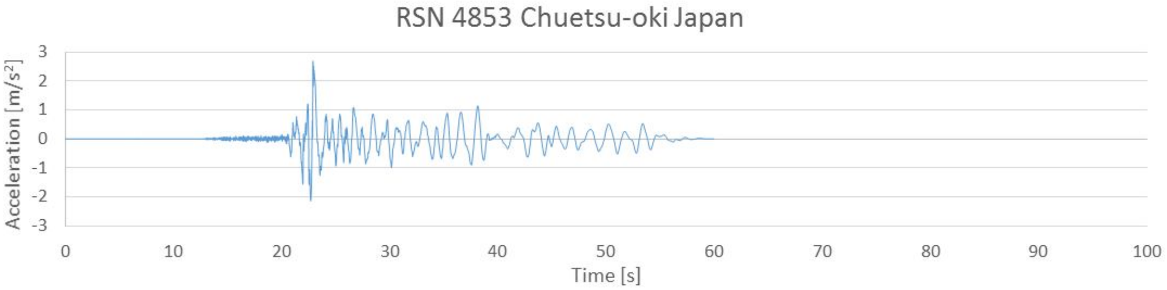

Figure 6.6: RSN4853 Unscaled ground motion time-history

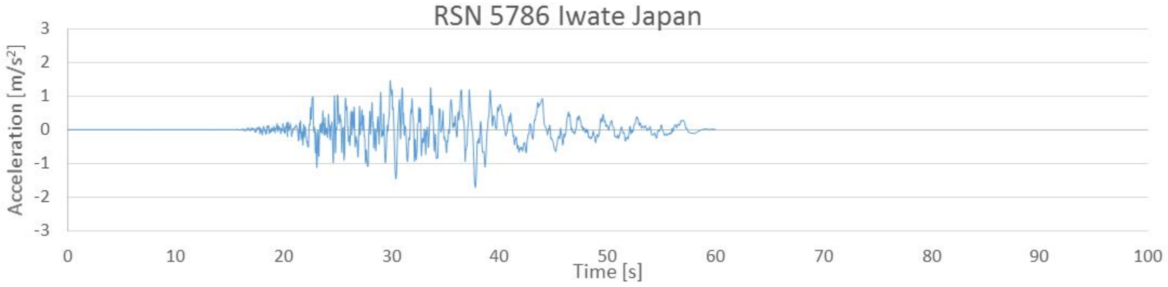

Figure 6.7: RSN5786 Unscaled ground motion time-history

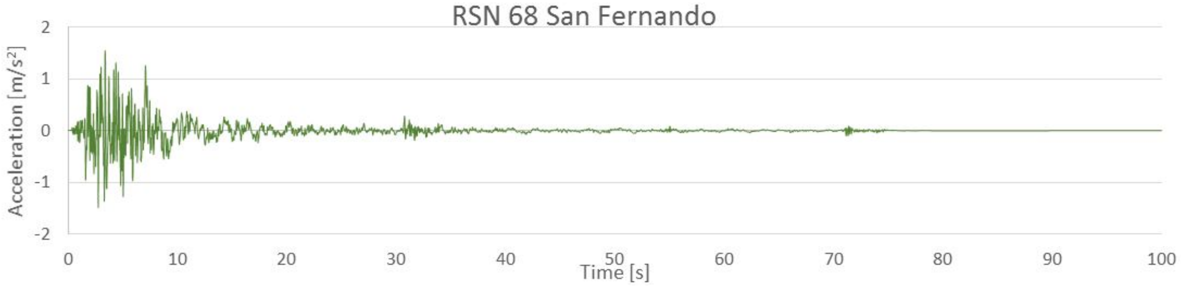

Figure 6.8: RSN68 Scaled ground motion time-history

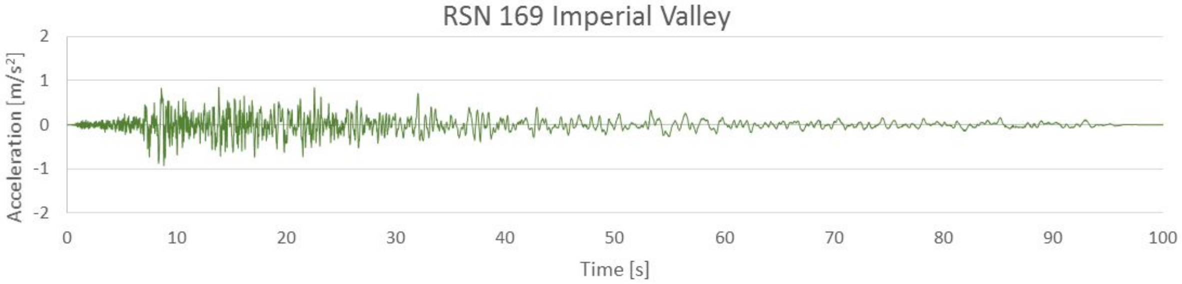

Figure 6.9: RSN169 Scaled ground motion time-history

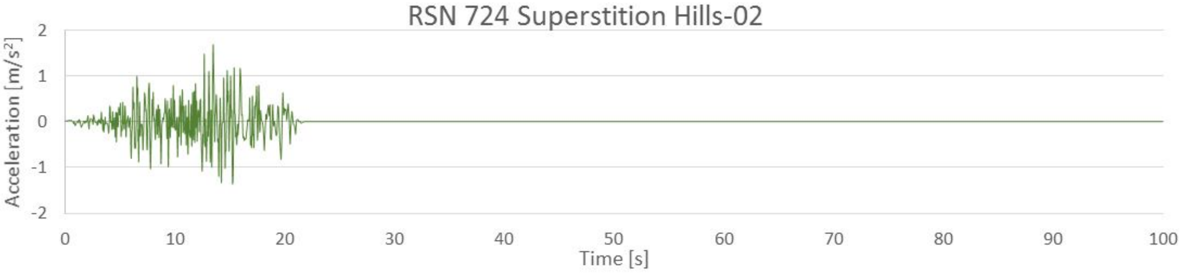

Figure 6.10: RSN724 Scaled ground motion time-history

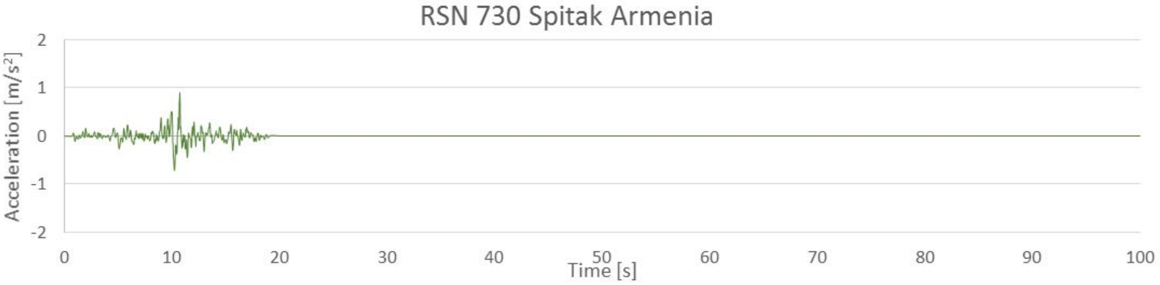

Figure 6.11: RSN730 Scaled ground motion time-history

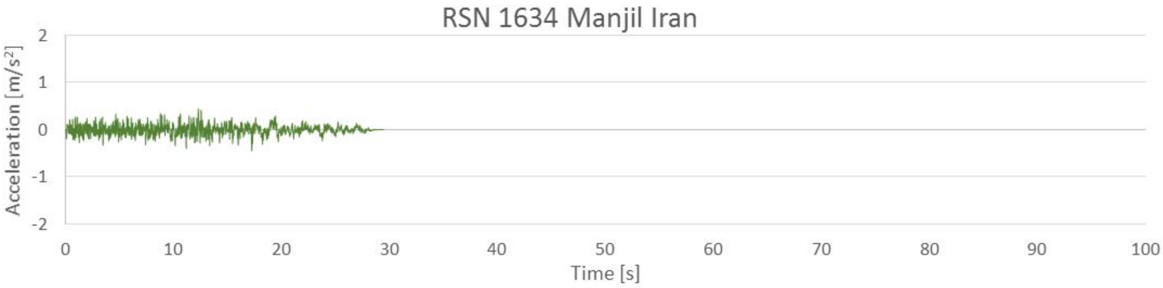

Figure 6.12: RSN1634 Scaled ground motion time-history

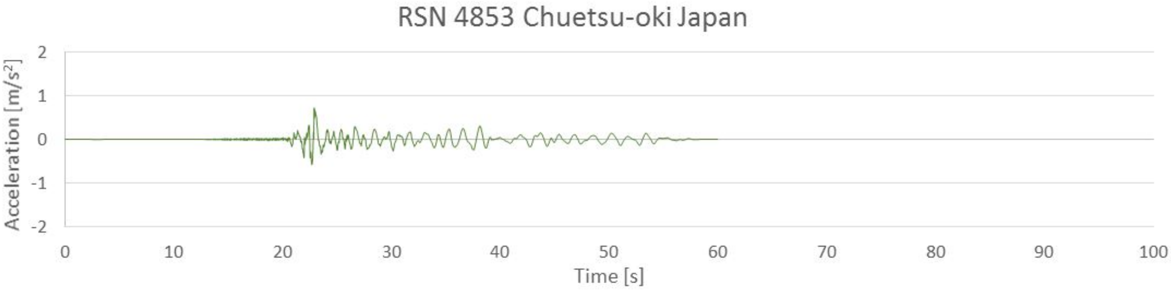

Figure 6.13: RSN4853 Scaled ground motion time-history

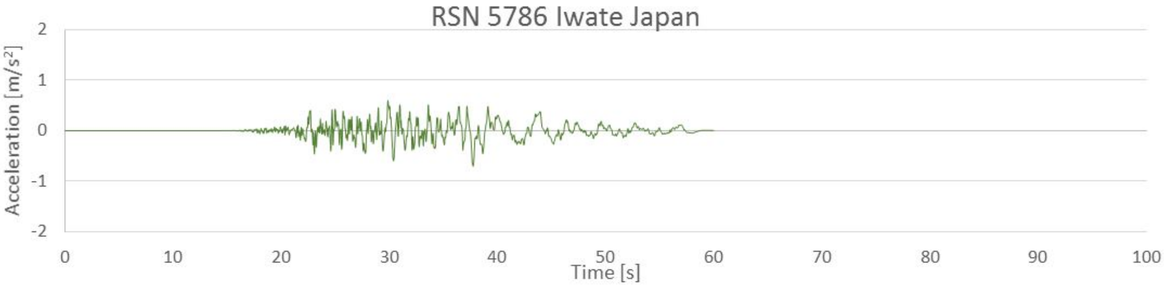

Figure 6.14: RSN5786 Scaled ground motion time-history

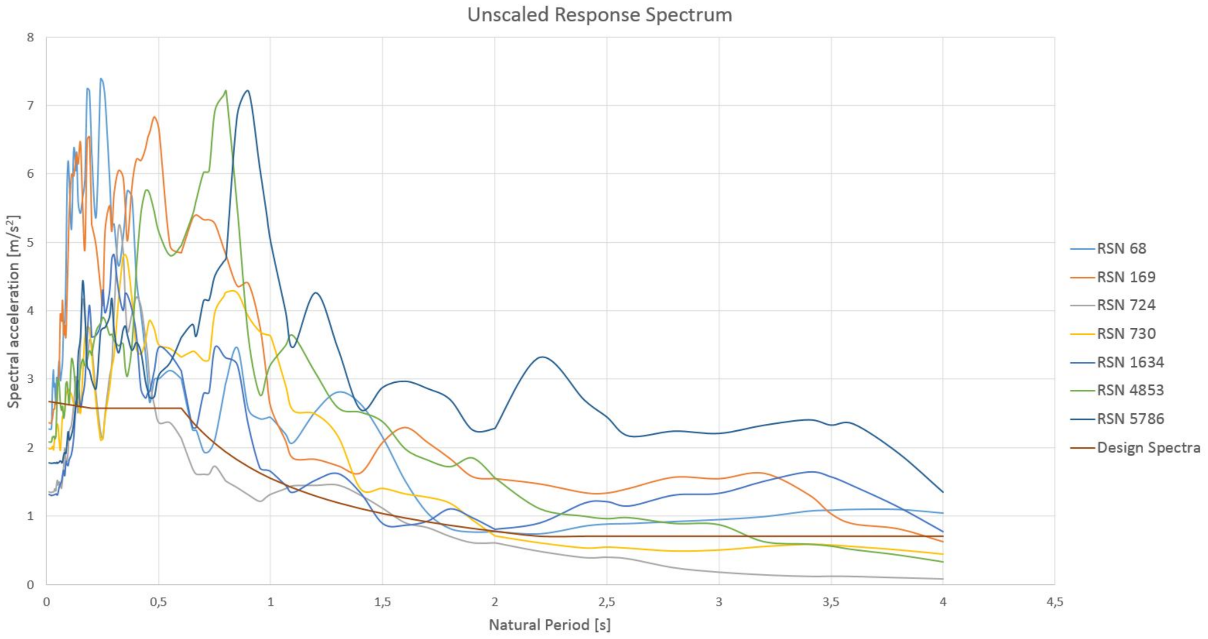

Figure 6.15: Unscaled response spectra for the selected earthquake records.

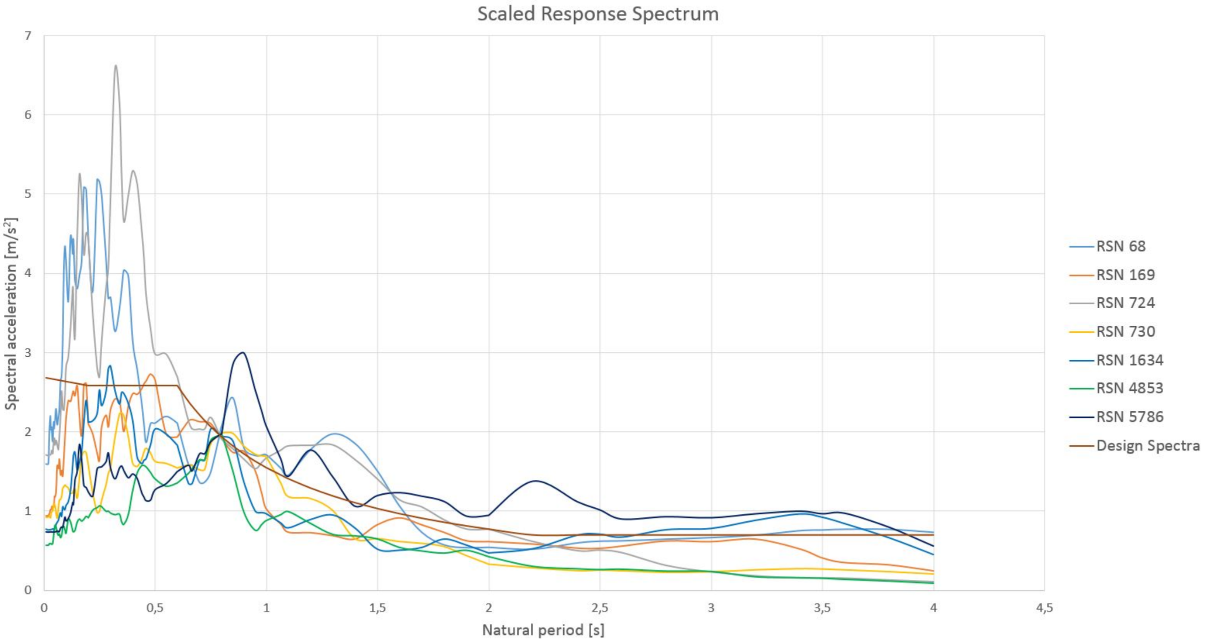

Figure 6.16: Scaled response spectra with $S_d(T_1, 5\%) = 1.96 m/s^2$, clearly different records have significantly different S_d for the lower periods.

Chapter 7

Non-linear response history analysis

7.1 Results and discussion

The results from the NRHA are presented in this section. Since the SPO results were satisfying regarding OpenSees vs. Seismostruct, the NRHA was only conducted using OpenSees. As mentioned in the Literature review, the response of the structure is highly dependent on the earthquake motion. First the records have been scaled such that the spectral acceleration at the first natural period of the selected spectra, match the spectral acceleration of the design spectrum at the first natural period, $S_d(T_1, 5\%) = 1.96\,m/s^2$, as described in the previous chapter. With this scaling it is expected that the structure remains elastic through all the earthquake motion records. Then the records have been scaled such that the spectral accelerations for the earthquake records match the elastic spectral acceleration, namely $S_e(T_1, 5\%) = 3.9 \times 1.96\,m/s^2 = 7.64\,m/s^2$. Where $q = 3.9$, which is the behavior factor. The structure is expected to withstand the earthquake records with such a scaling however, ductile or non-linear behavior will likely occur. In Table 7.1 the maximum base shear for both scalings are shown.

Table 7.1: Maximum base shear forces and displacement at control nodes from NRHA using S_d-scaling:

Earthquake Record	Maximum base shear S_d-scaling	Maximum base shear S_e-scaling
RSN68, San Fernando	601 kN	928 kN
RSN169, Imperial Valley	249 kN	835 kN
RSN724, Superstition Hills-02	524 kN	969 kN
RSN730, Spitak Armenia	397 kN	860 kN
RSN1634, Manjil Iran	177 kN	597 kN
RSN4853, Chuetsu-oki Japan	454 kN	846 kN
RSN5786, Iwate Japan	396 kN	825 kN

The results from the NRHA are presented in Figure 7.1 to 7.17. Depicted in Figure 7.1, the Base shear vs. Roof Drift Ratio (RDR) relationships for both scalings are shown. The structure remains elastic for all of the earthquake motions for the scaling using $S_d(T_1, 5\%)$ and for the scaling matched to $S_e(T_1, 5\%)$, it can be seen that ductile behavior is occurring for most of the motion records. For comparison the SPO curve from OpenSees is also included in the plot. Looking at the results from the analyses with scaling factors to match S_d, clearly none of the ground motion records induce any behavior that is close to the maximum seismic shear calculated in the SPO analyses. The response is showing good elastic behavior, and as expected – the maximum base shear vs. RDR points from the NRHA lie close to the elastic part of the SPO curve for the $S_d - scaling$. Figure 7.2 depicts the deflected shape of the building, when the maximum base shear occurs for each earthquake record. Figure 7.3 through Figure 7.9 show the deflected shape along with the 1st and 2nd mode shape, and a plot showing the displacement time-history for each ground motion. The first and second mode shape are scaled such that it matches the roof displacement for each ground motion.

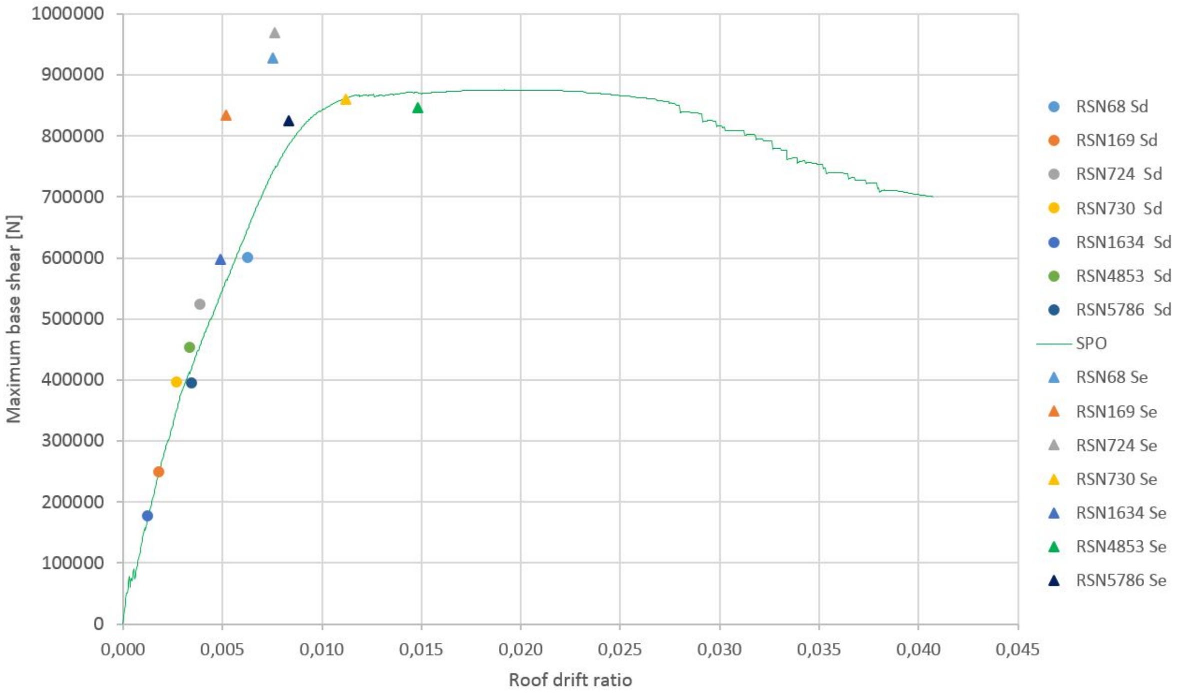

Figure 7.1: NRHA Base shear vs RDR plotted with the SPO curve from OpenSees. Both the results from the scaling with $S_d(T_1, 5\%)$ and $S_e(T_1, 5\%)$ are included

When looking at Figure 7.2 and Figure 7.3a through 7.9a, it is clearly the first mode that dominates the response for all the records, since the deflected shape more or less resembles a first mode. The second mode is included so that it can be seen that contribution from this mode is negligible. Even though the RSN68 more or less resembles first mode behavior, it is suspected that contributions from the second mode is significant. Recalling that $T_2 = 0.258s$ and the peak in spectral acceleration for RSN68, shown in Figure 6.16 in Chapter 6, this may cause the higher base shear compared to the other earthquake motions. Not surprisingly are the records RSN68 and RSN724 the ones causing the highest base shear. These two where the only ones that had spectral acceleration above the design spectrum for the shorter periods, as seen in Figure 6.16. When investigating the spectral acceleration for RSN169 it shows a clear dip at $T \approx 0.25s$, which could explain the low base shear. However, as Figure 7.4a reveals, RSN169 is also first mode dominant. Figure 7.3a through 7.9a also reveal that the contributions from the 2nd mode are almost negligible. Figure 7.3b to 7.9b shows the displacement time-histories for each ground motion record, which reveals a significant different displacement response for each of the records.

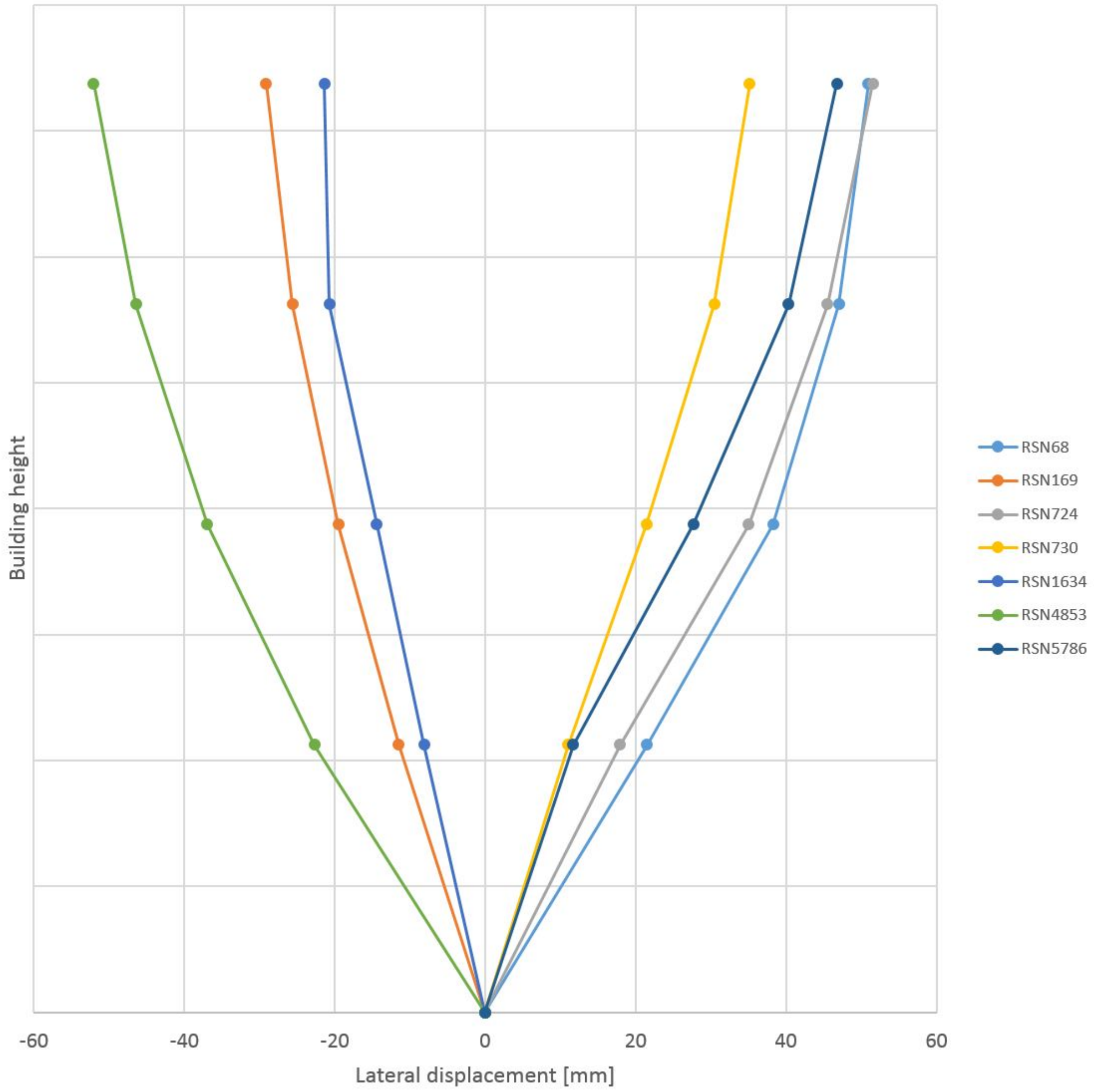

Figure 7.2: Plot showing the lateral displacement of the building at maximum base shear for each earthquake motion record scaled to $S_d(T_1, 5\%)$

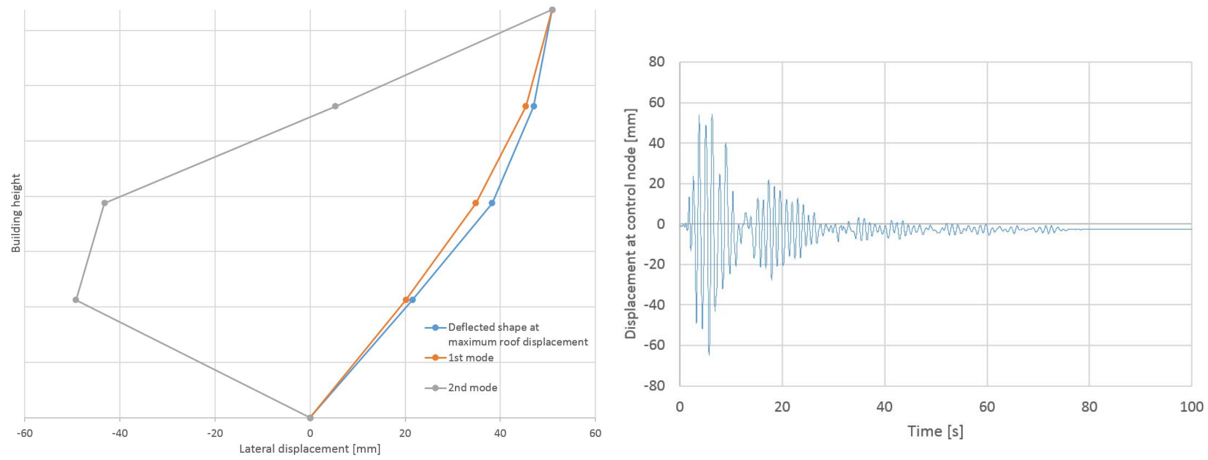

(a) Deflected shape at maximum base shear, plotted with 1st and 2nd mode shape

(b) Displacement history

Figure 7.3: RSN68 San Fernando scaled to $S_d(T_1, 5\%)$

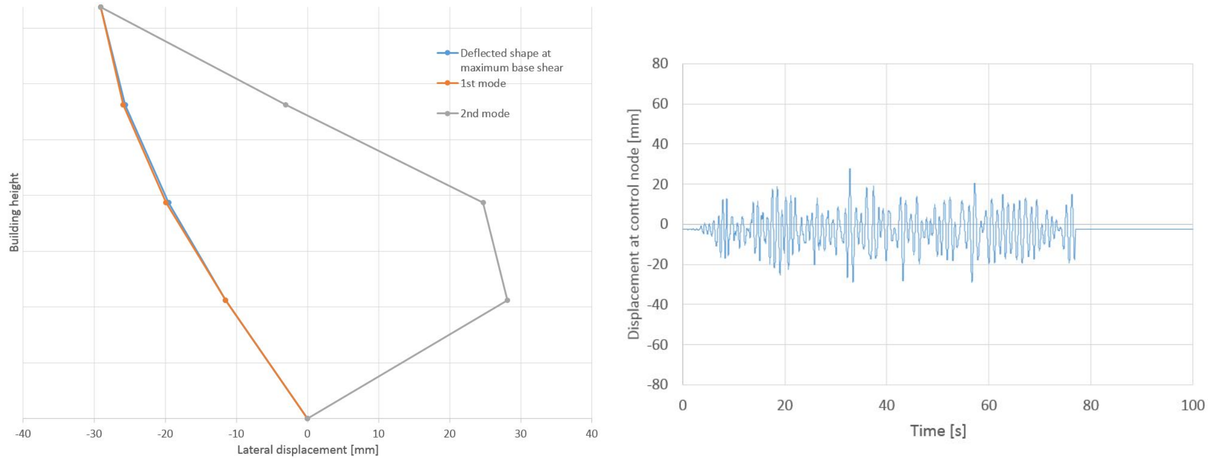

(a) Deflected shape at maximum base shear, plotted with 1st and 2nd mode shape

(b) Displacement history

Figure 7.4: RSN169 Imperial Valley scaled to $S_d(T_1, 5\%)$

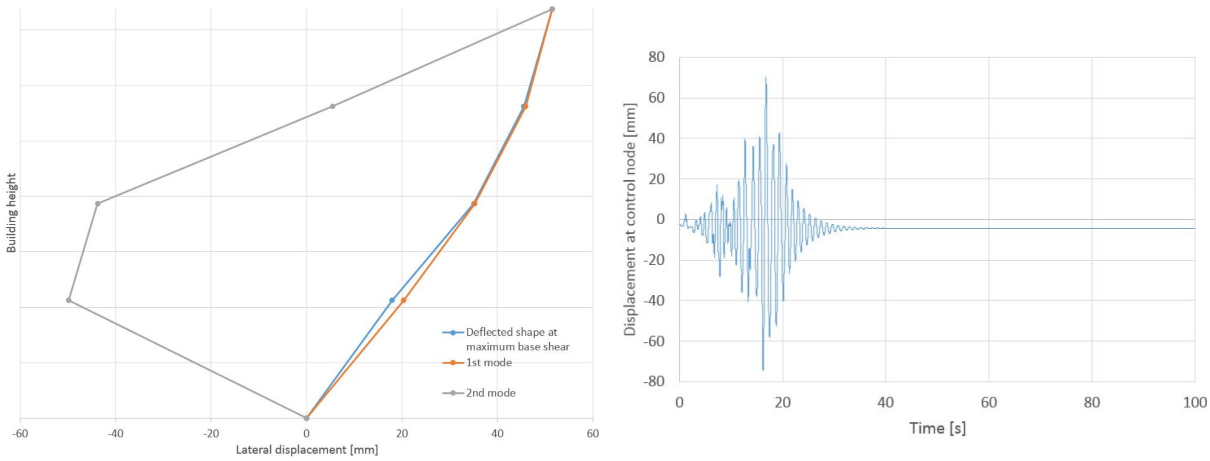

(a) Deflected shape at maximum base shear, plotted with 1st and 2nd mode shape

(b) Displacement history

Figure 7.5: RSN724 Superstition Hills-02 scaled to $S_d(T_1, 5\%)$

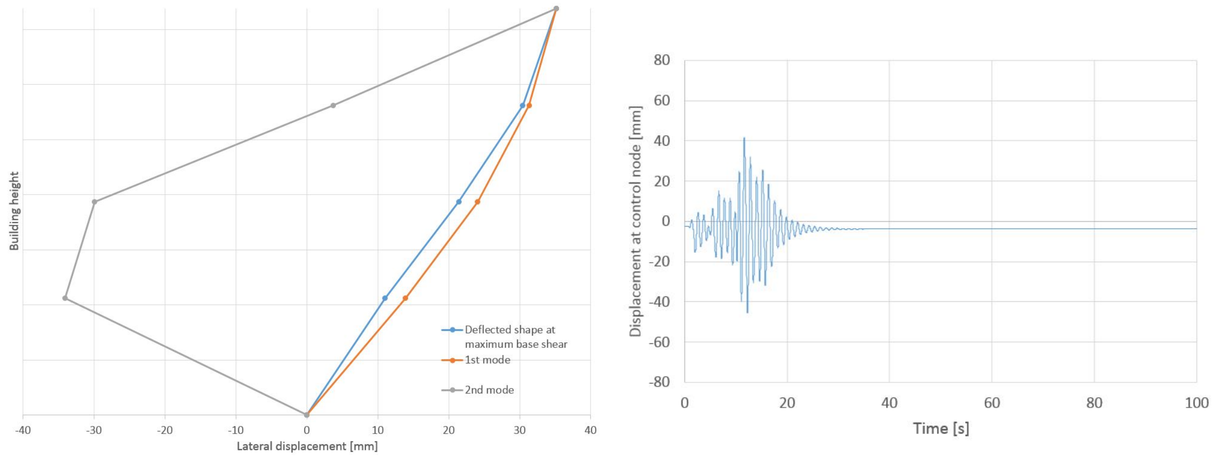

(a) Deflected shape at maximum base shear, plotted with 1st and 2nd mode shape

(b) Displacement history

Figure 7.6: RSN730 Spitak Armenia scaled to $S_d(T_1, 5\%)$

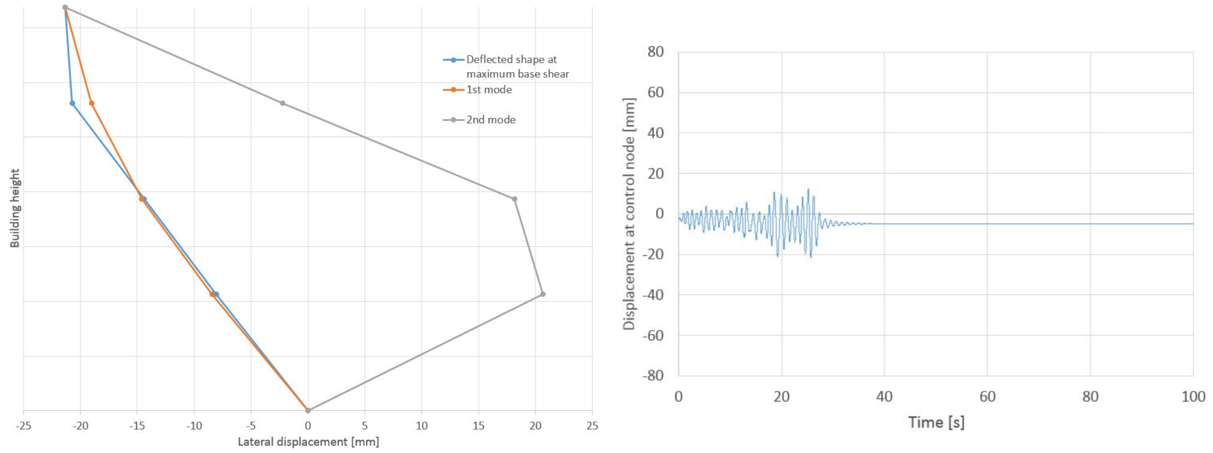

(a) Deflected shape at maximum base shear, plotted with 1st and 2nd mode shape

(b) Displacement history

Figure 7.7: RSN1634 Manjil Iran scaled to $S_d(T_1, 5\%)$

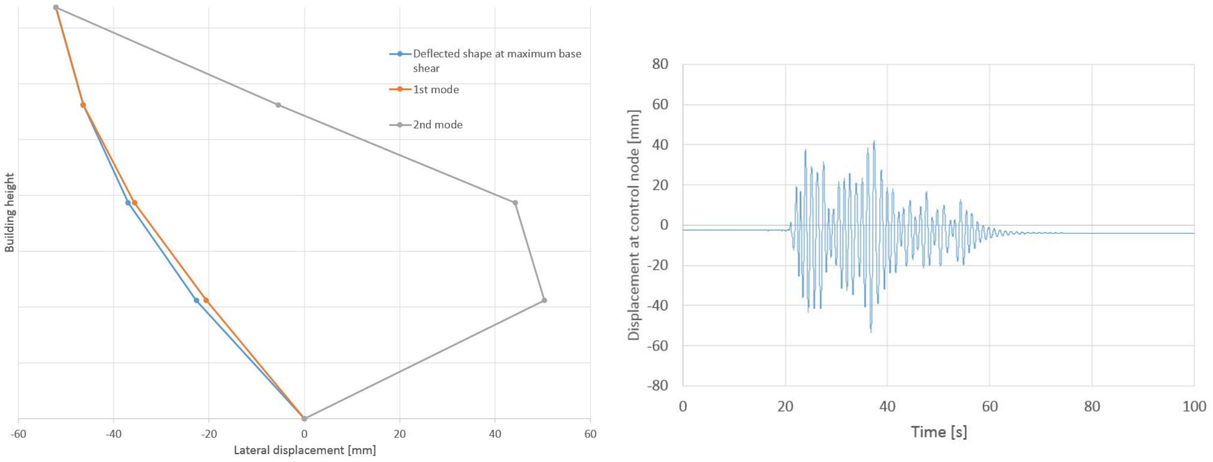

(a) Deflected shape at maximum base shear, plotted with 1st and 2nd mode shape

(b) Displacement history

Figure 7.8: RSN4853 Chuetsu-oki Japan scaled to $S_d(T_1, 5\%)$

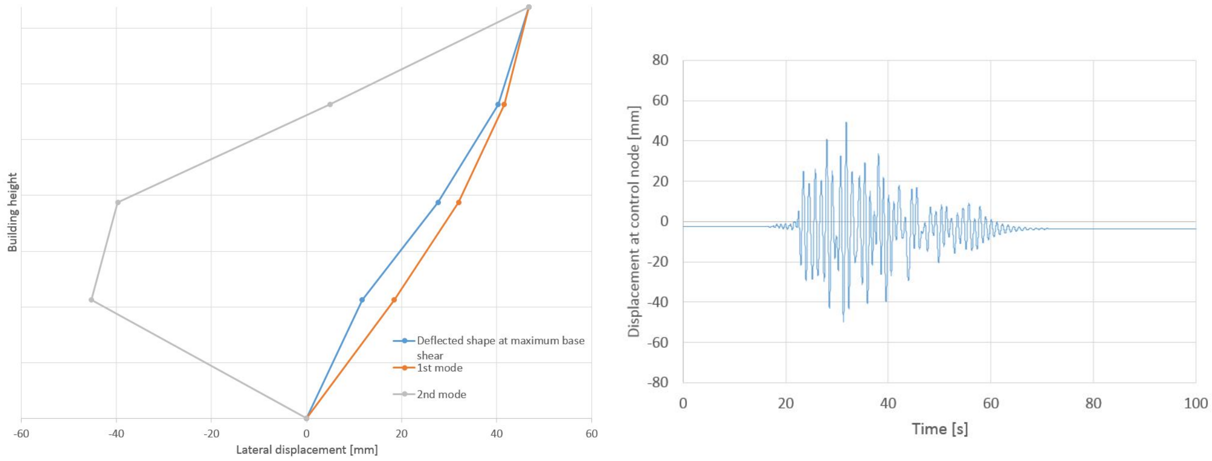

(a) Deflected shape at maximum base shear, plotted with 1st and 2nd mode shape

(b) Displacement history

Figure 7.9: RSN5786 Iwate Japan scaled to $S_d(T_1, 5\%)$

When a structure is subjected to a ground motion, the seismic energy from the earthquake must be transferred to the structure itself. The building can take up the seismic energy by transforming it to kinetic energy or elastic strain energy, and also dissipate it through damping and hysteric behavior [24]. Figure 7.10 to 7.13 shows the hysteric base shear vs displacement at the roof for the records scaled to $S_d(T_1, 5\%)$. Hysteresis energy can be expressed in terms of bending moment vs. rotation, axial force vs. axial displacement or shear vs. lateral displacement as shown here. Such plots show the cyclic behavior the structure is exhibiting during an earthquake. The hysteric energy that is being taken up by the building is the area inside these loops.

Clearly, the amount of energy transmitted from the different records varies greatly. Interestingly the RSN1634 record, which has the lowest amount of energy, has the highest Rrup=75.58 km as seen from Table 6.1 in Chapter 6, which is more that double the distance compared to the Rrup in RSN68 or RSN724 which are the records with the highest energies induced on the structure. Even though the shear/displacement time histories show hysteric behavior, they are causing the structure to alternate somewhat close to perfect linear elastic, back and forth from the second quadrant to the fourth quadrant, except for the RSN724 record which clearly shows non-linear behavior in Figure 7.11b.

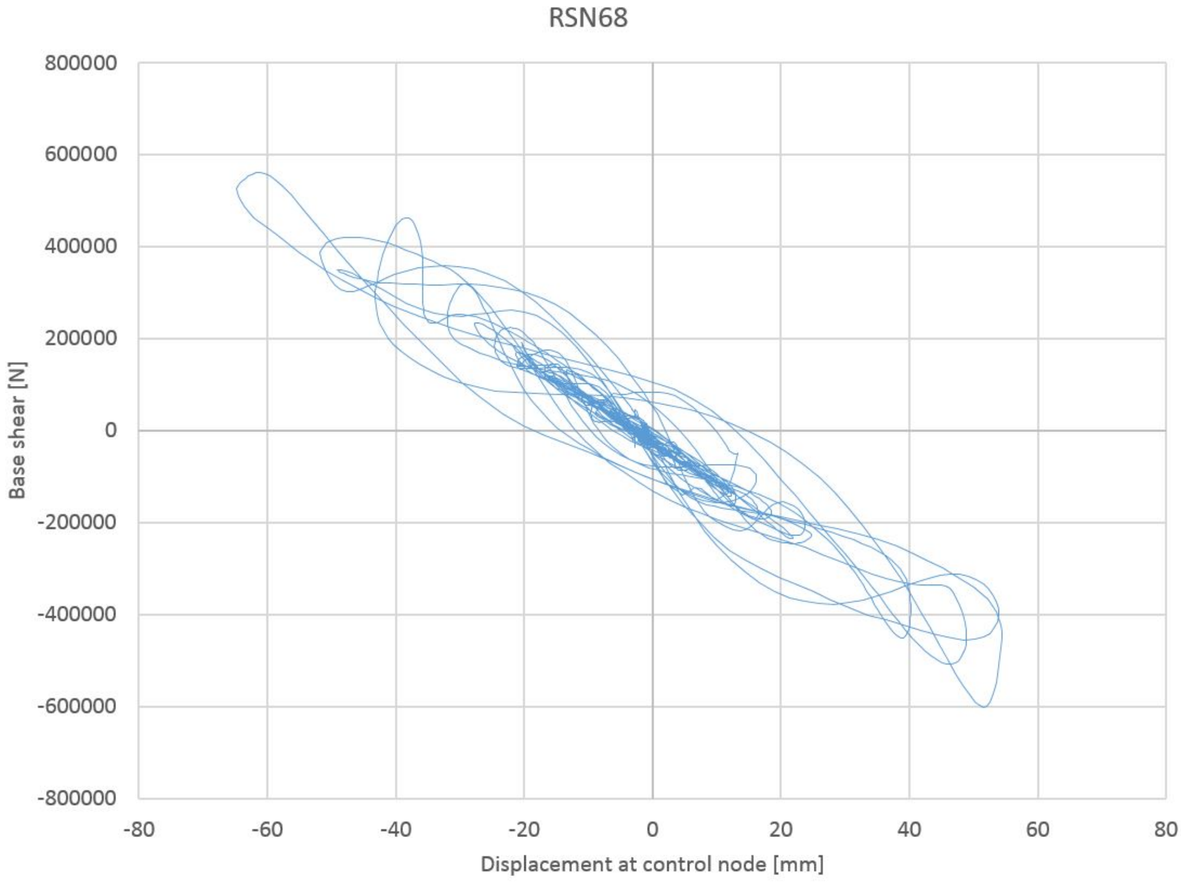

Figure 7.10: San Fernando earthquake hysteric base shear vs. roof displacement scaled to $S_d(T_1, 5\%)$

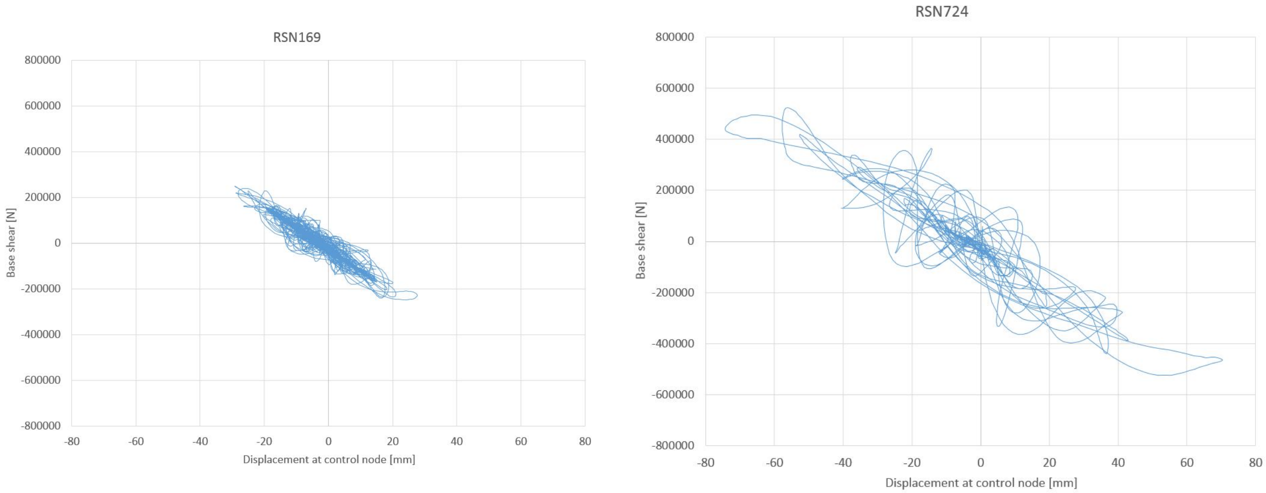

(a) Hysteric base shear Imperial Valley Earthquake scaled to $S_d(T_1, 5\%)$

(b) Hysteric base shear Superstition Hills-02 Earthquake scaled to $S_d(T_1, 5\%)$

Figure 7.11: Hysteric base shear vs. displacement at control node

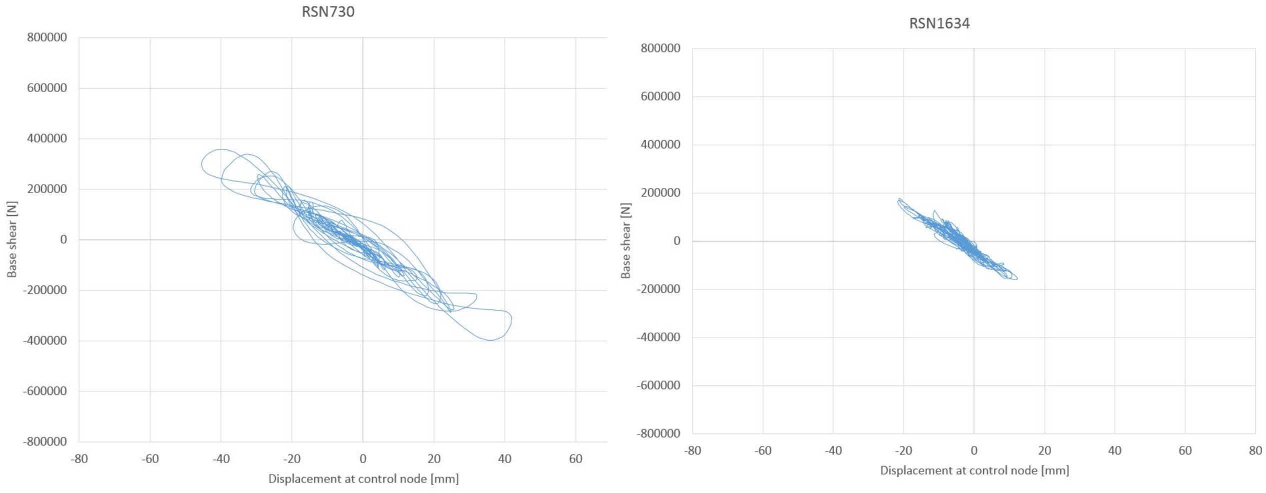

(a) Hysteric base shear Spitak Armenia Earthquake scaled to $S_d(T_1, 5\%)$

(b) Hysteric base shear Manjil Iran Earthquake scaled to $S_d(T_1, 5\%)$

Figure 7.12: Hysteric base shear vs. displacement at control node

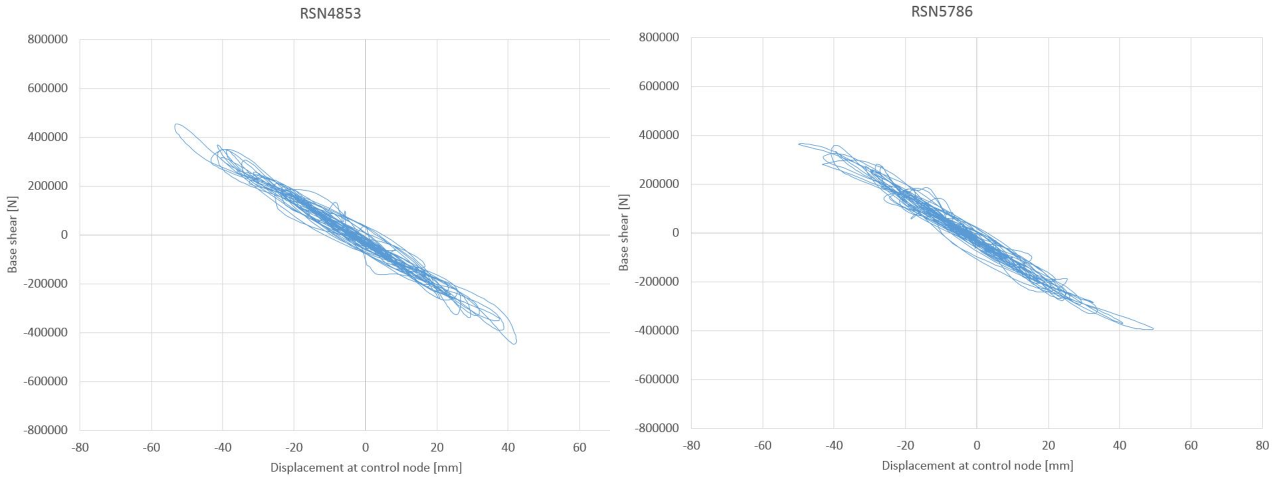

(a) Hysteric base shear Chuetsu-oki Japan Earthquake scaled to $S_d(T_1, 5\%)$

(b) Hysteric base shear Iwate Japan Earthquake scaled to $S_d(T_1, 5\%)$

Figure 7.13: Hysteric base shear vs. displacement at control node

Figure 7.14 to 7.17 shows the hysteric base shear vs. displacement for the records scaled to $S_e(T_1, 5\%)$. Obviously both displacement and base shear are significantly higher than for the scaling matched to $S_e(T_1, 5\%)$. The amount of energy induced on the structure is greatly increased and the curves shows that the structure has highly non-linear behavior for most of the records. The RSN4853 record and RSN5786 still resembles *close* to perfect linear behavior.

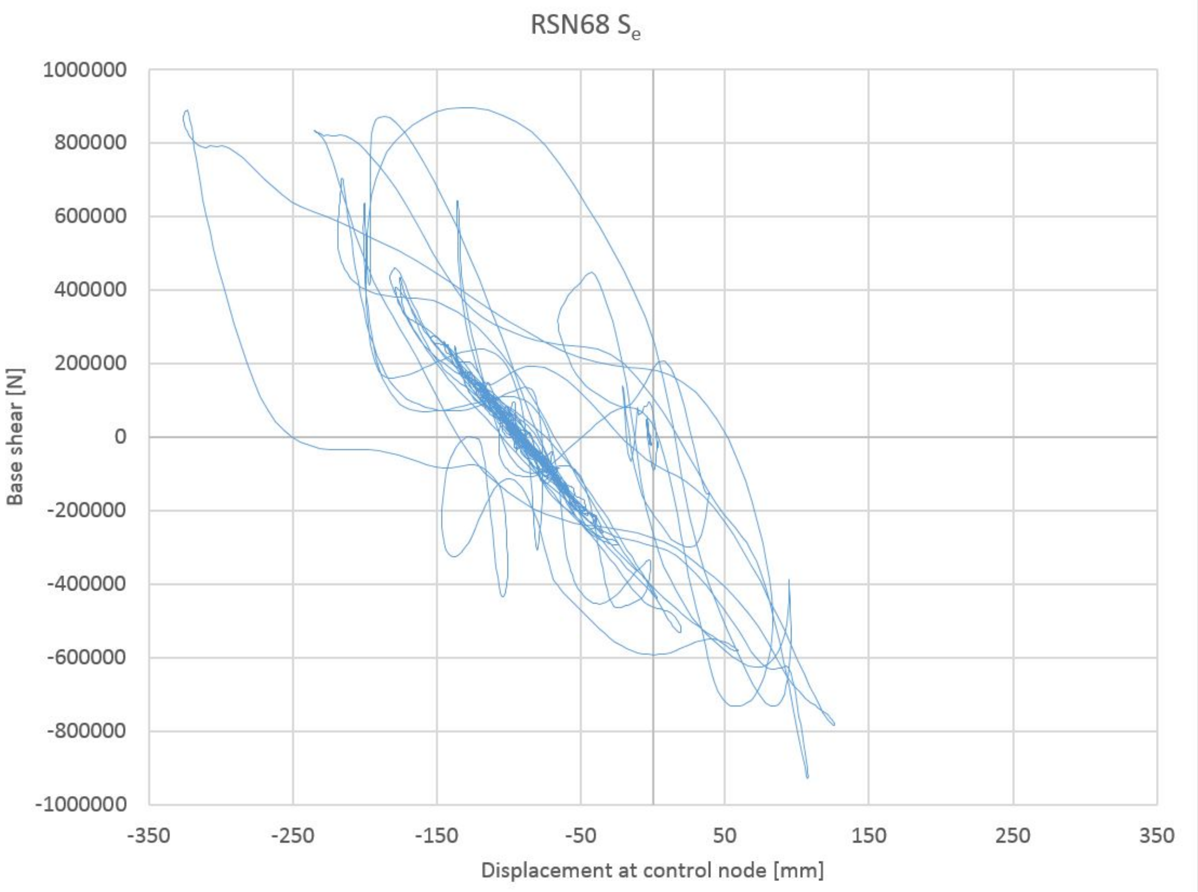

Figure 7.14: San Fernando earthquake hysteric base shear vs. roof displacement scaled to $S_e(T_1, 5\%)$

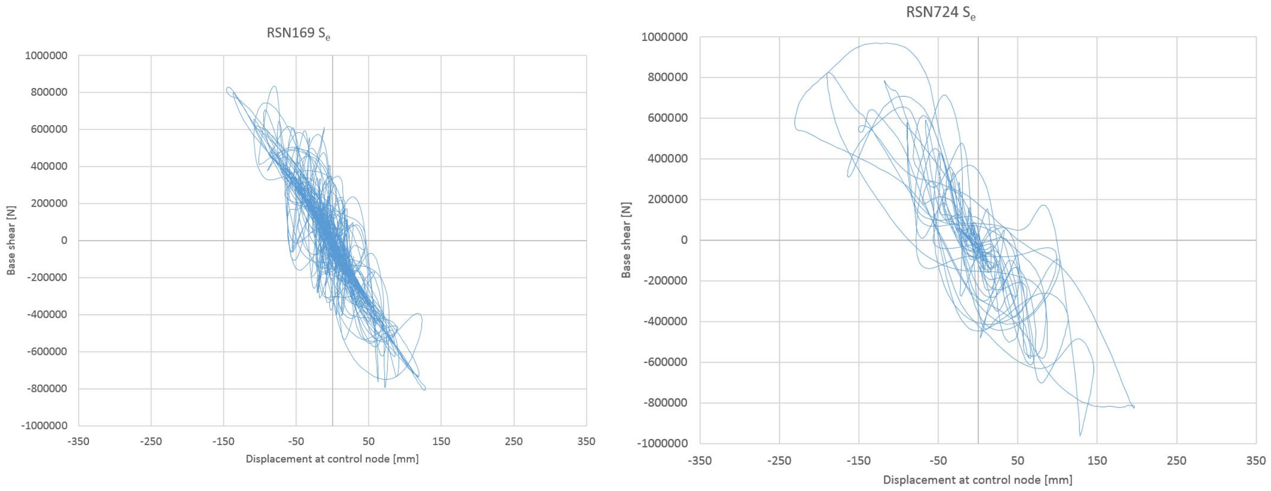

(a) Hysteric base shear Imperial Valley Earthquake scaled to $S_e(T_1, 5\%)$

(b) Hysteric base shear Superstition Hills-02 Earthquake scaled to $S_e(T_1, 5\%)$

Figure 7.15: Hysteric base shear vs. displacement at control node

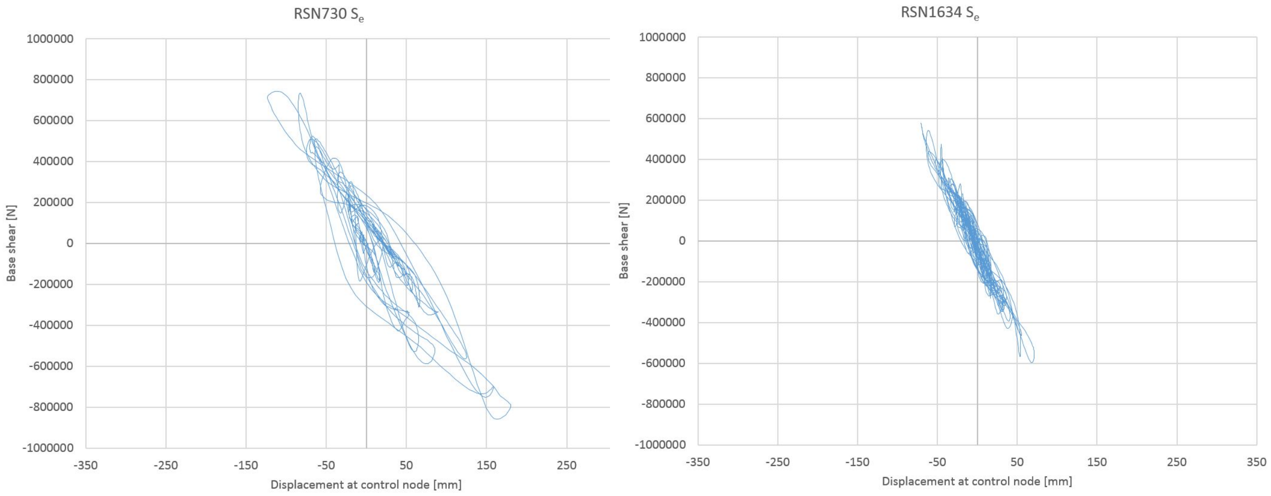

(a) Hysteric base shear Spitak Armenia Earthquake scaled to $S_e(T_1, 5\%)$

(b) Hysteric base shear Manjil Iran Earthquake scaled to $S_e(T_1, 5\%)$

Figure 7.16: Hysteric base shear vs. displacement at control node

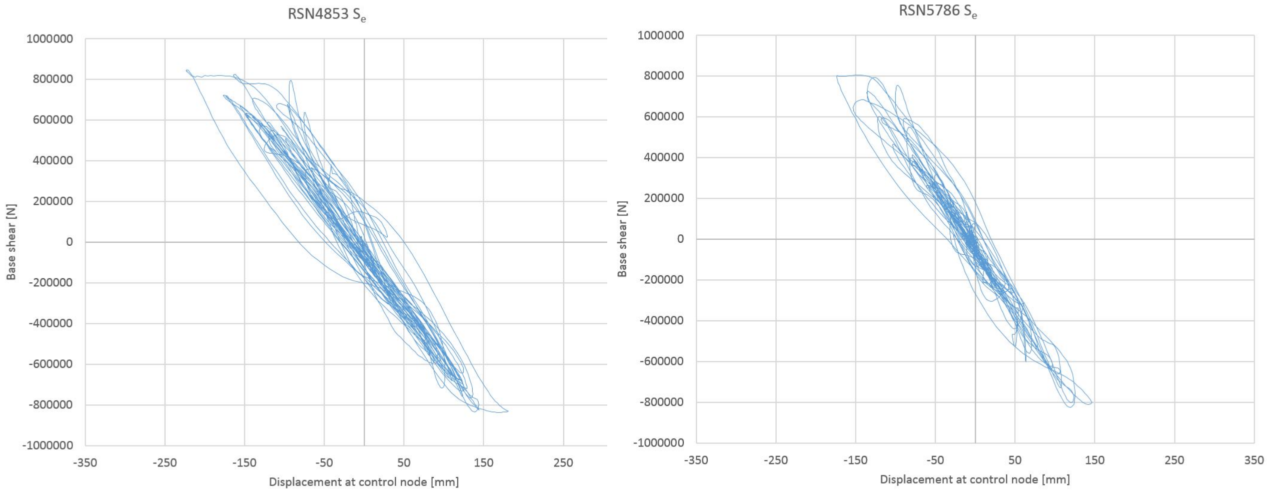

(a) Hysteric base shear Chuetsu-oki Japan Earthquake scaled to $S_e(T_1, 5\%)$

(b) Hysteric base shear Iwate Japan Earthquake scaled to $S_e(T_1, 5\%)$

Figure 7.17: Hysteric base shear vs. displacement at control node

Chapter 8

Incremental dynamic analysis

8.1 Results and discussion

The different earthquake motions have been scaled both up and down from the initial values of S_d at the fundamental period as discussed earlier. The damage measure used to assess the response are RDR and Interstorey Drift Ratio (IDR), both the overall maximum peak interstorey drift (θ_{max}) and for each floor (θ_n) are assessed. θ_{max} is a strong DM candidate for looking at structural damage on frame structures, since it relates well to both global and local story collapse [8]. For structures designed according to DCM in EN 1998-1, the forces in the elements are not causing the ultimate collapse, it is the displacements. The structure is designed to withstand significant ductile behavior, and the previous chapters has revealed that. Therefore the displacement or drift ratios are assessed in this chapter instead of element forces and stresses.

Figure 8.1 shows the roof drift ratio for the selected earthquake motions. Clearly, as mentioned earlier in the thesis, different time histories cause collapse at different IMs. Much of the reason for the variation in the response, is due to the different frequency characteristics in each ground motion. RSN68 is scaled up to $13.9 \times S_d(T_1, 5\%)$, which is the collapse-IM for that earthquake, while RSN1634 did not collapse until the IM was $72.50\,m/s^2$, or $37 \times S_d(T_1, 5\%)$. As depicted in Figure 8.1, RSN5786 is the earthquake record that induce collapse at the lowest spectral acceleration. All curves are showing a distinct linear-elastic region for the lowest IMs, until at least $S_d(T_1, 5\%) = 1.96\,m/s^2$ is reached on the vertical axis.

As discussed in the Literature review, the duration of the ground motion can possibly effect the structural damage, which in turn cause collapse. When investigating the duration of the selected ground motion and the collapse IM, they should therefore correlate in some way: The ground motion with the highest collapse IM should be the shortest in time, if duration have significant effect. Recalling the scaled ground motion time histories in Figure 6.8 to 6.14 in Chapter 6, RSN1634 is not the shortest in duration, but rather the ground motion with the lowest amplitude, after the scaling to $S_d(T_1)$ is done. On the other end of the collapse IM-scale, RSN5786, RSN169 and RSN68 are found. These earthquake records are however in the top three regarding duration with significant amplitude. Therefore the amplitude could as well as duration interfere with collapse capacity, but as discussed earlier, longer earthquake records have more cycles, which in turn results in significant stiffness degradation.

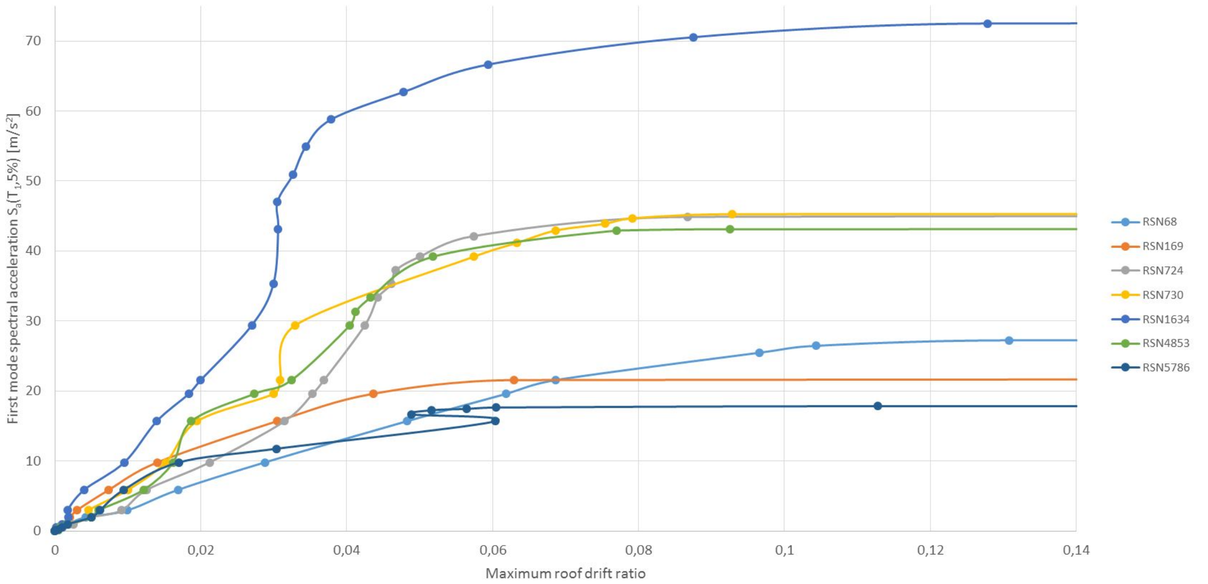

Figure 8.1: IDA curves showing maximum roof drift ratio, of the building with $T_1 = 0.790s$.

Figure 8.2 to 8.8 depict the RDR time-histories of the collapse IM and the intensity prior to collapse for each ground motion. These time-histories are a verification of actual collapse, since the divergence in the analyses could also be caused by numerical difficulties in the solver, e.g. localization issues. Clearly, a small increase in IM causes a significant increase in DM, resulting in collapse, as expected. However some of the time-histories are not showing an instant stop in RDR vs. time such as Figure 8.2 is depicting, though the IM is usually causing collapse at $RDR > 5 - 6\%$. The time-histories depicted in Figure 8.4, 8.5 and 8.7 are not showing the instant stop, however $RDR > 5 - 6\%$ is causing the structure to collapse.

The plots in Figure 8.2 to 8.8 shows the distinctive differences of the RDR vs. time prior to collapse. In Figure 8.2 it can be seen that the structure is able to come back, and still manage to converge for the $S_d(T_1) = 26.45\,m/s^2$, with $RDR \geq 10\%$, however the structure is collapsing for the next scaling, after 20 seconds, with $RDR \approx 12\%$. The times-history in Figure 8.3 show a linear increase of RDR, until collapse close to RDR=5%. The RSN724 ground motion record is causing a major jump in RDR in the time-history depicted in Figure 8.4. With an IM of $S_d(T_1) = 42.13\,m/s^2$, the structure is not even close to GI, with $RDR \approx 1\%$. The relatively small increase is causing the roof to drift away after 22 seconds. Figure 8.5 is showing the RSN730 time-history, and as for the RSN724 record, a small increase in IM is causing a jump in DM, followed by global instability or collapse. The RSN 1634 earthquake record is causing the structure to collapse instantly after 30 seconds, as shown in Figure 8.6. For the last two converging scalings of the RSN4853 record, it can be seen in Figure 8.7 that both of them have a linear increasing RDR, where the last converging is causing a jump after around 55 seconds, which ultimately leads to collapse. The RDR caused by the RSN5786 earthquake motion, is rapidly increasing after 45 seconds, as depicted in the time-history plot in Figure 8.8, resulting in collapse of the structure.

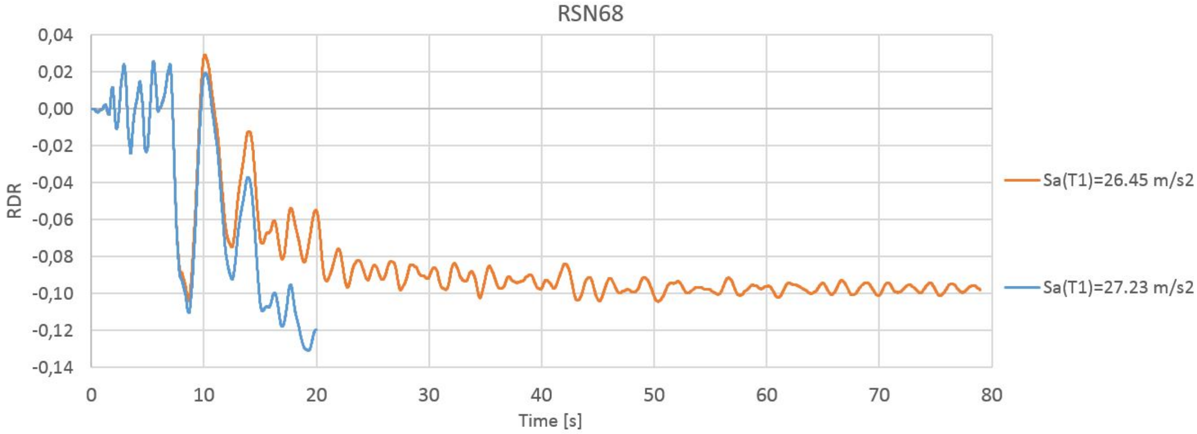

Figure 8.2: RDR Response of the last two scalings of RSN68, resulting in collapse at $T \approx 20$ s

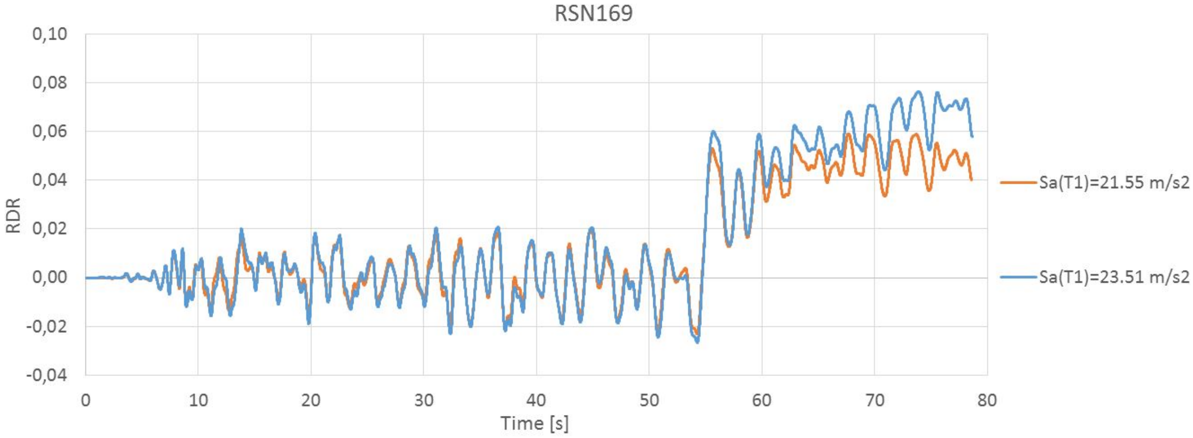

Figure 8.3: RDR Response of the last two scalings of RSN169, resulting in collapse at $T \approx 78$ s

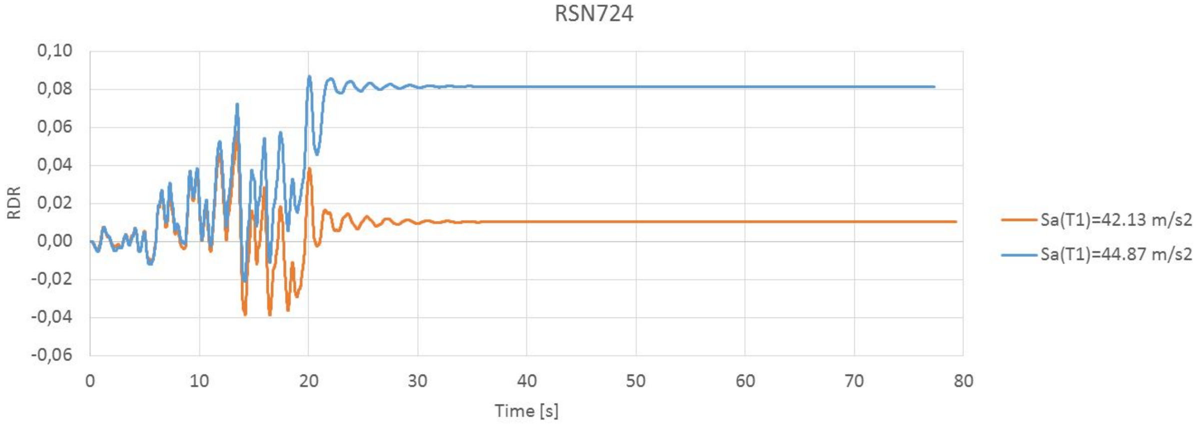

Figure 8.4: RDR Response of the last two converging scalings of RSN724, the time-history is not showing a collapse behavior, however the structure is collapsed at RDR=8%

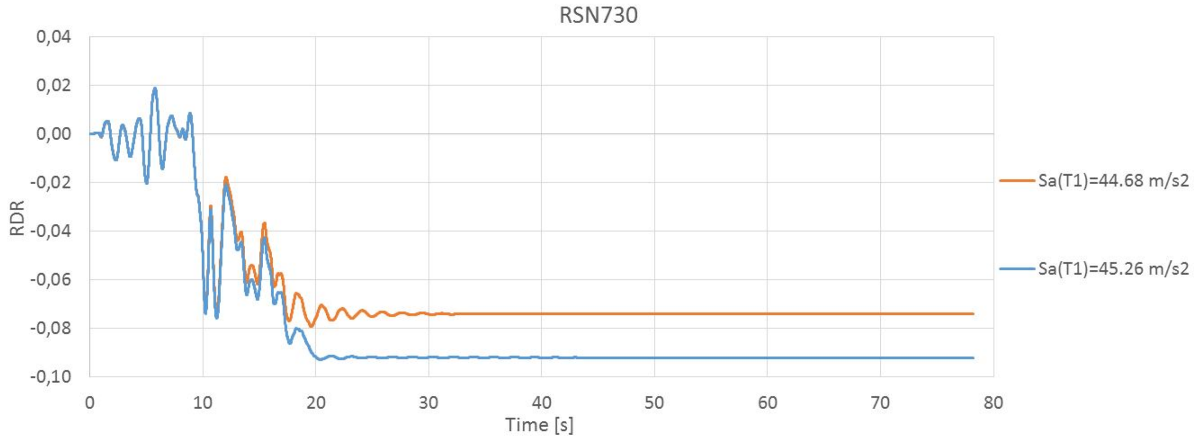

Figure 8.5: RDR Response of the last converging two scalings of RSN730, the time-history is not showing a collapse behavior, however the structure is collapsed at RDR≈9%

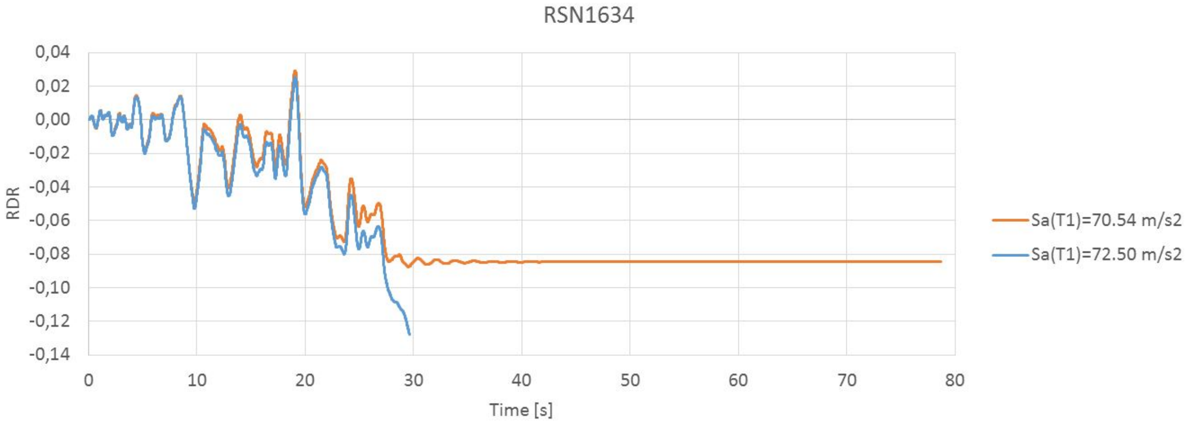

Figure 8.6: RDR Response of the last two scalings of RSN1634, resulting in collapse at $T \approx 30$ s

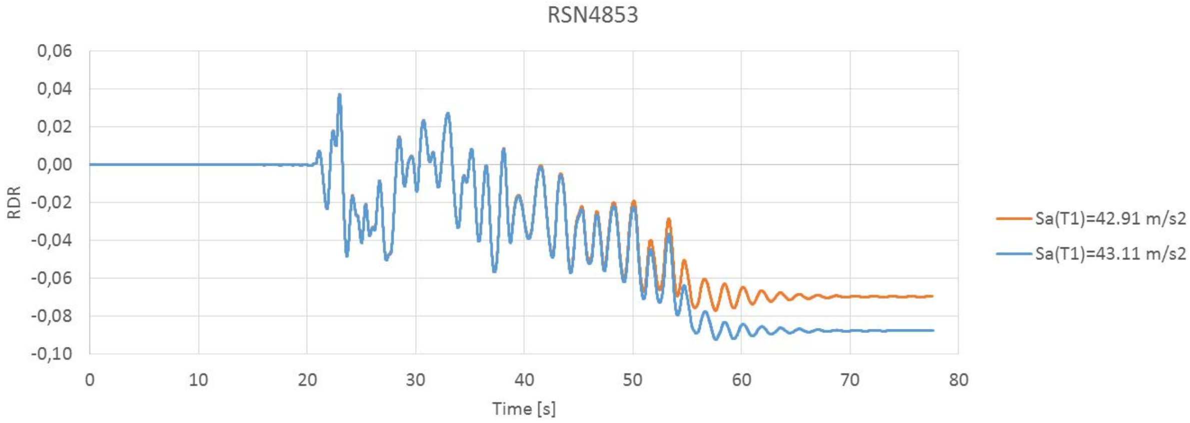

Figure 8.7: RDR Response of the last two converging scalings of RSN4853, the time-history is not showing a collapse behavior, however the structure is collapsed at RDR≈8.5%

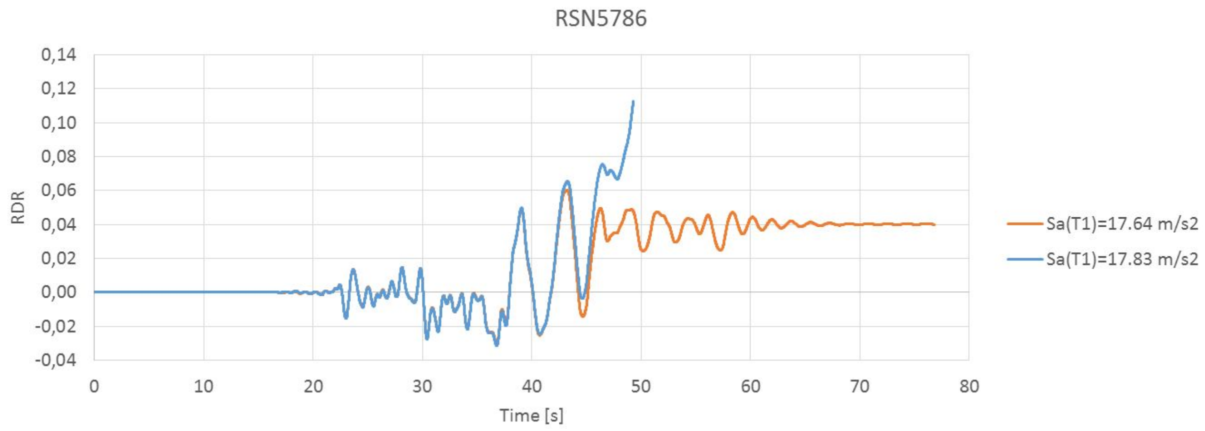

Figure 8.8: RDR Response of the last two scalings of RSN5786, resulting in collapse at $T \approx 50$ s

In Figure 8.9 the IDA curves with IDR as the DM are presented. The curves shows many of the same characteristics as the RDR plot in Figure 8.1, but clearly when looking at the *maximum interstorey drift ratio*, the DM is significantly higher. Figure 8.10 to 8.16 are depicting the maximum interstorey drift ratio for each of the selected ground motion records, at each floor. Clearly the collapse is initiated in the first floor for all ground motions. However, when looking at lower IM level, the drift in the upper floors are higher for both RSN724, RSN730 and RSN1634. The maximum interstorey drift ratio is in general highest for the first floor, then the second, third and lowest in the fourth floor. In Figure 8.9 the curves that are the highest on the IM axes shows hardening behavior, whilst the RSN68 and RSN169 are both softening cases. The RSN5786 cause somewhat softening behavior prior to the sudden decrease of DM. After the initial non-linearities for these records, they accelerate towards larger drift ratios, with little increase in IM, and eventually GI. Looking at the IDR in Figure 8.9, RSN730 and RSN1634 almost resembles a weaving behavior around the elastic slope. The weaving follows the equal displacement rule, which for moderate period structures, the non-linear global displacements can be approximated to the displacement from the elastic case [8].

The reason for these back and forth turns is that the structure in some segments or elements, experience an increase of the rate of DM accumulation and at other times a deceleration. This can stop or reverse the accumulation of DM and thus pull back the curve to lower DMs, as seen in Figure 8.1 and 8.9 [8], for the RSN5786 record. Severe hardening on the RDR and IDR curves in Figure 8.1 and 8.9, respectively is caused by the reduction of integration points, which is done to cope with the localization issues. This has been done manually in order to obtain convergence when the records have been scaled up and diverged.

Figure 8.10 to 8.16 are helpful in the determination of the collapsing floor, which in turn leads to global instability. As discussed earlier, the first floor is collapsing for all the recordings, but the response curve for the different floors has major differences. In Figure 8.10 it can be seen that the first floor columns are experiencing hardening behavior three times, after softening cases. The second floor is also experiencing major drift ratios after $S_d(T_1) > 20\,m/s^2$, although it is the first floor that is causing the structure to reach global dynamic instability. During the RSN169 earthquake record, it can be seen from Figure 8.11 that all the floors remain close to linear-elastic up to $S_d(T_1) \approx 10\,m/s^2$. An explanation for this behavior is likely to be period elongation: Looking at Figure 6.16 the RSN169 ground motion is the record with the lowest spectral acceleration in the range of $1.0s \leq T \leq 1.4s$, likely to be the elongated first period, which can cause the linear behavior seen in Figure 8.11. The snap-back turn in the first floor is likely to be numeric since the integration points are reduced to obtain convergence, as described previously in this section.

Figure 8.12 is showing the interstorey drift ratios for the RSN724 earthquake record. Note that the drift ratio for the second floor is higher than for the first floor, from $S_d(T_1) \approx 10m/s^2$ up to $S_d(T_1) \approx 33\,m/s^2$. This can be caused by contributions from higher order modes, which has higher spectral acceleration, but here as in the previous cases, the first floor is the floor with the highest drift ratios in the end. Severe hardening is also seen in most of the floors as well as snap-backs, which are caused by integration point reduction in the columns. Due to the RSN730 record, it is evident from Figure 8.13 that both the first and second floor experience major drift at the collapse IM, $S_d(T_1) \approx 45\,m/s^2$. Figure 8.14 is showing the response due to the RSN1634 motion record, and here it can be seen that all of the floors suffers from great drift ratios. The ultimate collapse is also here caused by local instability of the first floor. The response due to RSN4853, have moderate drift ratios for all floors, up to $S_d(T_1) \approx 20\,m/s^2$, when larger drifts occurs, as seen in Figure 8.15. The structure is experiencing a softening behavior prior to GI. In Figure 8.16, the IDA curves from the RSN5786 run are shown. The IDR for all floors are close to linear up to $S_d(T_1) \approx 10\,m/s^2$, where the first and second floor exhibits major drift ratios.

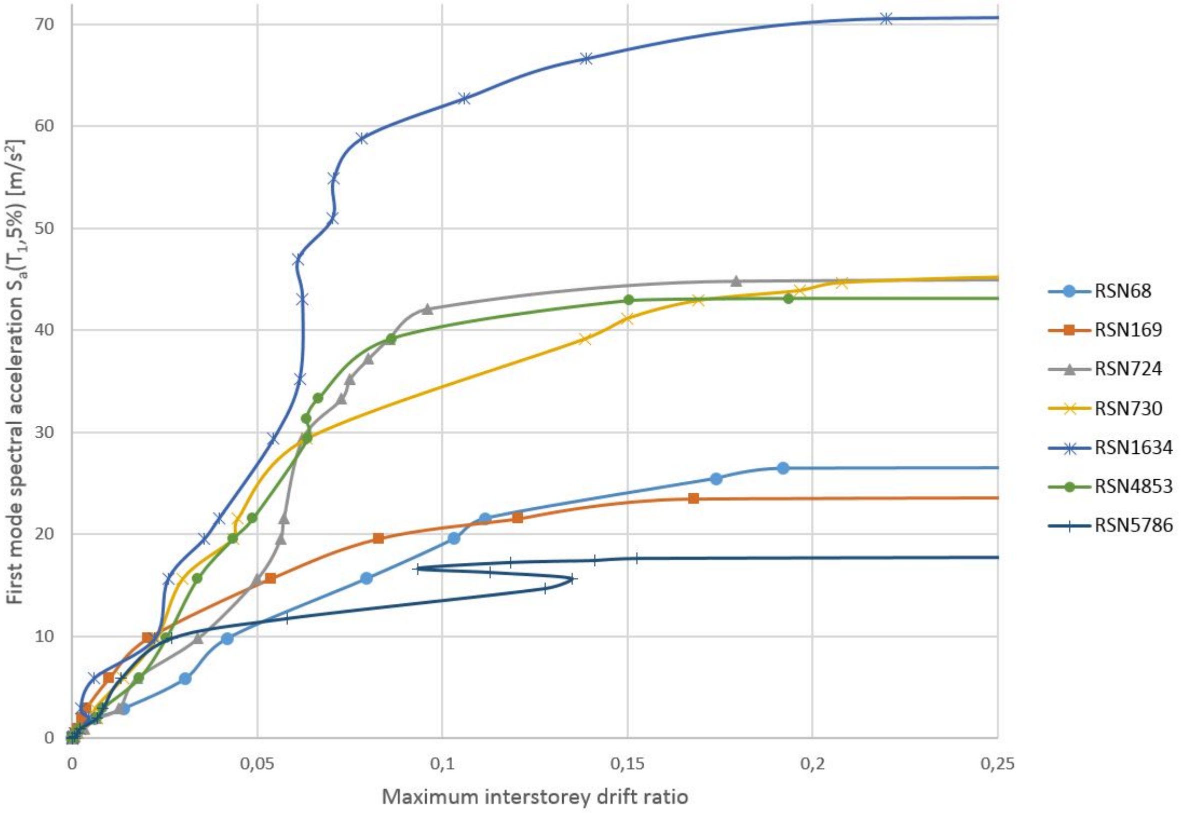

Figure 8.9: IDA curves showing maximum interstorey drift ratio for all the ground motion records.

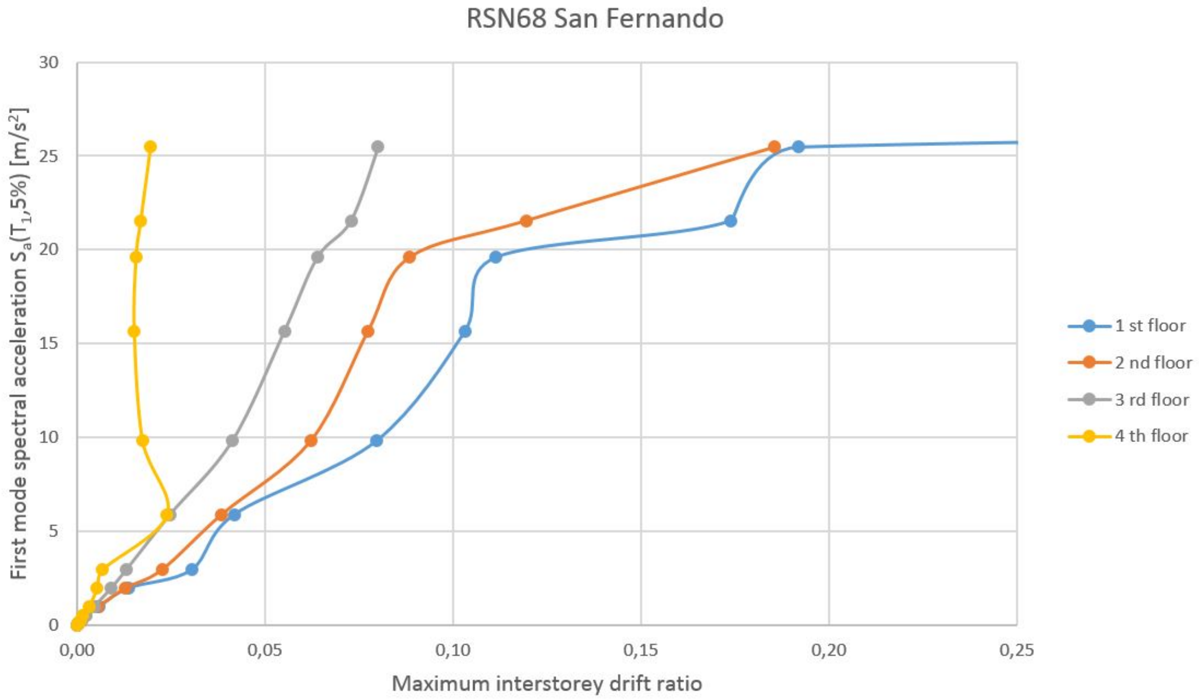

Figure 8.10: IDA curves showing maximum interstorey drift ratio for each floor, for the RSN68 record

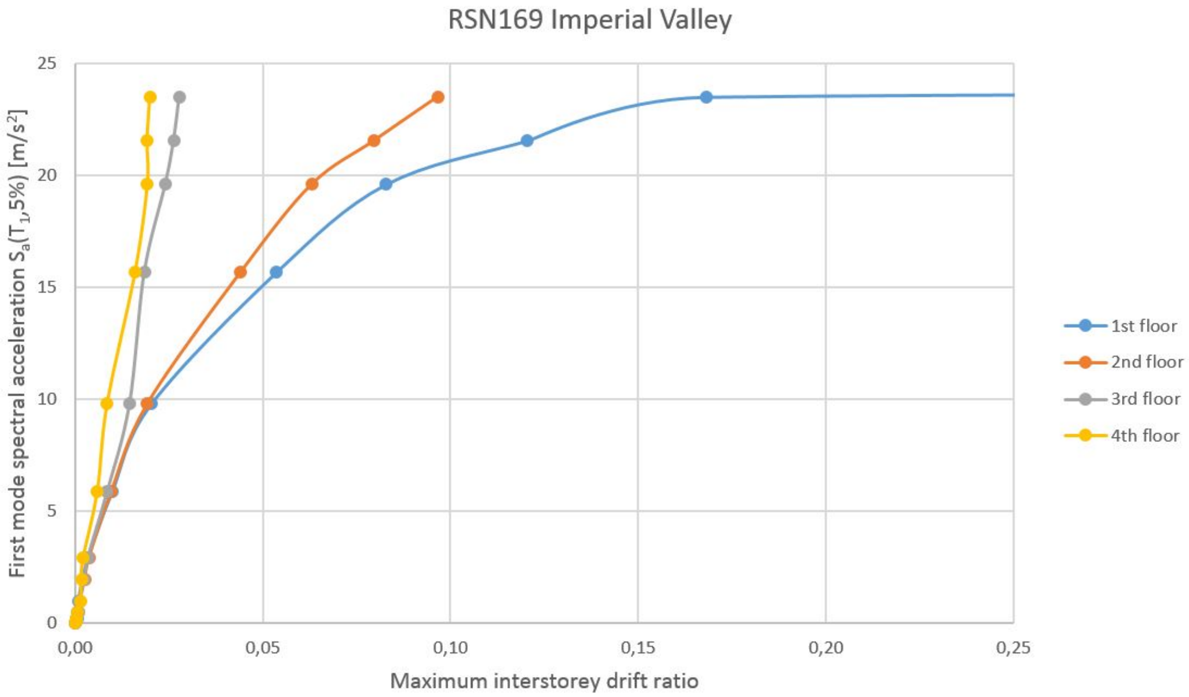

Figure 8.11: IDA curves showing maximum interstorey drift ratio for each floor, for the RSN169 record

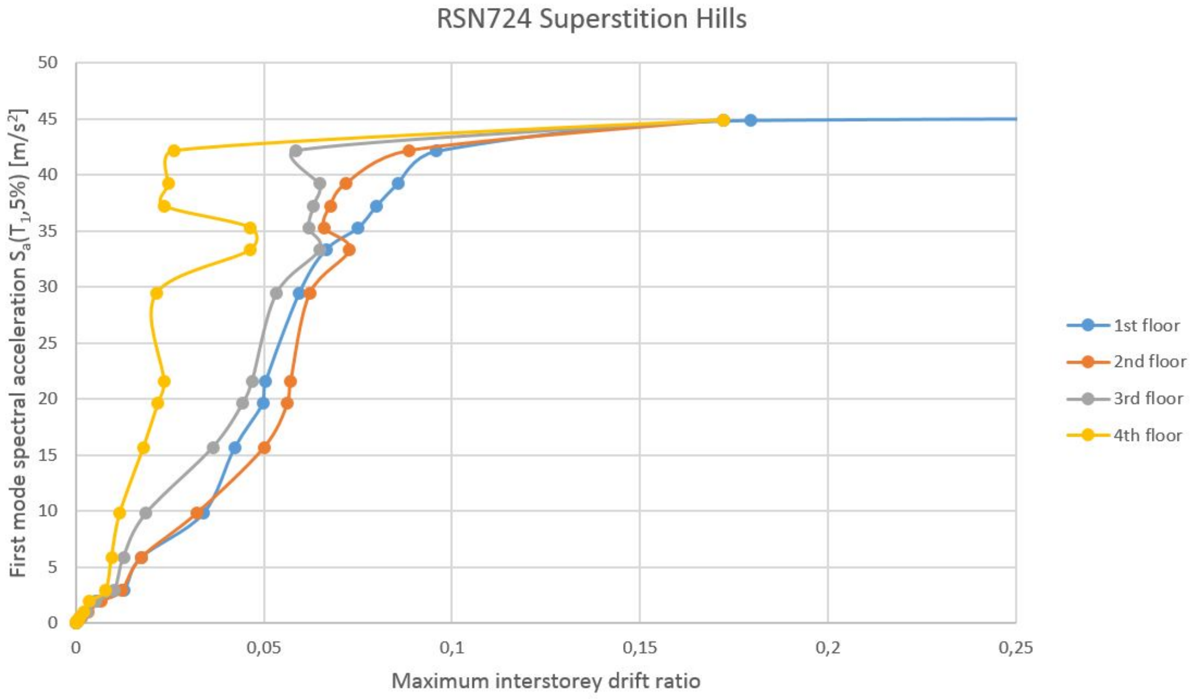

Figure 8.12: IDA curves showing maximum interstorey drift ratio for each floor, for the RSN724 record

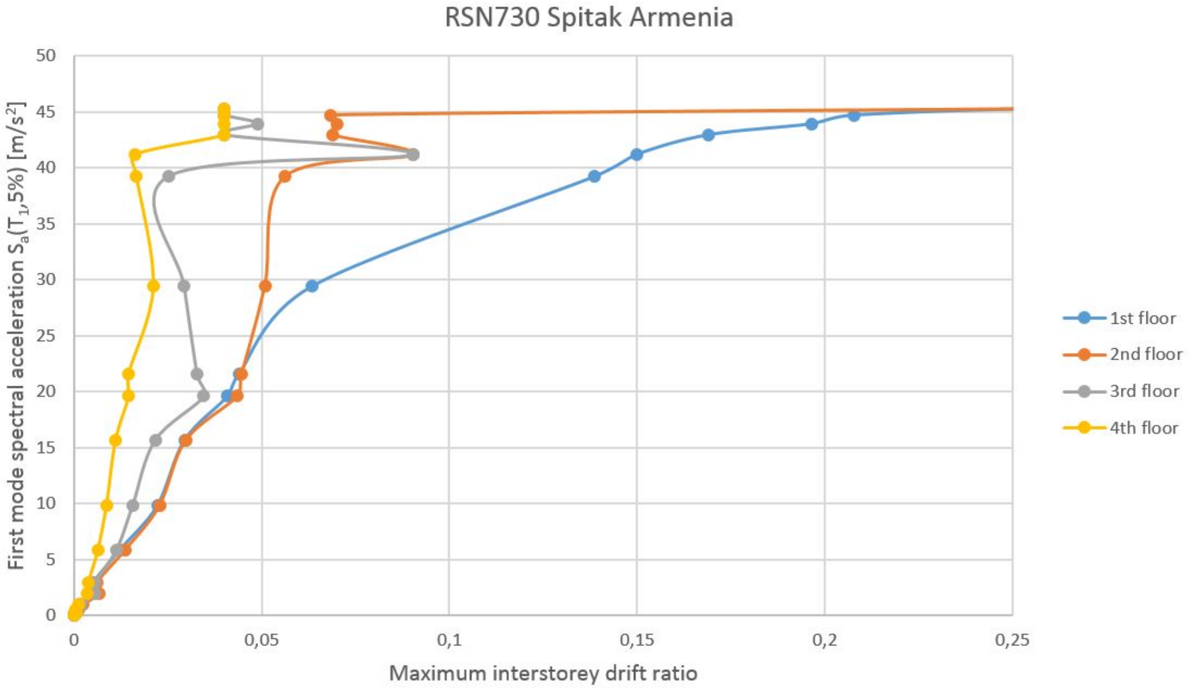

Figure 8.13: IDA curves showing maximum interstorey drift ratio for each floor, for the RSN730 record

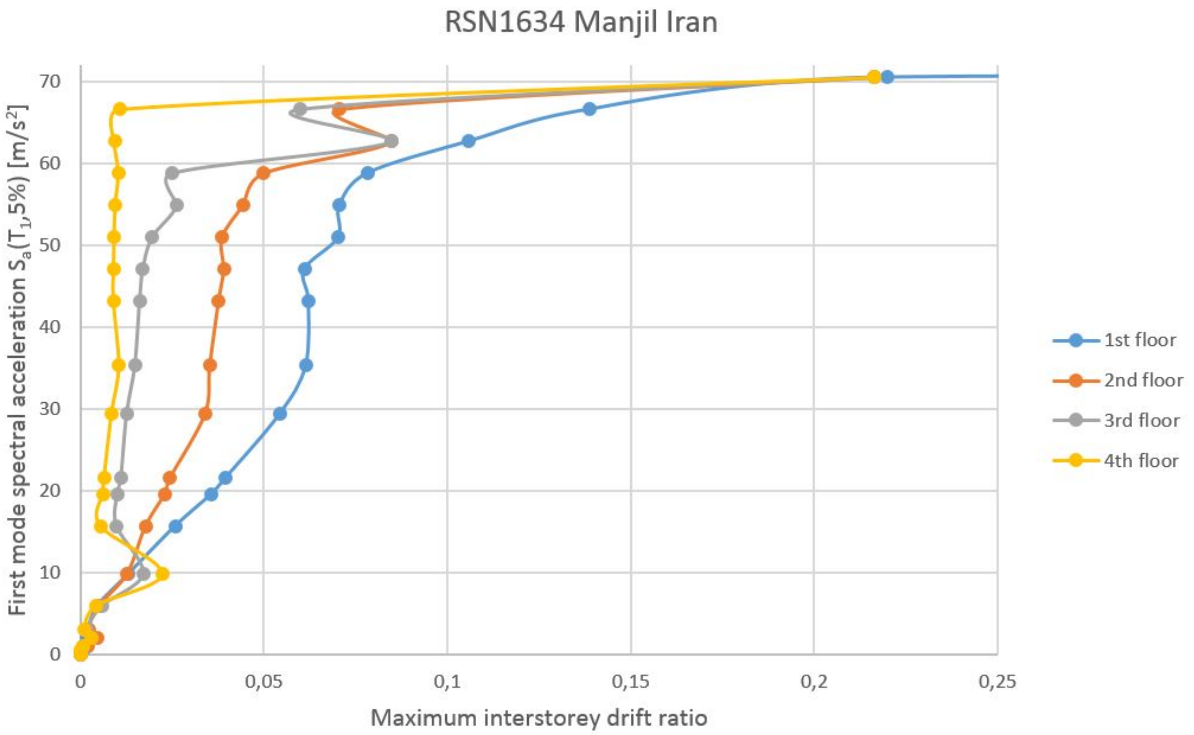

Figure 8.14: IDA curves showing maximum interstorey drift ratio for each floor, for the RSN1634 record

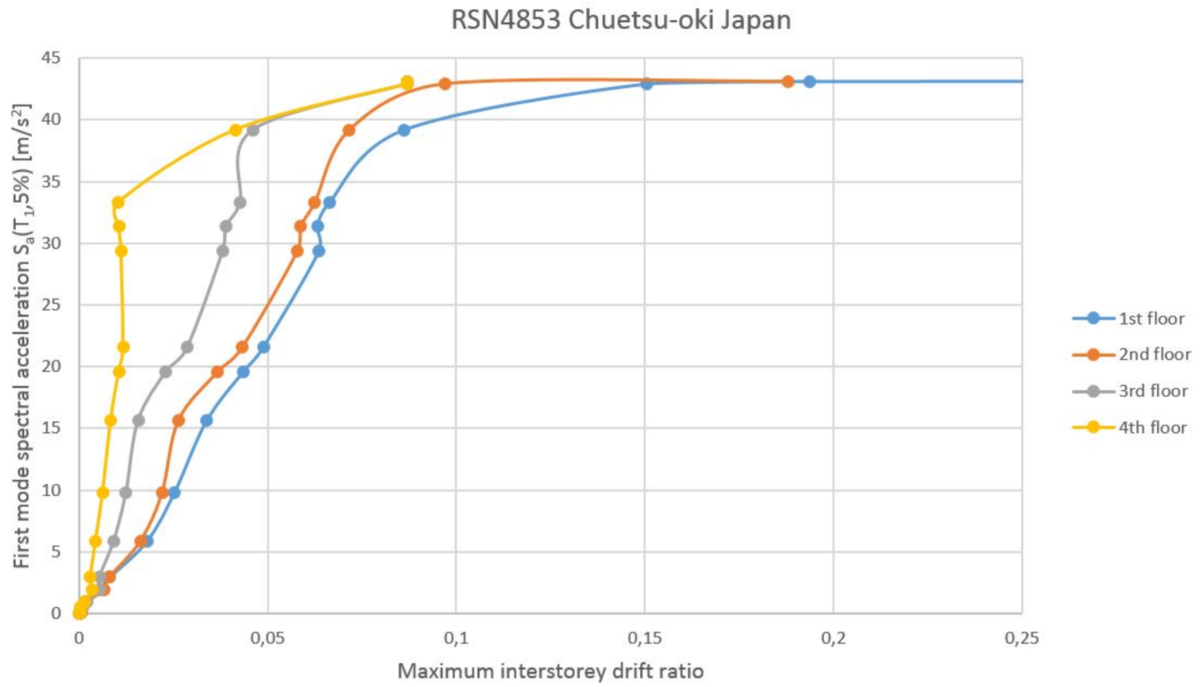

Figure 8.15: IDA curves showing maximum interstorey drift ratio for each floor, for the RSN4853 record

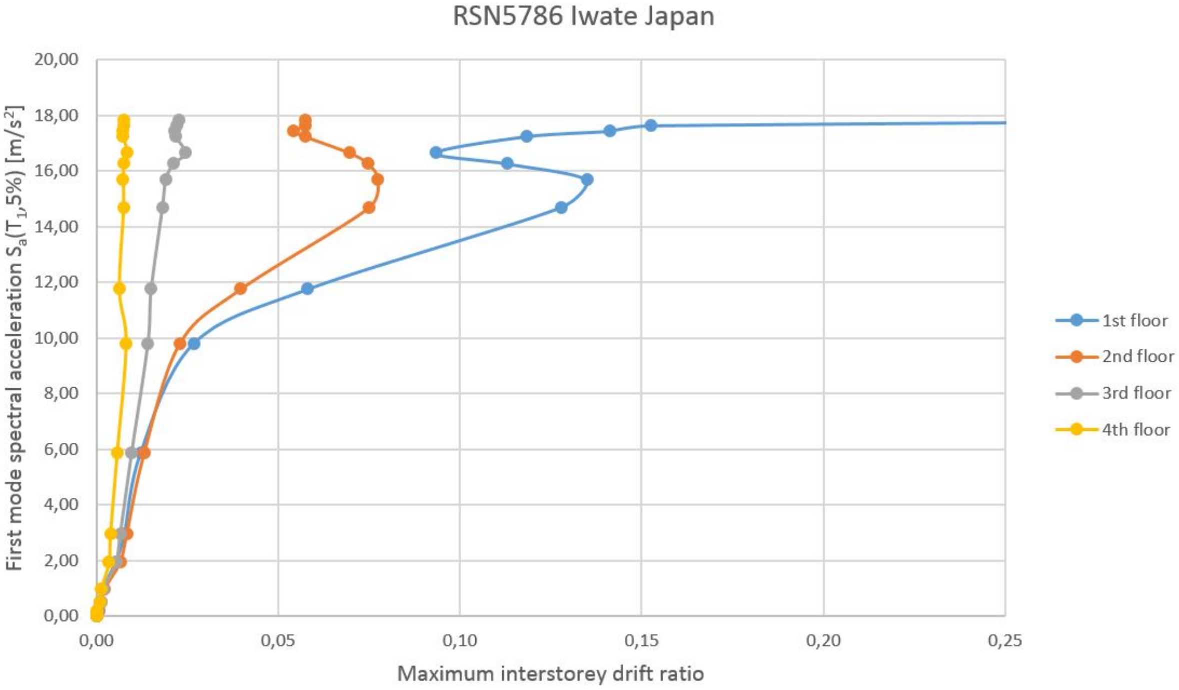

Figure 8.16: IDA curves showing maximum interstorey drift ratio for each floor, for the RSN5786 record

8.2 Probability of collapse and fragility curves

The assessment of probability of collapse from the different earthquake motions is presented in this section. In Figure 8.17 the collapse fragility curves are depicted. This gives a good picture of which first mode spectral acceleration levels cause collapse. Clearly, the different methods for fitting the fragility curves give different results. Recalling the three approaches presented in Chapter 2.1.2, the method using the median collapse IM as θ, and set the standard deviation to 0.4 as suggested by FEMA P695 [2] is the most conservative for most of the IM values. The method with the actual STD is barely more conservative for the lower IMs. As seen from Figure 8.17 the two procedures where the median is used in the creation of the CDF strongly agrees, and lies practically on top of each other. The mean method is the least conservative. It should be mentioned that an increase in number of selected earthquake motions would give more accurate CDF curves with data points from the empirical distribution spread along them, though due to the limited time, this has not been done.

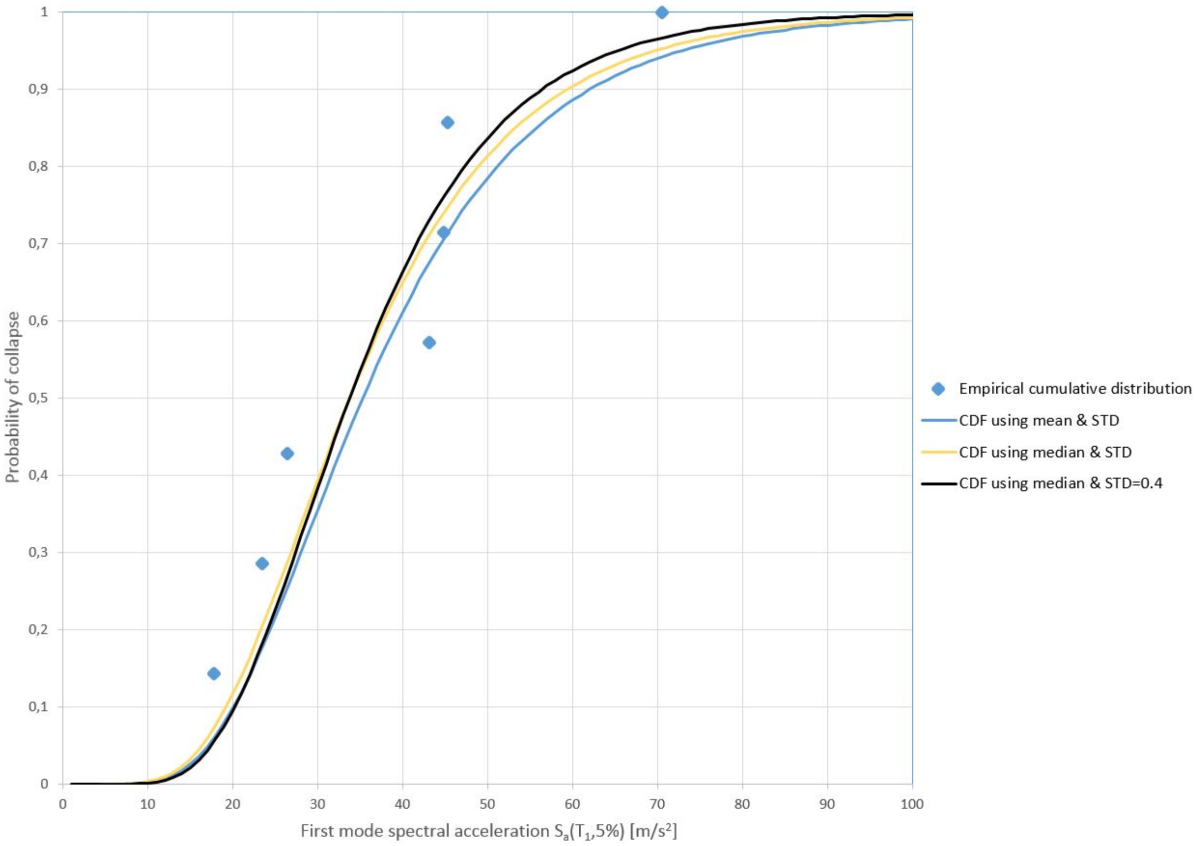

Figure 8.17: Fitted collapse fragility curves and the empirical cumulative distribution.

Chapter 9

Parameter study

9.1 Introduction

In order to both assess and verify the response of the structure, a parameter study is done. By introducing a deficiency in the structure, the response is to be assessed. All of the analyses that are presented here in this section are conducted using OpenSees. The weakness is imposed by increasing the height of the first floor from $4250mm$ to $6000mm$ without increasing the cross-section of the columns, nor changing the reinforcement, resulting in a softer building, and thus a higher first natural period. The NRHA has been conducted using $S_d(T_1, 5\%)$ due to the fact that the new building has not been designed according to Eurocode. By using S_d-scaling, it is expected that the results from the NRHA remains in the elastic range. The first four cracked natural periods for the new building are listed below. The change of the building is a realistic adjustment, since the first floor of both residential, and commercial office buildings often are higher. It is expected that the maximum base shear is lower and that lateral displacements are increased, thus the drift ratios are higher than before. Since the natural periods of the building are changed, the scaling factors need to be updated as well, in Table 9.1 the updated earthquake record scale factors are listed. Recalling Table 6.2 from Chapter 6, four out of seven scaling factor are increased. The scale factors are resulting in a spectral acceleration at the first natural period, $S_d(T_1, 5\%) = 1.458\, m/s^2$ for all the spectra. It should be mentioned that it is the same earthquake records as previously, obtained from PEER [17].

$$\mathbf{T} = [1.064 \quad 0.294 \quad 0.167 \quad 0.116]$$

The updated ground motions time histories are shown in Figure 9.1 to 9.7. In Figure 9.8 the revised scaled response spectra are depicted. Clearly a greater portion of the selected earthquake motions have an increased intensity when it comes to the spectral acceleration for the higher order modes (lower periods) than the response spectra for the original building. The change of the building is also resulting in a changed loading pattern for the SPO analysis, since this is applied using a modal pattern.

Table 9.1: Updated ground motion scaling factors, to match $S_d(T_1, 5\%) = 1.458\,m/s^2$

RSN	Scale factor
68	0.66
169	0.69
724	1.04
730	0.50
1634	1.01
4853	0.42
5786	0.36

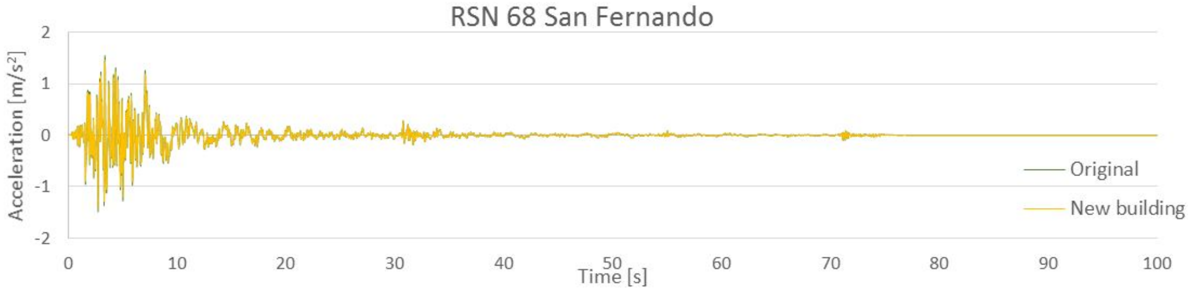

Figure 9.1: RSN68 Scaled ground motion time-history

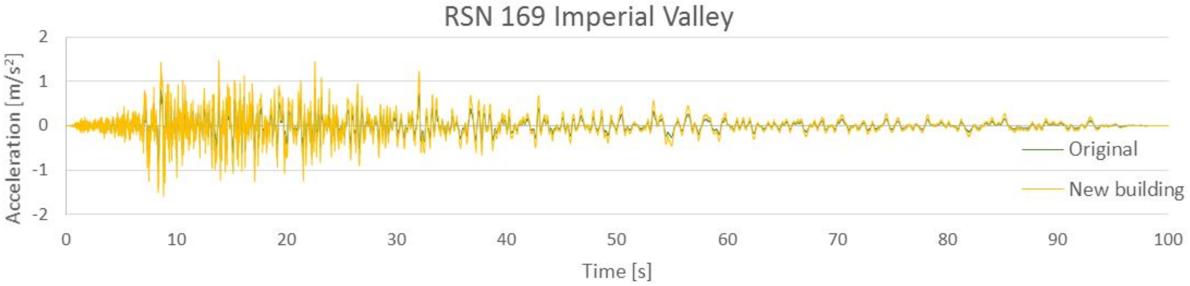

Figure 9.2: RSN169 Scaled ground motion time-history

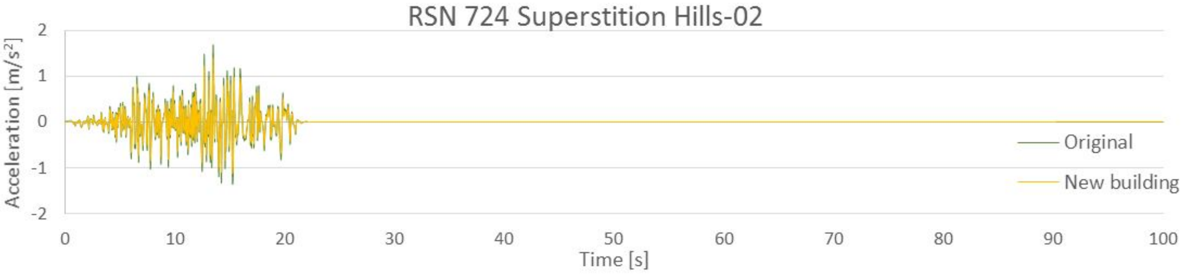

Figure 9.3: RSN724 Scaled ground motion time-history

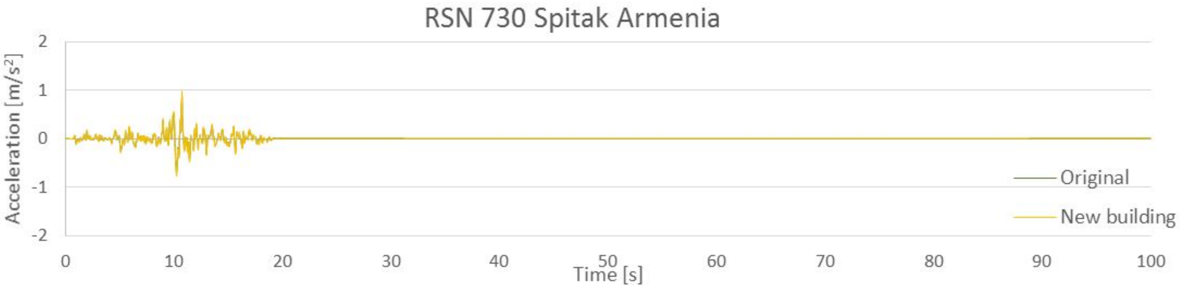

Figure 9.4: RSN730 Scaled ground motion time-history

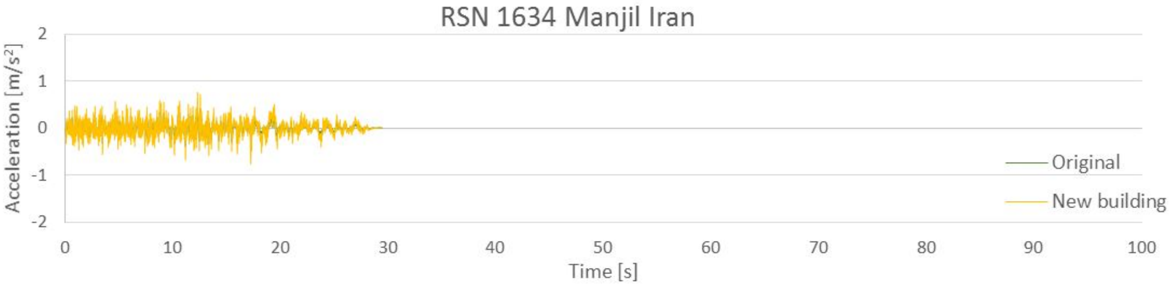

Figure 9.5: RSN1634 Scaled ground motion time-history

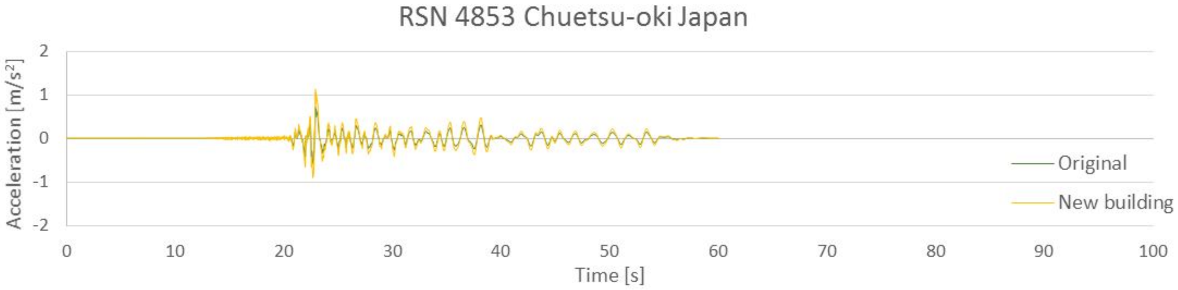

Figure 9.6: RSN4853 Scaled ground motion time-history

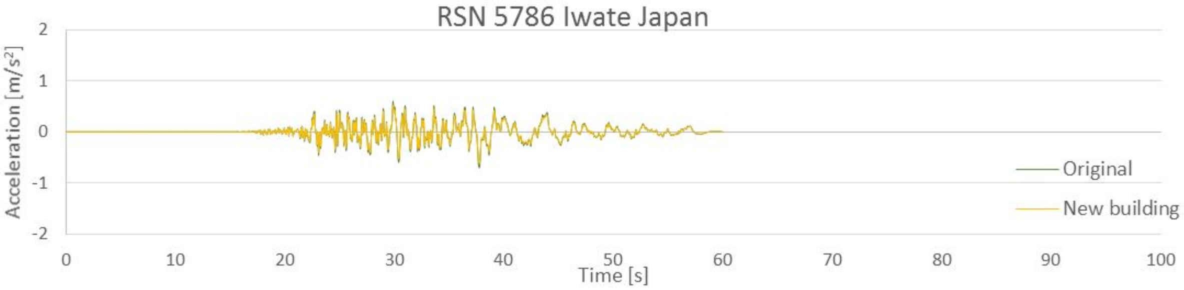

Figure 9.7: RSN5786 Scaled ground motion time-history

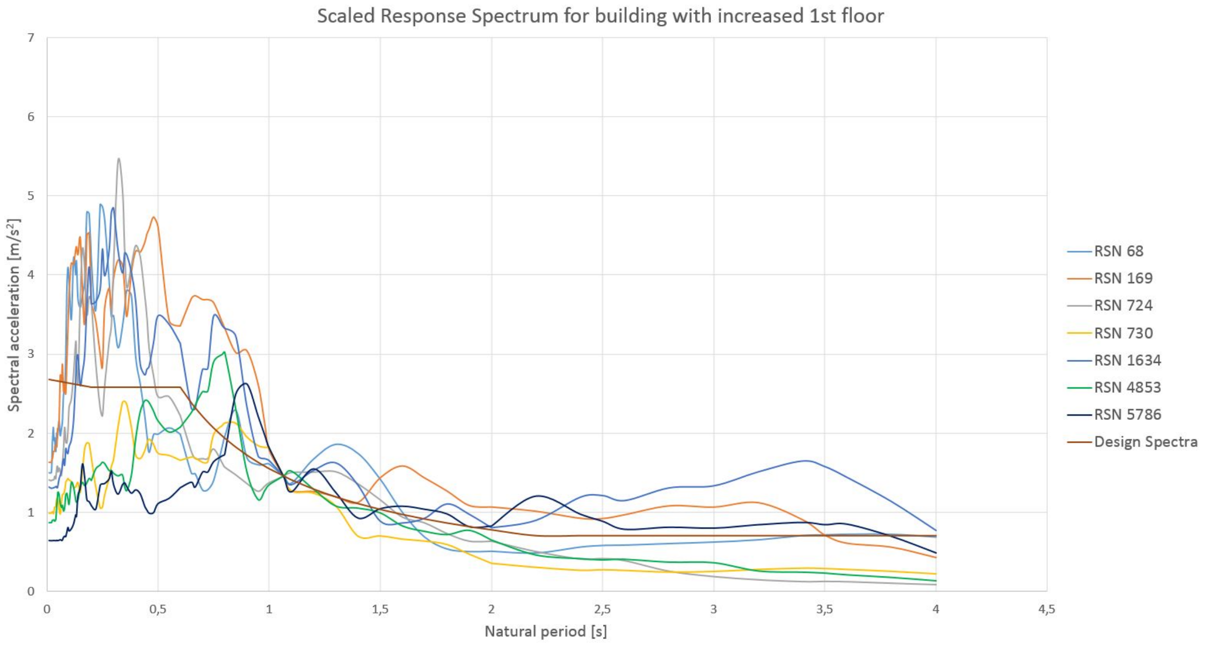

Figure 9.8: Scaled response spectra with $S_d(T_1, 5\%) = 1.458\, m/s^2$

9.2 Results and discussion

The results, here presented as base shear vs. RDR from both NRHA and SPO analysis, are shown in Figure 9.9. For comparison the results from the original building are also included.

The first floor of the building is increased with more than 40% without re-designing the load bearing columns and beams. Thus expecting that the capacity is significantly lower. Looking at the SPO curve in Figure 9.9, the maximum base shear is now 659 kN, recalling that the seismic base shear in the original building was significantly higher, namely 87 kN. The pushover curve is plotted until a loss of 20% of the maximum base shear. As expected, the base shear vs. RDR from the NRHA is pretty much the same as for the original building − none of the earthquake motions cause collapse. The structure is still in the linear-elastic region, and the NRHA results are spread around the linear part of the SPO curve. From the SPO curve one can observe that the global stiffness, here the tangent to the SPO curve, is reduced.

The IDA was also done for the new, updated structural model, and as for the other analyses, the capacity is clearly lower than for the original structure. In Figure 9.10 the IDA curves with the maximum roof drift ratio as DM, for the selected ground motions, scaled up and down from the initial $S_d(T_1, 5\%) = 1.458\, m/s^2$ are depicted. Clearly, when recalling Figure 8.1, one can see that the collapse IM is significantly lower. A good portion of the earthquake motions are causing hardening of the new building, as seen for the original. The new design is a typical *soft story* which is very unfortunate for seismic design and the capacity is significantly reduced.

Evidently RSN1634 is not the earthquake motion that is scaled the highest for the new building. Now, RSN724 is the IDA curve which is reaching the highest collapse IM. RSN724 is scaled up to $S_d(T_1, 5\%) = 50.45\, m/s^2$ until collapse is reached, which is a significantly lower IM than before. The reason for the change in collapse IMs, can be

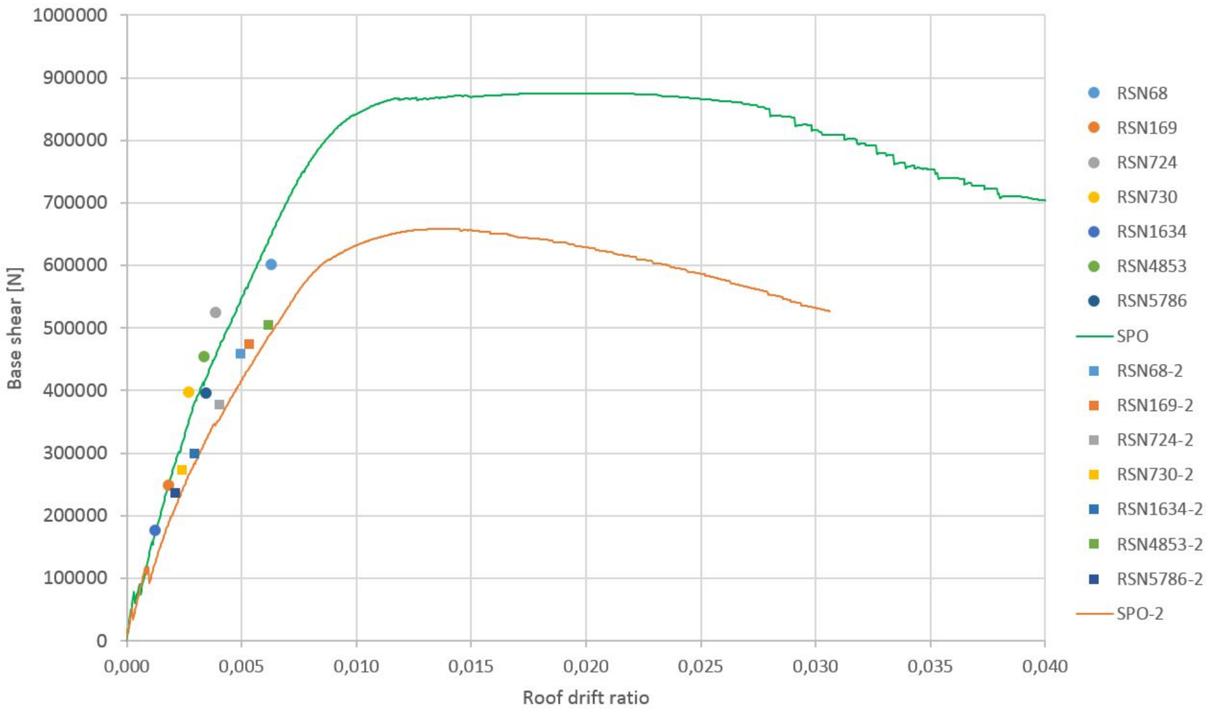

Figure 9.9: RDR from NRHA and SPO analysis, plotted with the results from the original building

explained by the scaled response spectra in Figure 9.8. Clearly, the building with the increased first floor is now much more exposed to the shorter periods, where the spectral acceleration is very high for most of the earthquake records, compared to the original spectra in Figure 6.16. Figure 9.11 illustrates the IDA curves with IDR as the DM.

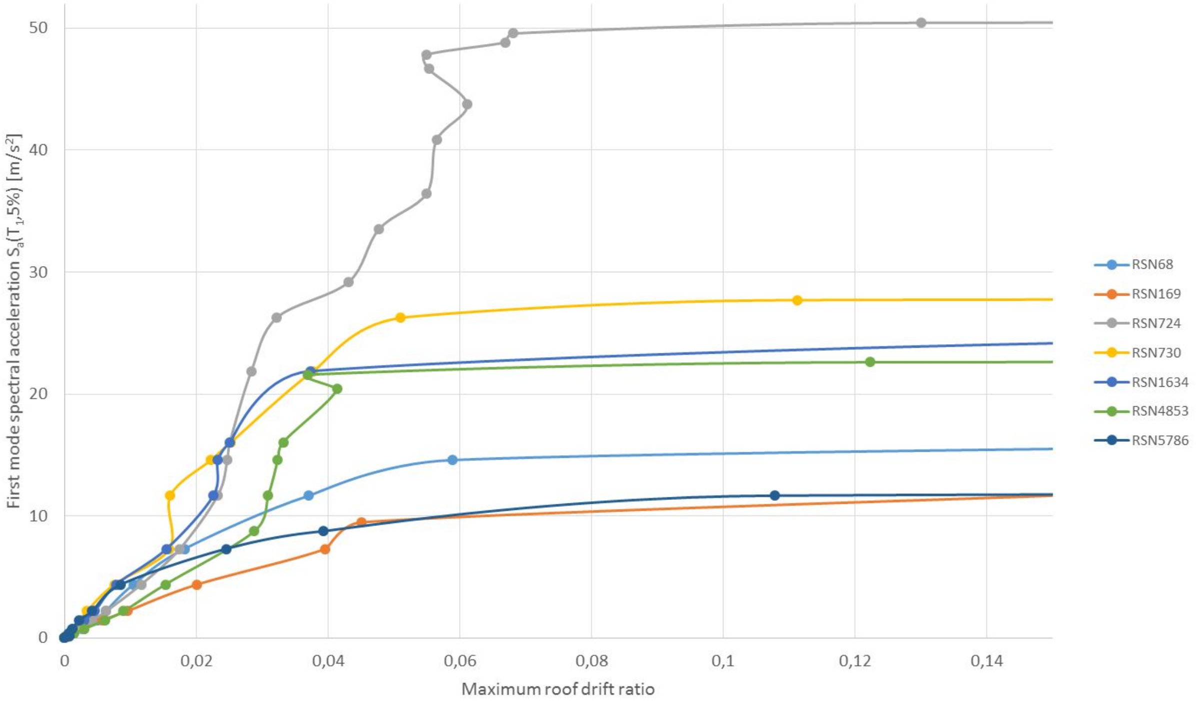

Figure 9.10: IDA curves showing maximum roof drift ratio, of the building with $T_1 = 1.064\,s$

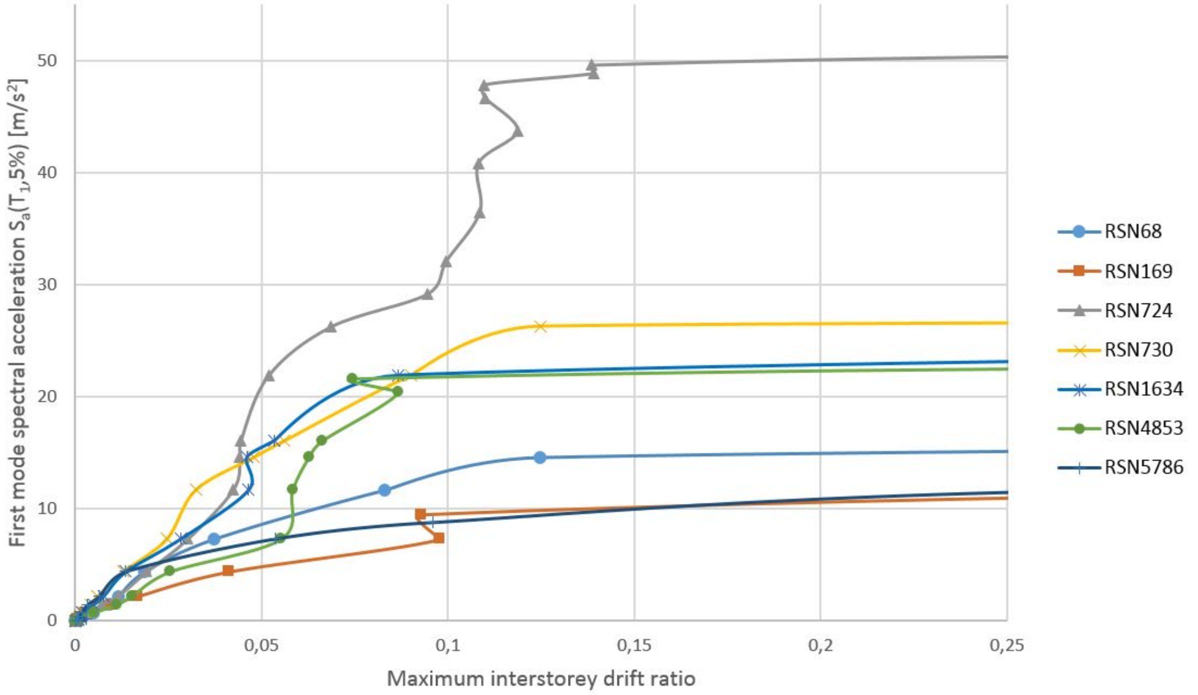

Figure 9.11: IDA curves showing maximum interstorey drift ratio, of the building with $T_1 = 1.064\,s$

9.3 Probability of collapse and fragility curves

In Figure 9.12 the fitted fragility curves and the empirical cumulative distribution are shown. Obviously, the probability of collapse is higher for the same spectral acceleration, compared to the original building. Here, the three curves obtained from the three approaches described in Chapter 2.1.2 are also included. Figure 9.13 is showing the fitted fragility curve and cumulative distribution for both of the buildings, and as discussed earlier, it is evident that the probability of collapse is higher for the new building, than for the original.

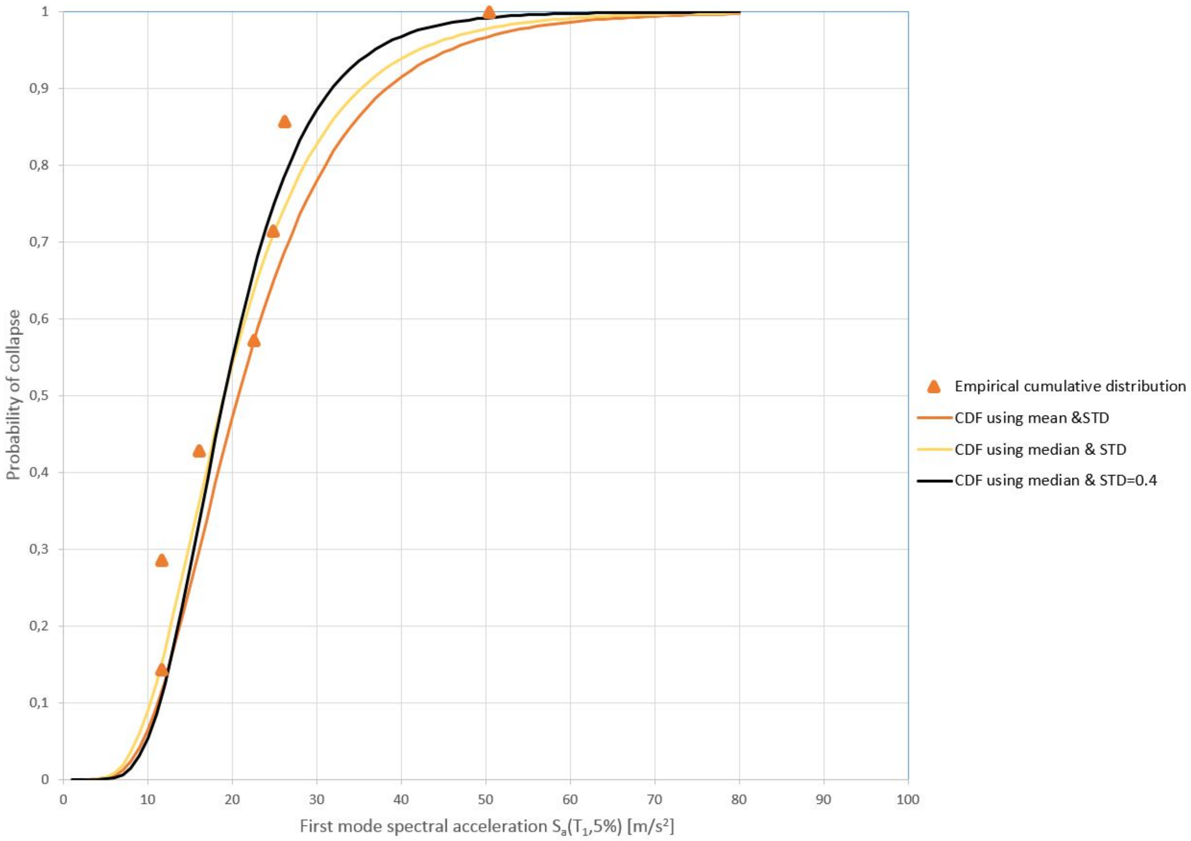

Figure 9.12: Fitted collapse Fragility curves and the empirical cumulative distribution for the building with $T_1 = 1.064\,s$

.

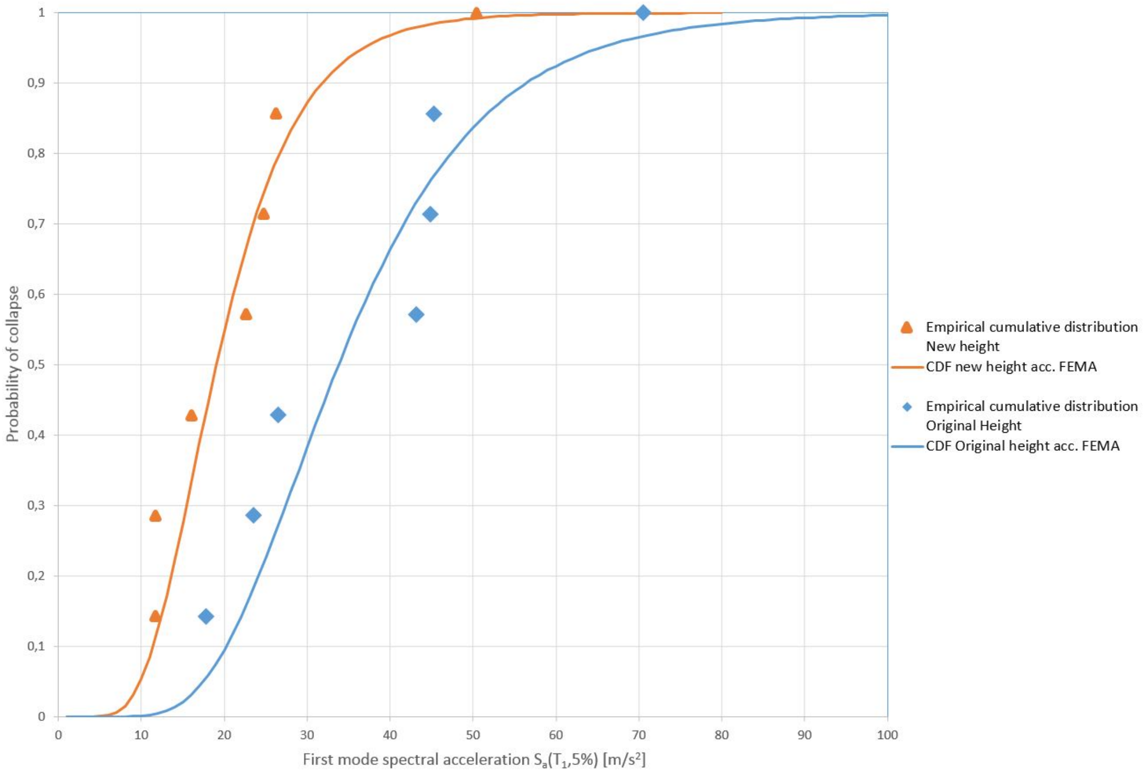

Figure 9.13: The fitted collapse fragility curves and the empirical cumulative distribution for both buildings

Chapter 10

Conclusion

Throughout the thesis the performance of the sample structure has been assessed using theory and advanced analysis methods. Performance based earthquake engineering is a research field in development, and analysis methods and procedures, as well as theory are constantly being developed and researched.

The theory that was presented in the Literature review has been applied and the results are presented and discussed in this thesis. The non-linear analyses conducted in this thesis are, as mentioned before, conducted using the characteristic material properties and not design values as used in the design chapter, giving stronger structural members. Both the non-linear material model applied here and the advanced analyses and integration schemes available in the OpenSees database, are important factors for estimating the actual performance of the building.

The over-capacity of structures designed according to Eurocode is one of the most important findings. It was expected that a Eurocode compliant building would be on the conservative side. However, performance-based earthquake engineering revealed that the building had significant higher collapse capacity. The non-linear static analysis results from both OpenSees and Seismostruct revealed good ductile behavior and a significant over-strength factor.

The non-linear response history analyses results were still in the elastic range for the S_d-scaling, however when the behavour factor, q was not accounted for in the response spectra, ductile, behavour occurred in the NRHA as well. The IDA revealed that the structure had tremendous amount of capacity. The sample structure was able to withstand large inelastic deformations and drifts prior to global instability and collapse in the IDA. The probabilistic approach using fragility curves illustrates the probability of collapse for the different spectral accelerations, rooted at the fundamental period. Fragility fitting is a reasonable approach for post-processing the results. The results from the parameter study were as expected: increasing the first floor without re-designing the columns and beams gives significantly lower collapse capacity.

The number of records chosen is a factor that is very likely to give refined results, especially for the IDA and the fragility assessment. The concrete material model and the element formulation have in some cases caused convergence issues. This has been dealt with by reducing the number of integration points. An alternative would be using a moment curvature relationship instead of the *Concrete04* material model. For further work on the subject it is recommended that the number of selected ground motion are increased in order to increase accuracy of the results.

Still a field under research, *PBEE* is a reliable approach for assessing the structural capacity. Effective and illustrative methods for post-processing the results and actual capacity are within reach – not just for academic purposes, but for the industry as well.

Bibliography

[1] Mander, J. B., Priestley, M. J., & Park, R. (1988). Theoretical stress-strain model for confined concrete. Journal of structural engineering, 114(8), 1804-1826.

[2] Federal Emergency Management Agency (FEMA). (2009). P695: Quantification of Building Seismic Performance Factors.

[3] Federal Emergency Management Agency (FEMA). (2005). P440: Improvement of Nonlinear Static Seismic Analysis Procedures

[4] Norge, Standard. NS-EN 1990:2002: Eurokode: Grunnlag for prosjektering av konstruksjoner (2008).

[5] Norge, Standard. NS-EN 1998-1: 2004: Eurokode 8: Prosjektering av konstruksjoner for seismisk påvirkning, Del 1: Allmenne regler, seismiske laster og regler for bygninger (2009).

[6] Norge, Standard. NS-EN 1992-1-1: 2004+ NA: 2008: Eurokode 2: Prosjektering av betongkonstruksjoner, Del 1-1: Allmenne regler og regler for bygninger. (2008).

[7] Pinho, R. (2007). Nonlinear dynamic analysis of structures subjected to seismic action (pp. 63-89). Springer Vienna.

[8] Vamvatsikos, D., & Cornell, C. A. (2002). Incremental dynamic analysis. Earthquake Engineering & Structural Dynamics, 31(3), 491-514.

[9] Vamvatsikos, D., & Fragiadakis, M. (2010). Incremental dynamic analysis for estimating seismic performance sensitivity and uncertainty. Earthquake Engineering and Structural Dynamics, 39(2), 141-163.

[10] Cook, R. D. (2007). Concepts and applications of finite element analysis. John Wiley & Sons.

[11] Baker,W. Jack (2015). Efficient Analytical Fragility Function Fitting Using Dynamic Structural Analysis. Earthquake Spectra, Volume 31, No. 1, 579-599.

[12] Moehle, J. P. (2008, October). Performance-based seismic design of tall buildings in the US. In 14th World Conference on Earthquake Engineering (CD), Beijing, China.

[13] Cemalovic, M. Earthquake analysis of structures using Non-Linear models (2015)

[14] A. Gharakhanloo. (2014)Distributed and concentrated inelasticity beam-column elements used in earthquake engineering.

[15] EFEHR, The 2013 European Seismic Hazard Model (ESHM13), $http://www.efehr.org:8080/jetspeed/portal/hazard.psml$ (Downloaded 09.02.16)

[16] Erduran, E. (2012). Evaluation of Rayleigh damping and its influence on engineering demand parameter estimates. Earthquake Engineering & Structural Dynamics, 41(14), 1905-1919.

[17] Ancheta, Bozorgnia, Darragh, Silva,Chiou,Stewart & Idriss, (2012). PEER NGA-West2 database: A database of ground motions recorded in shallow crustal earthquakes in active tectonic regions. In Proceedings, 15th World Conference on Earthquake Engineering.

[18] Calabrese, A., Almeida, J. P., & Pinho, R. (2010). Numerical issues in distributed inelasticity modeling of RC frame elements for seismic analysis. Journal of Earthquake Engineering, 14(S1), 38-68.

[19] SeismoSoft, S. (2010). SeismoStruct is a FEM-program developed for the analytical assessment of structures subjected to earthquake strong motion. Seismosoft Ltd, Version 7.0.6, 2016

[20] OpenSees, The Open System for Earthquake Engineering Simulation (OpenSees). OpenSees is a software framework for developing applications to simulate the performance of structural and geotechnical systems subjected to earthquakes. Pacific Earthquake Engineering Research Center, Version 2.4.6, 2013.

[21] Vecchio, F. J. (2001). Non-linear finite element analysis of reinforced concrete: at the crossroads?. Structural Concrete, 2(4), 201-212.

[22] Fajfar, P. & Dolsek, M. (2014). Pushover-Based Analysis in Performance-Based Seismic Engineering – A View from Europe. M. Fischinger (ed.), Performance-Based Seismic Engineering: Vision for an Earthquake Resilient Society, Geotechnical, Geological and Earthquake Engineering 32, Chapter 19.

[23] A.M. Mwafy, A.S. Elnashai (2000). Static pushover versus dynamic collapse analysis of RC buildings, Engineering Structures publ. 23 (2001) 407–424

[24] Raghunandan, M. Eera and Liel, Abbie B (2013). Effect of ground motion duration on earthquake-induced structural collapse, Structural Safety vol. 41, 119-133, Elsevier

[25] J. Hancock, J.J. Bommer and M. Eeri (2006). A State-of-Knowledge Review of the Influence of Strong-Motion Duration on Structural Damage, Earthquake Spectra vol. 22, No.3, 827-845

Appendix

OpenSees Scripts

```
######################################################################################
#
#2D Model of 4 Storey 5 bay frame
#Nina Øystad-Larsen & Fredrik Bjercke
#7/1/2016
#Metric units mm, g, N, sec
#
######################################################################################
wipe;
#Model Builder for 2D
model BasicBuilder -ndm 2 -ndf 3
set numModes 4;

#Create the nodes
source nodes.tcl

#Create the Materials
source materials.tcl

#Create the sections
source sections.tcl

#Create the Elements
source assignment.tcl

#Define recorders
source Recorder.tcl

#Determine eigenvalues for uncracked system
source Eigenvalues.tcl

#Apply the Gravity Analysis
source GravityAnalysis.tcl

#Determine eigenvalues for system with cracks from gravity loads
source Eigenvalues.tcl

#Apply the Pushover Analysis
source PushoverAnalysis.tcl

#Apply the response history analysis
source NRHA.tcl

#Determine eigenvalues for system with cracks from the seismic analysis
source Eigenvalues.tcl

wipe;
```

```
###########################################################################################
#
#Nodes of the 2D Model of 4 Story Optimal Building axis B
#Nina Øystad-Larsen & Fredrik Bjercke
#7/1/2016
#Metric units mm, ton, N, sec
#
###########################################################################################

set x1 0.0;     # mm
set x2 6000.0;  # mm
set x3 12000.0; # mm
set x4 16500.0; # mm
set x5 22500.0; # mm
set x6 28500.0; # mm
set z1 0.0;     # mm
set z2 4250.0;  # mm
set z3 7750.0;  # mm
set z4 11250.0; # mm
set z5 14750.0; # mm

set colWidth        400.0; # mm
set colHeight       400.0; # mm
set colWidthBdr     350.0; # mm
set colHeightBdr    350.0; # mm
set beamWidth       300.0; # mm
set beamHeight      500.0; # mm
set beamWidthRoof   260.0; # mm
set beamHeightRoof  450.0; # mm

# W/g = (0.001 tons/kg) x (N/mm3)/(m/s2) = tons/mm3
set massDens [expr 0.001*0.000025/9.81];

# Mass of columns in 1st storey joints - (0.001 tons/kg) x (kg/mm3)*mm*mm2 = tons
set mc1 [expr $massDens*($z2*$colWidth*$colHeight/2+($z3-$z2)*pow($colWidth,2)/2)];

# Mass of columns in 2nd storey joints - (0.001 tons/kg) x (kg/mm3)*mm*mm2 = tons
set mc2 [expr $massDens*(($z3-$z2)*pow($colWidth,2)/2+($z4-$z3)*pow($colWidth,2)/2)];

# Mass of columns in 3rd storey joints - (0.001 tons/kg) x (kg/mm3)*mm*mm2 = tons
set mc3 [expr $massDens*(($z4-$z3)*pow($colWidth,2)/2+($z5-$z4)*pow($colWidth,2)/2)];

# Mass of columns in roof joints - (0.001 tons/kg) x (kg/mm3)*mm*mm2 = tons
set mc4 [expr $massDens*($z5-$z4)*pow($colWidth,2)/2];

# Mass from slab and eigenweight of beams - (0.001 tons/kg) x (N/mm)/(m/s2) = tons/mm
set m123 [expr 0.001*32.164/9.81+$massDens*$beamWidth*($beamHeight-150.0)];

# Mass from slab and eigenweight of beams - (0.001 tons/kg) x (N/mm)/(m/s2) = tons/mm
set mroof [expr 0.001*28.900/9.81+$massDens*$beamWidth*($beamHeight-150.0)];


#Define the Ground Level Nodes
#node $nodeTag (ndm $coords) <-mass (ndf $MassValues)>
node 1 $x1  $z1 -mass   0.0 0.0 0.0
node 2 $x2  $z1 -mass   0.0 0.0 0.0
node 3 $x3  $z1 -mass   0.0 0.0 0.0
node 4 $x4  $z1 -mass   0.0 0.0 0.0
node 5 $x5  $z1 -mass   0.0 0.0 0.0
node 6 $x6  $z1 -mass   0.0 0.0 0.0

#Define the First Story Nodes
#node $nodeTag (ndm $coords) <-mass (ndf $MassValues)>
node 11 $x1 $z2 -mass   [expr $m123*($x2-$x1)/2.0+$mc1] 0.0 0.0
node 12 $x2 $z2 -mass   [expr $m123*($x3-$x1)/2.0+$mc1] 0.0 0.0
node 13 $x3 $z2 -mass   [expr $m123*($x4-$x2)/2.0+$mc1] 0.0 0.0
node 14 $x4 $z2 -mass   [expr $m123*($x5-$x3)/2.0+$mc1] 0.0 0.0
node 15 $x5 $z2 -mass   [expr $m123*($x6-$x4)/2.0+$mc1] 0.0 0.0
node 16 $x6 $z2 -mass   [expr $m123*($x6-$x5)/2.0+$mc1] 0.0 0.0
```

```
#Define the Second Story Nodes
#node $nodeTag (ndm $coords) <-mass (ndf $MassValues)>
node 21 $x1 $z3 -mass   [expr $m123*($x2-$x1)/2.0+$mc2] 0.0 0.0
node 22 $x2 $z3 -mass   [expr $m123*($x3-$x1)/2.0+$mc2] 0.0 0.0
node 23 $x3 $z3 -mass   [expr $m123*($x4-$x2)/2.0+$mc2] 0.0 0.0
node 24 $x4 $z3 -mass   [expr $m123*($x5-$x3)/2.0+$mc2] 0.0 0.0
node 25 $x5 $z3 -mass   [expr $m123*($x6-$x4)/2.0+$mc2] 0.0 0.0
node 26 $x6 $z3 -mass   [expr $m123*($x6-$x5)/2.0+$mc2] 0.0 0.0

#Define the Third Story Nodes
#node $nodeTag (ndm $coords) <-mass (ndf $MassValues)>
node 31 $x1 $z4 -mass   [expr $m123*($x2-$x1)/2.0+$mc3] 0.0 0.0
node 32 $x2 $z4 -mass   [expr $m123*($x3-$x1)/2.0+$mc3] 0.0 0.0
node 33 $x3 $z4 -mass   [expr $m123*($x4-$x2)/2.0+$mc3] 0.0 0.0
node 34 $x4 $z4 -mass   [expr $m123*($x5-$x3)/2.0+$mc3] 0.0 0.0
node 35 $x5 $z4 -mass   [expr $m123*($x6-$x4)/2.0+$mc3] 0.0 0.0
node 36 $x6 $z4 -mass   [expr $m123*($x6-$x5)/2.0+$mc3] 0.0 0.0

#Define the Fourth Story (=Roof) Nodes
#node $nodeTag (ndm $coords) <-mass (ndf $MassValues)>
node 41 $x1 $z5 -mass   [expr $mroof*($x2-$x1)/2.0+$mc4] 0.0 0.0
node 42 $x2 $z5 -mass   [expr $mroof*($x3-$x1)/2.0+$mc4] 0.0 0.0
node 43 $x3 $z5 -mass   [expr $mroof*($x4-$x2)/2.0+$mc4] 0.0 0.0
node 44 $x4 $z5 -mass   [expr $mroof*($x5-$x3)/2.0+$mc4] 0.0 0.0
node 45 $x5 $z5 -mass   [expr $mroof*($x6-$x4)/2.0+$mc4] 0.0 0.0
node 46 $x6 $z5 -mass   [expr $mroof*($x6-$x5)/2.0+$mc4] 0.0 0.0

#Single Point Constraints
fix 1 1 1 1
fix 2 1 1 1
fix 3 1 1 1
fix 4 1 1 1
fix 5 1 1 1
fix 6 1 1 1

puts "finished creating the nodes, masses and boundary conditions..."
```

```
########################################################################################
#
#Materials for the 2D Model of 3 Story frame
#Nina Øystad-Larsen & Fredrik Bjercke
#7/1/2016 Revised 20/2/2016
#Metric units mm, g, N, sec, MPa
#
########################################################################################


# General concrete and reinforcement parameters
set kam8 8.0;   set Akam8  [expr 3.14159*($kam8/2.0)*($kam8/2.0)];
set kam10 10.0; set Akam10 [expr 3.14159*($kam10/2.0)*($kam10/2.0)];
set kam16 16.0; set Akam16 [expr 3.14159*($kam16/2.0)*($kam16/2.0)];
set kam18 18.0; set Akam18 [expr 3.14159*($kam18/2.0)*($kam18/2.0)];
set kam20 20.0; set Akam20 [expr 3.14159*($kam20/2.0)*($kam20/2.0)];
set kam25 25.0; set Akam25 [expr 3.14159*($kam25/2.0)*($kam25/2.0)];
set kam32 32.0; set Akam32 [expr 3.14159*($kam32/2.0)*($kam32/2.0)];

set fcm [expr -30.0];           #Value of C30/37 cylinder compressive strength from EN
    1992-1-1 Table 3.1. N/mm2
set fctm [expr 2.9];            #Mean value of axial tensile strength of C30/37. N/mm2
set Ec 33000.0;                 #For C30/37 according to EN 1992-1-1 Table 3.1. N/mm2
set epsc1 [expr -2.2/1000.0];   #Compressive strain in concrete at peak stress from EN
    1992-1-1 Table 3.1
set epscu [expr -3.5/1000.0];   #Ultimate compressive strain in concrete from Table 3.1
    in EN 1992-1-1. Mander is not applied due to complexity
set epsctu [expr $fctm/$Ec];    #Tensile strain in concrete at peak stress
set nu 0.0;                     #For cracked concrete, taken from EN 1992-1-1 section
    3.1.3(4)

set fyk [expr 500.0];           #B500NC  N/mm2
set Es 200000.0;                #EN 1992-1-1 section 3.2.7(4). N/mm2
set epsuk [expr 7.5/100.0];     #Characteristic strain in steel at maximum force
    according to EN 1992-1-1 Table C.1. This is not to be confused with the yield strain,
    which is [expr $fyk/$Es] according to EN 1992-1-1 Figure 3.8.
set haRatio 0.005;              #To avoid convergence issues.
set mu [expr $epsuk/$fyk/$Es];  #EN 1992-1-1 Figure 3.8


########################################################################################

# Cover concrete Unconfined. according to mander:
#                          $matTag $fc          $ec          $ecu  $Ec <$fct $et>
#OLD: uniaxialMaterial Concrete04  1     $fcm $epsc1 $epscu $Ec $fctm $epsctu

uniaxialMaterial Concrete04  1     -35.59479775 -0.001977329 -0.006 32838.02131 $fctm
    $epsctu

########################################################################################
    #
########################################################################################
    #

# Confined concrete in 300x500 beam ends
set L1B [expr $beamHeight-70.0-12.0];
set L2B [expr $beamWidth-70.0-12.0];
set SBE 100.0;


# Application of C04 - The confinement factor was determined by hand calculation and
    comapred to Seismostruct.
#                          $matTag  $fc             $ec             $ecu            $Ec
    <$fct $et>
uniaxialMaterial Concrete04  2      -39.15427753    -0.005556568    -0.018700233
    32838.02131     $fctm $epsctu


########################################################################################
```

```
# Confined concrete in middle part of 300x500 beams
set SBM 200.0;
# Application of C04 - The confinement factor was determined by hand calculation and
    comapred to Seismostruct.
#                          $matTag $fc         $ec               $ecu             $Ec
    <$fct $et>
uniaxialMaterial Concrete04  3     -35.59479775 -0.004251426    -0.012085128
    32838.02131         $fctm $epsctu

#########################################################################################

#########################################################################################

# Confined concrete in 260x450 beam ends
set L1B [expr $beamHeight-70.0-12.0];
set L2B [expr $beamWidth-70.0-12.0];
set SBE 100.0;

# Application of C04 - The confinement factor was determined by hand calculation and
    comapred to Seismostruct.
#                          $matTag  $fc             $ec             $ecu             $Ec
    <$fct $et>
uniaxialMaterial Concrete04  8      -40.93401741    -0.00620914     -0.022658513
    32838.02131     $fctm $epsctu


#########################################################################################

# Confined concrete in middle part of 260x450 beams
set SBM 200.0;
# Application of C04 - The confinement factor was determined by hand calculation and
    comapred to Seismostruct.
#                          $matTag $fc          $ec              $ecu             $Ec
    <$fct $et>
uniaxialMaterial Concrete04  9     -35.59479775 -0.004251426    -0.015035178
    32838.02131     $fctm $epsctu

#########################################################################################

#########################################################################################
# Confined concrete in 400x400 column ends
# Application of C04 - The confinement factor was determined by hand calculation and
    comapred to Seismostruct.
#                          $matTag $fc           $ec               $ecu              $Ec
    <$fct $et>
uniaxialMaterial Concrete04  4     -53.39219663 -0.010777139      -0.021979928
    32838.02131 $fctm $epsctu


set L1C [expr $colWidth-70.0-12.0];
set SCE 100.0;


#########################################################################################

# Confined concrete in middle part of 400x400 columns
set SCM 200.0;
# Application of C04 - The confinement factor was determined by hand calculation and
    comapred to Seismostruct.
#                          $matTag $fc          $ec            $ecu           $Ec
    <$fct $et>
uniaxialMaterial Concrete04  5     -37.73048562 -0.005034511  -0.010873209  32838.02131
    $fctm $epsctu

#########################################################################################
#########################################################################################

# Confined concrete in 350x350 column ends
# Application of C04 -  The confinement factor was determined by hand calculation and
    comapred to Seismostruct.
```

```
#                          $matTag $fc          $ecu         $ecu          $Ec
    <$fct $et>
uniaxialMaterial Concrete04  6     -43.78160123 -0.007253254 -0.018867173   32838.02131
    $fctm $epsctu

set L1C [expr $colWidthBdr-70.0-12.0];
set SC350E 175.0;


##########################################################################################
##########################################################################################
# Confined concrete in middle part of 350x350 columns
set SC350M 275.0;
# Application of C04 - The confinement factor was determined by hand calculation and
    comapred to Seismostruct.
#                          $matTag $fc          $ec             $ecu            $Ec
    <$fct $et>
uniaxialMaterial Concrete04  7     -35.66598735 -0.004277529    -0.010274619
    32838.02131  $fctm $epsctu


##########################################################################################
##########################################################################################

# Reinforcement B500C
#                         $matTag $Fy  $E0 $b
uniaxialMaterial Steel01    10    $fyk $Es $haRatio


puts "materials are defined..."
```

```
#########################################################################################
#
#Sections for the 2D Model of 3 Story frame
#Nina Øystad-Larsen & Fredrik Bjercke
#7/1/2016
#Metric units mm, g, N, sec
#
#########################################################################################

# Define cross-section parameters
# ------------------------------------------
# set some paramaters

# Cover + half the stirrup diameter
set cover [expr 35.0+6.0];

# Beam cover + stirrup diameter + half the longitudinal bar diameter
set dclb [expr 35.0+12.0+11.0];

# Effective flange width of beams
set beff 1600.0;

# Column cover + stirrup diameter + half the longitudinal bar diameter
set dclc [expr 35.0+12.0+20.0];

# Slab height
set hslab 150.0;

# some variables derived from the parameters
set yb  [expr $beamHeight/2.0];
set zb  [expr $beamWidth/2.0];
set zbf [expr $beff/2.0];

set ybRoof  [expr $beamHeightRoof/2.0]; # Roof level beam height
set zbRoof  [expr $beamWidthRoof/2.0];  # Roof level beam width

set yc      [expr $colHeight/2.0];
set zc      [expr $colWidth/2.0];
set ycBdr   [expr $colHeightBdr/2.0];
set zcBdr   [expr $colWidthBdr/2.0];

puts "section parameters are set..."

#ooooooooooooooooooooooooooooooooooooooooooooooooooooooooooooooooooooooooooooooooooooooooo
# 1st, 2nd and 3rd storey beams (300x500 beams)
# Define cross-section for nonlinear beam ends
# ----------------------------------------------------------------------------

section Fiber 1 {
    # Create the concrete cover fibers for the beams:
    # patch rect $matTag $numSubdivY $numSubdivZ  $yI               $zI
        $yJ                         $zJ
    patch rect     1         2          20       [expr $yb-$cover] [expr -$zbf]
        $yb                         $zbf
    patch rect     1         2          2        [expr $yb-$hslab]  [expr -$zbf]        [
        expr $yb-$cover]            [expr -$zbf+$cover]
    patch rect     1         2          2        [expr $yb-$hslab]  [expr $zb-$cover]   [
        expr $yb-$cover]            $zbf
    patch rect     1         2          10       [expr $yb-$hslab] [expr -$zbf+$cover]  [
        expr $yb-$hslab+$cover] [expr -$zb+$cover]
    patch rect     1         2          10       [expr $yb-$hslab] [expr $zb-$cover]    [
        expr $yb-$hslab+$cover] [expr $zbf-$cover]
    patch rect     1         2          2        [expr -$yb]        [expr -$zb]         [
        expr $yb-$hslab]            [expr -$zb+$cover]
    patch rect     1         2          2        [expr -$yb]        [expr $zb-$cover]   [
        expr $yb-$hslab]            $zb
    patch rect     1         30         2        [expr -$yb]        [expr -$zb+$cover]  [
        expr -$yb+$cover]           [expr $zb-$cover]

    # Create the confined concrete in the flanges (part of the slab):
```

```
    # patch rect $matTag $numSubdivY $numSubdivZ     $yI                    $zI
        $yJ                $zJ
    patch rect     2         30        20         [expr $yb-$hslab+$cover] [expr -$zbf+
        $cover] [expr $yb-$cover] [expr -$zb+$cover]
    patch rect     2         30        20         [expr $yb-$hslab+$cover] [expr $zb-
        $cover] [expr $yb-$cover] [expr $zbf-$cover]

    # Create the confined concrete core fibers for the ends of the beams:
    # patch rect $matTag $numSubdivY $numSubdivZ     $yI                 $zI
        $yJ                $zJ
    patch rect     2         30        20         [expr -$yb+$cover] [expr -$zb+$cover] [
        expr $yb-$cover] [expr $zb-$cover]

    # Create the reinforcing fibers (top, top, bottom, bottom)
    #              $matTag $numFiber $areaFiber      $yStart             $zStart
        $yEnd              $zEnd
    layer straight 10          2        $Akam18   [expr $yb-$dclb]  [expr -$zb+$dclb] [
        expr $yb-$dclb]  [expr $zb-$dclb]
    layer straight 10          1        $Akam16   [expr $yb-$dclb]  [expr -$zb+$dclb] [
        expr $yb-$dclb]  [expr $zb-$dclb]
    layer straight 10          2        $Akam18   [expr -$yb+$dclb] [expr -$zb+$dclb] [
        expr -$yb+$dclb] [expr $zb-$dclb]
    layer straight 10          1        $Akam16   [expr -$yb+$dclb] [expr -$zb+$dclb] [
        expr -$yb+$dclb] [expr $zb-$dclb]
    # Create the reinforcing fibers in the slab (top, bottom)
    #              $matTag $numFiber $areaFiber      $yStart                    $zStart
        $yEnd                    $zEnd
    layer straight 10         4       $Akam10   [expr $yb-$dclb]           [expr -$zbf+
        $dclb]  [expr $yb-$dclb]        [expr -$zb+$dclb]
    layer straight 10         4       $Akam10   [expr $yb-$dclb]           $zb
        [expr $yb-$dclb]        [expr $zbf-$dclb]
    layer straight 10         3       $Akam10   [expr $yb-$hslab+$dclb]    [expr -$zbf+
        $dclb]  [expr $yb-$hslab+$dclb] [expr -$zb+$dclb]
    layer straight 10         3       $Akam10   [expr $yb-$hslab+$dclb]    $zb
        [expr $yb-$hslab+$dclb] [expr $zbf-$dclb]
}

##########################################################################################

# Define cross-section for middle part of nonlinear beams
# ----------------------------------------------------------------------------------------

section Fiber 2 {
    # Create the concrete cover fibers for the beams:
    # patch rect $matTag $numSubdivY $numSubdivZ  $yI               $zI
        $yJ                 $zJ
    patch rect     1         2          20       [expr $yb-$cover] [expr -$zbf]
        $yb                 $zbf
    patch rect     1         2          2        [expr $yb-$hslab]  [expr -$zbf]        [
        expr $yb-$cover]    [expr -$zbf+$cover]
    patch rect     1         2          2        [expr $yb-$hslab]  [expr $zbf-$cover]  [
        expr $yb-$cover]    $zbf
    patch rect     1         2          10       [expr $yb-$hslab] [expr -$zbf+$cover]  [
        expr $yb-$hslab+$cover] [expr -$zb+$cover]
    patch rect     1         2          10       [expr $yb-$hslab] [expr $zb-$cover]    [
        expr $yb-$hslab+$cover] [expr $zbf-$cover]
    patch rect     1         2          20       [expr -$yb]        [expr -$zb]         [
        expr $yb-$hslab]    [expr -$zb+$cover]
    patch rect     1         2          20       [expr -$yb]        [expr $zb-$cover]   [
        expr $yb-$hslab]    $zb
    patch rect     1         30         2        [expr -$yb]        [expr -$zb+$cover]  [
        expr -$yb+$cover]   [expr $zb-$cover]

    # Create the confined concrete in the flanges (part of the slab):
    # patch rect $matTag $numSubdivY $numSubdivZ     $yI                    $zI
        $yJ                $zJ
    patch rect     3         30        20         [expr $yb-$hslab+$cover] [expr -$zbf+
        $cover] [expr $yb-$cover] [expr -$zb+$cover]
    patch rect     3         30        20         [expr $yb-$hslab+$cover] [expr $zb-
        $cover] [expr $yb-$cover] [expr $zbf-$cover]
    # Create the confined concrete core fibers for the beams:
    # patch rect $matTag $numSubdivY $numSubdivZ     $yI             $zI
        $yJ                $zJ
    patch rect     3         30        20       [expr -$yb+$cover] [expr -$zb+$cover] [
        expr $yb-$cover] [expr $zb-$cover]

    # Create the reinforcing fibers (top, bottom, bottom)
    #              $matTag $numFiber $areaFiber      $yStart             $zStart
        $yEnd             $zEnd
    layer straight 10        2        $Akam18   [expr $yb-$dclb]  [expr -$zb+$dclb] [
        expr $yb-$dclb]  [expr $zb-$dclb]
    layer straight 10        2        $Akam18   [expr -$yb+$dclb] [expr -$zb+$dclb] [
        expr -$yb+$dclb] [expr $zb-$dclb]
    layer straight 10        1        $Akam16   [expr -$yb+$dclb] [expr -$zb+$dclb] [
        expr -$yb+$dclb] [expr $zb-$dclb]

    # Create the reinforcing fibers in the slab (top, bottom)
    #              $matTag $numFiber $areaFiber      $yStart                    $zStart
        $yEnd                       $zEnd
    layer straight 10        4        $Akam10   [expr $yb-$dclb]           [expr -$zbf+
        $dclb]  [expr $yb-$dclb]        [expr -$zb+$dclb]
    layer straight 10        4        $Akam10   [expr $yb-$dclb]           $zb
        [expr $yb-$dclb]        [expr $zbf-$dclb]
    layer straight 10        3        $Akam10   [expr $yb-$hslab+$dclb]    [expr -$zbf+
        $dclb]  [expr $yb-$hslab+$dclb] [expr -$zb+$dclb]
    layer straight 10        3        $Akam10   [expr $yb-$hslab+$dclb]    $zb
        [expr $yb-$hslab+$dclb] [expr $zbf-$dclb]
}

#ooooooooooooooooooooooooooooooooooooooooooooooooooooooooooooooooooooooooooooooooooooooooo

# 4th storey (=roof) beams (260x450 beams)

# Define cross-section for beam ends
# ----------------------------------------------------------------------------

section Fiber 14 {
    # Create the concrete cover fibers for the beams:
    # patch rect $matTag $numSubdivY $numSubdivZ  $yI                   $zI
        $yJ                             $zJ
    patch rect     1         2          20       [expr $ybRoof-$cover] [expr -$zbf]
        $ybRoof                         $zbf
    patch rect     1         2          2        [expr $ybRoof-$hslab]  [expr -$zbf]
        [expr $ybRoof-$cover]           [expr -$zbf+$cover]
    patch rect     1         2          2        [expr $ybRoof-$hslab]  [expr $zbf-$cover
        ]       [expr $ybRoof-$cover]           $zbf
    patch rect     1         2          10       [expr $ybRoof-$hslab] [expr -$zbf+$cover
        ]       [expr $ybRoof-$hslab+$cover]    [expr -$zbRoof+$cover]
    patch rect     1         2          10       [expr $ybRoof-$hslab] [expr $zbRoof-
        $cover]     [expr $ybRoof-$hslab+$cover]    [expr $zbf-$cover]
    patch rect     1         2          20       [expr -$ybRoof]        [expr -$zbRoof]
        [expr $ybRoof-$hslab]           [expr -$zbRoof+$cover]
    patch rect     1         2          20       [expr -$ybRoof]        [expr $zbRoof-
        $cover]     [expr $ybRoof-$hslab]           $zbRoof
    patch rect     1         30         2        [expr -$ybRoof]        [expr -$zbRoof+
        $cover] [expr -$ybRoof+$cover]          [expr $zbRoof-$cover]

    # Create the confined concrete in the flanges (part of the slab):
    # patch rect $matTag $numSubdivY $numSubdivZ     $yI                        $zI
        $yJ                   $zJ
    patch rect     8         30        20         [expr $ybRoof-$hslab+$cover] [expr -
        $zbf+$cover]        [expr $ybRoof-$cover] [expr -$zbRoof+$cover]
    patch rect     8         30        20         [expr $ybRoof-$hslab+$cover] [expr
        $zbRoof-$cover] [expr $ybRoof-$cover] [expr $zbf-$cover]

    # Create the confined concrete core fibers for the ends of the beams:
    # patch rect $matTag $numSubdivY $numSubdivZ     $yI                 $zI
        $yJ                $zJ
    patch rect     8         40        20         [expr -$ybRoof+$cover] [expr -$zbRoof+
        $cover] [expr $ybRoof-$cover] [expr $zbRoof-$cover]

    # Create the reinforcing fibers (top, top, bottom)
    #              $matTag $numFiber $areaFiber      $yStart             $zStart
        $yEnd             $zEnd
    layer straight 10          3       $Akam16   [expr $ybRoof-$dclb]  [expr -$zbRoof+
        $dclb] [expr $ybRoof-$dclb]  [expr $zbRoof-$dclb]
    layer straight 10          3       $Akam16   [expr -$ybRoof+$dclb] [expr -$zbRoof+
        $dclb] [expr -$ybRoof+$dclb] [expr $zbRoof-$dclb]

    # Create the reinforcing fibers in the slab (top, bottom)
    #              $matTag $numFiber $areaFiber      $yStart                    $zStart
        $yEnd                       $zEnd
    layer straight 10         4       $Akam10   [expr $ybRoof-$dclb]           [expr -
        $zbf+$dclb]     [expr $ybRoof-$dclb]        [expr -$zbRoof+$dclb]
    layer straight 10         4       $Akam10   [expr $ybRoof-$dclb]           $zbRoof
        [expr $ybRoof-$dclb]        [expr $zbf-$dclb]
    layer straight 10         3       $Akam10   [expr $ybRoof-$hslab+$dclb]    [expr -
        $zbf+$dclb]     [expr $ybRoof-$hslab+$dclb] [expr -$zbRoof+$dclb]
    layer straight 10         3       $Akam10   [expr $ybRoof-$hslab+$dclb]    $zbRoof
        [expr $ybRoof-$hslab+$dclb] [expr $zbf-$dclb]
}

#########################################################################################

# Define cross-section for middle part of beams
# ---------------------------------------------------------------------------------------

section Fiber 24 {
    # Create the concrete cover fibers for the beams:
    # patch rect $matTag $numSubdivY $numSubdivZ  $yI                   $zI
        $yJ                             $zJ
    patch rect     1         2          20       [expr $ybRoof-$cover] [expr -$zbf]
        $ybRoof                         $zbf
    patch rect     1         10         2        [expr $ybRoof-$hslab]  [expr -$zbf]
        [expr $ybRoof-$cover]           [expr -$zbf+$cover]
    patch rect     1         10         2        [expr $ybRoof-$hslab]  [expr $zbf-$cover
        ]       [expr $ybRoof-$cover]           $zbf
    patch rect     1         2          10       [expr $ybRoof-$hslab] [expr -$zbf+$cover
        ]       [expr $ybRoof-$hslab+$cover]    [expr -$zbRoof+$cover]
    patch rect     1         2          10       [expr $ybRoof-$hslab] [expr $zbRoof-
        $cover]     [expr $ybRoof-$hslab+$cover]    [expr $zbf-$cover]
    patch rect     1         2          2        [expr -$ybRoof]        [expr -$zbRoof]
        [expr $ybRoof-$hslab]           [expr -$zbRoof+$cover]
    patch rect     1         2          2        [expr -$ybRoof]        [expr $zbRoof-
        $cover]     [expr $ybRoof-$hslab]          $zbRoof
    patch rect     1         2          2        [expr -$ybRoof]        [expr -$zbRoof+
        $cover] [expr -$ybRoof+$cover]          [expr $zbRoof-$cover]

    # Create the confined concrete in the flanges (part of the slab):
    # patch rect $matTag $numSubdivY $numSubdivZ     $yI                        $zI
        $yJ                   $zJ
    patch rect     9         10        20         [expr $ybRoof-$hslab+$cover] [expr -
        $zbf+$cover]        [expr $ybRoof-$cover] [expr -$zbRoof+$cover]
    patch rect     9         10        20         [expr $ybRoof-$hslab+$cover] [expr
        $zbRoof-$cover] [expr $ybRoof-$cover] [expr $zbf-$cover]

    # Create the confined concrete core fibers for the beams:
    # patch rect $matTag $numSubdivY $numSubdivZ     $yI                 $zI
        $yJ                   $zJ
    patch rect     9            40        20     [expr -$ybRoof+$cover] [expr -$zbRoof+
        $cover] [expr $ybRoof-$cover] [expr $zbRoof-$cover]

    # Create the reinforcing fibers i the beam (top, bottom)
    #              $matTag $numFiber $areaFiber      $yStart             $zStart
        $yEnd             $zEnd
    layer straight 10        2         $Akam16   [expr $ybRoof-$dclb]   [expr -$zbRoof+
        $dclb] [expr $ybRoof-$dclb]  [expr $zbRoof-$dclb]
    layer straight 10        3         $Akam16   [expr -$ybRoof+$dclb] [expr -$zbRoof+
        $dclb] [expr -$ybRoof+$dclb] [expr $zbRoof-$dclb]
    # Create the reinforcing fibers in the slab (top, bottom)
    #              $matTag $numFiber $areaFiber      $yStart                    $zStart
        $yEnd                       $zEnd
    layer straight 10         4       $Akam10   [expr $ybRoof-$dclb]           [expr -
        $zbf+$dclb]     [expr $ybRoof-$dclb]        [expr -$zbRoof+$dclb]
    layer straight 10         4       $Akam10   [expr $ybRoof-$dclb]           $zbRoof
        [expr $ybRoof-$dclb]        [expr $zbf-$dclb]
    layer straight 10         3       $Akam10   [expr $ybRoof-$hslab+$dclb]    [expr -
        $zbf+$dclb]     [expr $ybRoof-$hslab+$dclb] [expr -$zbRoof+$dclb]
    layer straight 10         3       $Akam10   [expr $ybRoof-$hslab+$dclb]    $zbRoof
        [expr $ybRoof-$hslab+$dclb] [expr $zbf-$dclb]
}

puts "beam sections are created..."

#ooooooooooooooooooooooooooooooooooooooooooooooooooooooooooooooooooooooooooooooooooooooooo

# 400x400 Columns

#########################################################################################

# Define cross-section for nonlinear interior column ends
# ---------------------------------------------------------------------------------------

section Fiber 3 {
    # Create the concrete cover fibers for the columns:
    # patch rect $matTag $numSubdivY $numSubdivZ     $yI              $zI
        $yJ                $zJ
    patch rect     1         2          20         [expr $yc-$cover]  [expr -$zc]
        $yc                 $zc
    patch rect     1         2          20         [expr -$yc]         [expr -$zc]
        [expr -$yc+$cover] $zc
    patch rect     1         20         2          [expr -$yc+$cover] [expr -$zc]        [
        expr $yc-$cover]  [expr -$zc+$cover]
    patch rect     1         20         2          [expr -$yc+$cover] [expr $zc-$cover] [
        expr $yc-$cover]  $zc

    # Create the confined concrete core fibers for the columns:
    # patch rect $matTag $numSubdivY $numSubdivZ     $yI              $zI
        $yJ                $zJ
    patch rect     4         20        20          [expr -$yc+$cover] [expr -$zc+$cover] [
        expr $yc-$cover] [expr $zc-$cover]

    # Create the reinforcing fibers
    #              $matTag $numFiber $areaFiber   $yStart           $zStart
        $yEnd               $zEnd
    layer straight 10          2        $Akam32   [expr $yc-$dclc]  [expr -$zc+$dclc]   [
        expr $yc-$dclc]     [expr $zc-$dclc]
    layer straight 10          1        $Akam20   [expr $yc-$dclc]  [expr -$zc+$dclc]   [
        expr $yc-$dclc]     [expr $zc-$dclc]
    layer straight 10          2        $Akam20   0.0               [expr -$zc+$dclc]
        0.0                 [expr $zc-$dclc]
    layer straight 10          2        $Akam32   [expr -$yc+$dclc] [expr -$zc+$dclc]   [
        expr -$yc+$dclc]    [expr $zc-$dclc]
    layer straight 10          1        $Akam20   [expr -$yc+$dclc] [expr -$zc+$dclc]   [
        expr -$yc+$dclc]    [expr $zc-$dclc]
}

# Define cross-section for middle part of nonlinear interior columns
# -----------------------------------------------------------------------------------

section Fiber 4 {
    # Create the concrete cover fibers for the columns:
    # patch rect $matTag $numSubdivY $numSubdivZ     $yI                $zI
        $yJ                 $zJ
    patch rect     1         2          20         [expr $yc-$cover]  [expr -$zc]
        $yc                 $zc
    patch rect     1         2          20         [expr -$yc]         [expr -$zc]
        [expr -$yc+$cover] $zc
    patch rect     1         20         2         [expr -$yc+$cover] [expr -$zc]         [
        expr $yc-$cover]  [expr -$zc+$cover]
    patch rect     1         20         2         [expr -$yc+$cover] [expr $zc-$cover] [
        expr $yc-$cover]  $zc

    # Create the confined concrete core fibers for the columns:
    # patch rect $matTag $numSubdivY $numSubdivZ     $yI              $zI
        $yJ               $zJ
    patch rect     5         20        20         [expr -$yc+$cover] [expr -$zc+$cover] [
        expr $yc-$cover] [expr $zc-$cover]

    # Create the reinforcing fibers
    #              $matTag $numFiber $areaFiber   $yStart           $zStart
        $yEnd              $zEnd
    layer straight 10          2        $Akam32   [expr $yc-$dclc]  [expr -$zc+$dclc]   [
        expr $yc-$dclc]     [expr $zc-$dclc]
    layer straight 10          1        $Akam20   [expr $yc-$dclc]  [expr -$zc+$dclc]   [
        expr $yc-$dclc]     [expr $zc-$dclc]
    layer straight 10          2        $Akam20   0.0               [expr -$zc+$dclc]
        0.0                 [expr $zc-$dclc]
    layer straight 10          2        $Akam32   [expr -$yc+$dclc] [expr -$zc+$dclc]   [
        expr -$yc+$dclc]    [expr $zc-$dclc]
    layer straight 10          1        $Akam20   [expr -$yc+$dclc] [expr -$zc+$dclc]   [
        expr -$yc+$dclc]    [expr $zc-$dclc]
}


#oooooooooooooooooooooooooooooooooooooooooooooooooooooooooooooooooooooooooooooooooooooooooo
# 350x350 Columns
##########################################################################################
# Define cross-section for nonlinear border column ends
# ---------------------------------------------------------------------------------------

section Fiber 5 {
    # Create the concrete cover fibers for the columns:
    # patch rect $matTag $numSubdivY $numSubdivZ     $yI              $zI
        $yJ               $zJ
    patch rect     1         2          20        [expr $ycBdr-$cover]  [expr -$zcBdr]
        $ycBdr                 $zcBdr
    patch rect     1         2          20        [expr -$ycBdr]         [expr -$zcBdr]
        [expr -$ycBdr+$cover] $zcBdr
    patch rect     1         20         2         [expr -$ycBdr+$cover] [expr -$zcBdr]
        [expr $ycBdr-$cover]  [expr -$zcBdr+$cover]
    patch rect     1         20         2         [expr -$ycBdr+$cover] [expr $zcBdr-
        $cover] [expr $ycBdr-$cover]  $zcBdr

    # Create the confined concrete core fibers for the columns:
    # patch rect $matTag $numSubdivY $numSubdivZ     $yI              $zI
        $yJ               $zJ
    patch rect     6         20        20         [expr -$ycBdr+$cover] [expr -$zcBdr+
        $cover] [expr $ycBdr-$cover] [expr $zcBdr-$cover]

    # Create the reinforcing fibers
    #              $matTag $numFiber $areaFiber   $yStart               $zStart
        $yEnd                  $zEnd
    layer straight 10          2        $Akam25   [expr $ycBdr-$dclc]   [expr -$zcBdr+
        $dclc]  [expr $ycBdr-$dclc]     [expr $zcBdr-$dclc]
    layer straight 10          1        $Akam25   [expr $ycBdr-$dclc]   [expr -$zcBdr+
        $dclc]  [expr $ycBdr-$dclc]     [expr $zcBdr-$dclc]
    layer straight 10          2        $Akam25   0.0                   [expr -$zcBdr+
        $dclc]  0.0                     [expr $zcBdr-$dclc]
    layer straight 10          2        $Akam25   [expr -$ycBdr+$dclc]  [expr -$zcBdr+
        $dclc]  [expr -$ycBdr+$dclc]    [expr $zcBdr-$dclc]
    layer straight 10          1        $Akam25   [expr -$ycBdr+$dclc]  [expr -$zcBdr+
        $dclc]  [expr -$ycBdr+$dclc]    [expr $zcBdr-$dclc]
}

# Define cross-section for middle part of border interior columns
# ---------------------------------------------------------------------------------------
section Fiber 6 {
    # Create the concrete cover fibers for the columns:
    # patch rect $matTag $numSubdivY $numSubdivZ     $yI                $zI
        $yJ                 $zJ
    patch rect     1         2          20        [expr $ycBdr-$cover]  [expr -$zcBdr]
        $ycBdr                 $zcBdr
    patch rect     1         2          20        [expr -$ycBdr]         [expr -$zcBdr]
        [expr -$ycBdr+$cover] $zcBdr
    patch rect     1         20         2         [expr -$ycBdr+$cover] [expr -$zcBdr]
        [expr $ycBdr-$cover]  [expr -$zcBdr+$cover]
    patch rect     1         20         2         [expr -$ycBdr+$cover] [expr $zcBdr-
        $cover] [expr $ycBdr-$cover]  $zcBdr

    # Create the confined concrete core fibers for the columns:
    # patch rect $matTag $numSubdivY $numSubdivZ     $yI              $zI
        $yJ                $zJ
    patch rect     7         20        20         [expr -$ycBdr+$cover] [expr -$zcBdr+
        $cover] [expr $ycBdr-$cover] [expr $zcBdr-$cover]

    # Create the reinforcing fibers
    #              $matTag $numFiber $areaFiber   $yStart           $zStart
        $yEnd               $zEnd
    layer straight 10          2        $Akam25   [expr $ycBdr-$dclc]   [expr -$zcBdr+
        $dclc]  [expr $ycBdr-$dclc]     [expr $zcBdr-$dclc]
    layer straight 10          1        $Akam25   [expr $ycBdr-$dclc]   [expr -$zcBdr+
        $dclc]  [expr $ycBdr-$dclc]     [expr $zcBdr-$dclc]
    layer straight 10          2        $Akam25   0.0                   [expr -$zcBdr+
        $dclc]  0.0                 [expr $zcBdr-$dclc]
    layer straight 10          2        $Akam25   [expr -$ycBdr+$dclc] [expr -$zcBdr+
        $dclc]  [expr -$ycBdr+$dclc]    [expr $zcBdr-$dclc]
    layer straight 10          1        $Akam25   [expr -$ycBdr+$dclc] [expr -$zcBdr+
        $dclc]  [expr -$ycBdr+$dclc]    [expr $zcBdr-$dclc]
}

puts "Column sections are created."
```

```
##########################################################################################
    ##
#
#Recorder for 2D Model of 4 Storey 5 bay frame
#Nina Øystad-Larsen & Fredrik Bjercke
#Metric units mm, kg, N, sec
#
##########################################################################################
    ##
set dataDir Output;
file mkdir $dataDir; # create data directory
#Recorder
#Record the eigen values
for { set k 1 } { $k <= $numModes } { incr k } {
    recorder Node -file [format "modes/mode%i.out" $k] -node 11 21 31 41 -dof 1  "eigen
        $k"
}

#Record the column axial loads
# when an element is called to ouput force they output the forces in the global coord
    system at the element ends, i.e. 2d 3dof: Fx1 Fy1 Mz1 Fx2 Fy2 Mz2
# NB: Since the loads are divided by $NstepGravity the output must be multiplied by this
    factor.
    recorder Element -file $dataDir/ColumnForces.out -ele 111 112 113 114 115 116 121 122
        123 124 125 126 131 132 133 134 135 136 141 142 143 144 145 146 force

    #Record the local forces in beams
# when an element is called to ouput force they output the forces in the global coord
    system at the element ends, i.e. 2d 3dof: Fx1 Fy1 Mz1 Fx2 Fy2 Mz2
# NB: Since the loads are divided by $NstepGravity the output must be multiplied by this
    factor.
    recorder Element -file $dataDir/BeamSt1Forces.out -eleRange 11  15 localForce
    recorder Element -file $dataDir/BeamSt2Forces.out -eleRange 21  25 localForce
    recorder Element -file $dataDir/BeamSt3Forces.out -eleRange 31  35 localForce
    recorder Element -file $dataDir/BeamSt4Forces.out -eleRange 41  45 localForce

    #Record the displacement
    recorder Node -file $dataDir/ControlDisp4th.out -time -node 41 -dof 1 disp
    recorder Node -file $dataDir/ControlDisp3rd.out -time -node 31 -dof 1 disp
    recorder Node -file $dataDir/Vertdisp3rd.out -time -node 31 -dof 2 disp
    recorder Node -file $dataDir/ControlDisp2nd.out -time -node 21 -dof 1 disp
    recorder Node -file $dataDir/ControlDisp1st.out -time -node 11 -dof 1 disp

    #Record the velocity
    recorder Node -file $dataDir/ControlVel3rd.out -time -node 31 -dof 1 vel

    # Record the base shear
    recorder Node -file $dataDir/BaseShearNode1.out -time -node 1 -dof 1 reaction
    recorder Node -file $dataDir/BaseShearNode2.out -time -node 2 -dof 1 reaction
    recorder Node -file $dataDir/BaseShearNode3.out -time -node 3 -dof 1 reaction
    recorder Node -file $dataDir/BaseShearNode4.out -time -node 4 -dof 1 reaction
    recorder Node -file $dataDir/BaseShearNode5.out -time -node 5 -dof 1 reaction
    recorder Node -file $dataDir/BaseShearNode6.out -time -node 6 -dof 1 reaction

    #Record the plastic deformations - column 1 is the axial deformation, columns 2 and 3
        are rotations at the 2 ends,
    recorder Element -file $dataDir/ColumnSt1PlasRot.out -time -eleRange 111    116
        plasticDeformation
    recorder Element -file $dataDir/ColumnSt2PlasRot.out -time -eleRange 121    122
        plasticDeformation
    recorder Element -file $dataDir/ColumnSt3PlasRot.out -time -eleRange 131    132
        plasticDeformation
    recorder Element -file $dataDir/BeamPlasRotSt1.out -time -eleRange 11   15
        plasticDeformation
    recorder Element -file $dataDir/BeamPlasRotSt2.out -time -eleRange 21   25
        plasticDeformation
    recorder Element -file $dataDir/BeamPlasRotSt3.out -time -eleRange 31   35
        plasticDeformation
    recorder Element -file $dataDir/BeamPlasRotSt4.out -time -eleRange 41   45
        plasticDeformation
    #Drift recorder one for each floor
    recorder Drift -file $dataDir/Drift1.out    -time -iNode 3  -jNode 13 -dof1 -
        perpDirn2
    recorder Drift -file $dataDir/Drift2.out    -time -iNode 13 -jNode 23 -dof1 -
        perpDirn2
    recorder Drift -file $dataDir/Drift3.out    -time -iNode 23 -jNode 33 -dof1 -
        perpDirn2
    recorder Drift -file $dataDir/Drift4.out    -time -iNode 33 -jNode 43 -dof1 -
        perpDirn2
    recorder Drift -file $dataDir/DriftRoof.out -time -iNode 3  -jNode 43 -dof1 -
        perpDirn2

puts "Recorders are defined..."
#########################################################################################
    ##
#End of Script
```

```
#######################################################################################
#2D Model of 3 Story frame
#Script to compute the natural periods and mode shapes
#Nina Øystad-Larsen & Fredrik Bjercke
#7/1/2016
#Units: N, mm, kg
#
#######################################################################################

# The eigenvalues are calculated using eigen command and stored in lambda variable
set lambda [eigen  $numModes];
#The periods and frequencies of the structure are calculated
set omega {}
set f {}
set T {}
set pi 3.141593
puts "Eigenvalue calculation begins..."
foreach lam $lambda {
    lappend omega [expr sqrt($lam)]
    lappend f [expr sqrt($lam)/(2*$pi)]
    lappend T [expr (2*$pi)/sqrt($lam)]
}
puts "The natural periods of the system are: $T"

# The periods are stored in a Periods.txt file inside of directory "modes".

set period "modes/Periods.txt"
set Periods [open $period "w"]
foreach t $T {
    puts $Periods " $t"
}
close $Periods

puts "Periods are stored..."

# Record mode shapes

record

puts "the eigenvalues have been recorded..."
```

```
#########################################################################################
#Script for Pushover Analysis
#########################################################################################
source PushoverLoad.tcl
puts "Pushover Analysis Starts..."
#System
system BandGeneral;
constraints Plain;
numberer Plain
test EnergyIncr 1.0e-2 200

set algorithmType Newton
algorithm $algorithmType;

set ControlDisplacementNode 41;
set ControlDisplacementDOF 1;
set Dmax 1000.0;
set Dincr 0.5;

# Determine the corrective step based on the displacement increment dU
#                                       node                       dof             init
    Jd minStepsize maxStepsize
integrator DisplacementControl $ControlDisplacementNode $ControlDisplacementDOF $Dincr;
    # 1   $Dincr      $Dincr;

#Perform pushover

analysis Static;
set Nsteps [expr int($Dmax/$Dincr)];
set NSA [analyze $Nsteps];
if {$NSA == 0} {
puts "All steps have converged. Non-linear static analysis OK."
}
if {$NSA != 0} {
puts " No convergence.. must try something else."
set NSA 0;
set controlDisp 0.0;
set D0 0.0;
set Dstep [expr ($controlDisp-$D0)/($Dmax-$D0)]
while {$Dstep < $Dmax && $NSA == 0} {
set controlDisp [nodeDisp $ControlDisplacementNode $ControlDisplacementDOF]
set Dstep [expr ($controlDisp-$D0)/($Dmax-$D0)]
set NSA [analyze 1]
if {$NSA != 0} {
puts "Trying Newton with Initial Tangent .."
test NormDispIncr $Tol 2000 0
algorithm Newton -initial
set NSA [analyze 1 ]
test $TestType $Tol $maxNumIter 0
algorithm $algorithmType
}
if {$NSA != 0} {
puts "Trying Broyden .."
algorithm Broyden 8
set NSA [analyze 1 ]
algorithm $algorithmType
}
if {$NSA != 0} {
puts "Trying NewtonWithLineSearch .."
algorithm NewtonLineSearch .8
set NSA [analyze 1 ]
algorithm $algorithmType
}
if {$NSA != 0} {
puts "Trying BFGS .."
algorithm BFGS
set NSA [analyze 1 ]
algorithm $algorithmType
}
}
```

```
    if {$NSA != 0} {
        puts "DispControl Analysis FAILED"
        } else {
        puts "DispControl Analysis SUCCESSFUL"
    }
}

#########################################################################################
#                       END OF INPUT                            #
#########################################################################################
```

```
##########################################################################################
#2D Model of 3 Story frame
#Nina Øystad-Larsen & Fredrik Bjercke
#7/1/2016
#Metric units mm, kg, N, sec
#
##########################################################################################

#set scale factor
set g 9810.0;
set sc68    1;
set sc169   1;
set sc724   1;
set sc730   1;
set sc1634  1;
set sc4853  1;
set sc5786  1;

set Scalefactor68 [expr $sc68*0.70*$g];
set Scalefactor169 [expr $sc169*0.40*$g];
set Scalefactor724 [expr $sc724*1.26*$g];
set Scalefactor730 [expr $sc730*0.46*$g];
set Scalefactor1634 [expr $sc1634*0.59*$g];
set Scalefactor4853 [expr $sc4853*0.27*$g];
set Scalefactor5786 [expr $sc5786*0.41*$g];


#Define time series
#timeSeries Path    $tag    -dt $dt     -filePath $filePath                 <-factor
    $cFactor>
timeSeries  Path    68      -dt 0.01    -filePath RSN68_SFERN_PEL090.tcl    -factor
    $Scalefactor68
#timeSeries Path    169     -dt 0.01    -filePath RSN169_IMPVALL.H_H-DLT262.tcl -factor
    $Scalefactor169
#timeSeries Path    724     -dt 0.01    -filePath RSN724_SUPER.B_B-PLS045.tcl   -factor
    $Scalefactor724
#timeSeries Path    730     -dt 0.01    -filePath RSN730_SPITAK_GUK000.tcl  -factor
    $Scalefactor730
#timeSeries Path    1634    -dt 0.01    -filePath RSN1634_MANJIL_184-UP.tcl -factor
    $Scalefactor1634
#timeSeries Path    4853    -dt 0.01    -filePath RSN4853_CHUETSU_65019EW.tcl   -factor
    $Scalefactor4853
#timeSeries Path    5786    -dt 0.01    -filePath RSN5786_IWATE_54038EW.tcl -factor
    $Scalefactor5786



#Apply time series
#pattern UniformExcitation $patternTag $dir -accel $tsTag <-vel0 $vel0> <-fact $cFactor>
pattern UniformExcitation   2           1   -accel 68
#pattern UniformExcitation  2           1   -accel 169
#pattern UniformExcitation  2           1   -accel 724
#pattern UniformExcitation  2           1   -accel 730
#pattern UniformExcitation  2           1   -accel 1634
#pattern UniformExcitation  2           1   -accel 4853
#pattern UniformExcitation  2           1   -accel 5786


#Define damping
set T1      0.79035;
set T3      0.2;
set w1      [expr 0.707*6.2831/$T1];
set w3      [expr 6.2831/$T3];
set ksi1    [expr 5.0/100.0];
set alphaM  [expr $ksi1*2*$w1*$w3/($w1+$w3)];
set betaK   [expr $ksi1*2/($w1+$w3)];
set betaKinit   0.0;
set betaKcomm   0.0;
#rayleigh $alphaM $betaK $betaKinit $betaKcomm
rayleigh $alphaM $betaK $betaKinit $betaKcomm;
```

```
wipeAnalysis

#Analysis
constraints Plain
numberer RCM
system BandGeneral
test NormDispIncr 1.0e-1 200;
algorithm BFGS


# Hilber-Hughes-Taylor Method
set HHTalpha 0.9;
#set Ngamma 0.6;
#set Nbeta 0.3025;
integrator HHT $HHTalpha;

# Newmarks method
set Ngamma 0.5;
set Nbeta 0.25;
#integrator Newmark $Ngamma $Nbeta

#Perform analysis
analysis Transient

set NRHA [analyze 7943 0.01];
if {$NRHA == 0} {
    puts "All steps have converged. Non-linear response history analysis OK"
}
if {$NRHA != 0} {
    puts "Convergence issues. Non-linear response history analysis not OK "
}
```

```
##########################################################################################
#2D Model of 3 Story frame
#Script to compute the natural periods and mode shapes
#Nina Øystad-Larsen & Fredrik Bjercke
#7/1/2016
#Units: N, mm, kg
#
##########################################################################################

# The eigenvalues are calculated using eigen command and stored in lambda variable
set lambda [eigen  $numModes];
#The periods and frequencies of the structure are calculated
set omega {}
set f {}
set T {}
set pi 3.141593
puts "Eigenvalue calculation begins..."
foreach lam $lambda {
    lappend omega [expr sqrt($lam)]
    lappend f [expr sqrt($lam)/(2*$pi)]
    lappend T [expr (2*$pi)/sqrt($lam)]
}
puts "The natural periods of the system are: $T"

# The periods are stored in a Periods.txt file inside of directory "modes".

set period "modes/Periods.txt"
set Periods [open $period "w"]
foreach t $T {
    puts $Periods " $t"
}
close $Periods

puts "Periods are stored..."

# Record mode shapes

record

puts "the eigenvalues have been recorded..."
```